POLITECNICO DI TORINO

Master's Degree
in Energy and Nuclear Engineering

Master's Thesis

System-level hydraulic modeling of the PbLi loop for the Breeding Blanket of a tokamak

Supervisors
Dr. Antonio Froio
Prof.ssa Laura Savoldi
Prof. Roberto Zanino

Candidate
Andrea Batti
matricola: 251494

October 2020

Ai miei nonni, ai miei genitori, a mia sorella

† A mio nonno Antonio

Acknowledgements

First of all, I thank my mother and father for supporting me from afar during this long and important journey that began six years ago. Thank you for always being there in both happy and difficult times.

I also thank my sister, Alessandra, for being close to me during these four years spent together and making my days lighter. As an older brother, I'll always be there.

I would especially like to thank my grandparents, who, although far away, have always been close to my thoughts. Thanks to their help, today I am who I am.

I thank my supervisor, Dr. Antonio Froio, for his great availability and for guiding me during this thesis work. I also thank my co-supervisors, prof. Savoldi and prof. Zanino, for worms given me the opportunity to work on the subject of fusion and the advice given to me in the drafting of my work.

Special thanks also go to Francesca, Marcello, Luigina, Luigi, Maria Grazia and Daniela for the wonderful moments spent together. Thank you very much for lifting me up and making me see the light.

I thank my friends Beatrice and William, with whom I spent many happy moments during my studies. I will never forget the thousand coffees taken together.

I thank all my classmates for making the days spent between one lesson and another more carefree. I will always have happy memories of this shared journey together.

I also thank all my friends that I got to know during these six years. Thanks for the great chats and the good times we spent together.

Finally, I wanted to address my grandfather Antonio. The night before he left, I saw him in a dream, in the same hospital bed, looking at me with a bright smile on his face. From that day to today I always carry that smile in my heart and in my thoughts, and I will always carry it.

Ringraziamenti

Prima di tutto, ringrazio mia madre e mio padre per avermi supportato a distanza durante questo lungo ed importante percorso iniziato sei anni fa. Grazie per esserci stati sempre sia nei momenti felici che in quelli difficili.

Ringrazio anche mia sorella, Alessandra, per essermi stata vicina durante questi quattro anni vissuti insieme e avermi reso le giornate più leggere. Da fratello maggiore, io ci sarò sempre.

Vorrei ringraziare soprattutto i miei nonni, che seppur lontani, sono sempre stati vicini con il pensiero. Grazie al loro aiuto, oggi sono la persona che sono.

Ringrazio il mio relatore, il Dott. Antonio Froio, per la sua grandissima disponibilità e per avermi guidato durante questo lavoro di tesi. Ringrazio inoltre i miei correlatori, la prof.ssa Savoldi e il prof. Zanino, per vermi dato l'opportunità di poter lavorare sul tema della fusione e dei consigli datomi nella stesura del mio lavoro.

Un ringraziamento speciale va anche a Francesca, Marcello, Luigina, Luigi, Maria Grazia e Daniela per i bellissimi momenti passati insieme. Grazie di cuore per avermi rialzato e per avermi fatto vedere la luce.

Ringrazio i miei amici Beatrice e William, con cui ho speso molti momenti felici durante i miei studi. Non dimenticherò mai i mille caffè presi insieme.

Ringrazio tutti i miei compagni di corso per aver reso più spensierate le giornate passate tra una lezione e l'altra. Avrò sempre un ricordo felice di questo viaggio condiviso insieme.

Ringrazio anche tutti i miei amici che ho avuto modo di conoscere durante questi sei anni. Grazie per le bellissime chiacchierate e i bei momenti passati insieme.

Infine, volevo rivolgere un pensiero a mio nonno Antonio. La notte prima che se ne andò via, lo vidi in un sogno, nella stesso letto dell'ospedale, che mi guardava con un sorriso smagliante in viso. Da quel giorno ad oggi mi porto sempre quel sorriso nel mio cuore e nei miei pensieri, e lo porterò sempre.

Abstract

The breeding blanket (BB) is a key part of future fusion reactors. Its purposes are: 1) absorbing the energy from neutrons produced in the plasma by the fusion nuclear reactions between deuterium and tritium (D-T), 2) breeding further tritium fuel and 3) shielding other radiation-susceptible components. The Water-Cooled Lithium-Lead (WCLL) is one of the candidate design options for the European DEMO nuclear fusion reactor. The current design is based on pressurized water as coolant, liquid lithium-lead (PbLi) as breeder-multiplier and EUROFER as structural material. However, this design is in a pre-conceptual phase and it is important to analyze with numerical models the behavior of the system from the different points of view, e.g. neutronics, thermal-mechanics and thermal-hydraulics.
In view of the relatively large electrical conductivity of the liquid metal used as breeder-multiplier, the flow regime in the PbLi loop are strongly susceptible to magnetic field and this causes the onset of a magneto-hydrodynamic (MHD) flow. The magnetic field in a fusion reactor is principally composed by a toroidal and a poloidal component which changes based on the position within the reactor. In general, for an electro-conductive fluid that flows under a magnetic field, the pressure drop is the sum of ordinary-hydrodynamic (OHD) pressure drop (Δp_{OHD}) and magneto-hydrodynamic pressure drop (Δp_{MHD}). For high value of magnetic field, it possible to consider only the MHD case in which the overall pressure drop can be split into the distributed (Δp_{2D}) and concentrated losses (Δp_{3D}).
With respect to the OHD case, the MHD pressure drops have different correlations based on the geometry of the channel, orientation of the magnetic field, cross section variation and presence of obstacles. The aim of this work is to develop a 1-D model through the Modelica language for the PbLi loop, to characterize the pressure drop inside the BB region. In this study, the 2018 WCLL design of the PbLi loop is considered. First, the correlations for each type of pressure loss are implemented with the Modelica language and are compared and validated with the available experimental results. Then, all the components of the PbLi loops are modeled according to the different types of pressure losses (Δp_{2D} and/or Δp_{3D}), taking into account the corresponding geometry, fluid properties and magnetic field parameters. Finally, the model is applied both for the OB and the IB loops in nominal operation and in two possible transients.

Sommario

Il breeding blanket (BB) è una parte fondamentale dei futuri reattori a fusione. I suoi scopi sono: 1) assorbire l'energia dei neutroni prodotta nel plasma dalle reazioni nucleari di fusione tra deuterio e trizio (D-T), 2) produrre ulteriore trizio e 3) schermare gli altri componenti sensibili alle radiazioni. Il Water-Cooled Lithium-Lead (WCLL) è uno delle configurazioni candidate per il reattore europeo a fusione nucleare DEMO. Il progetto attuale si basa su acqua pressurizzata come refrigerante, litio-piombo liquido (PbLi) come moltiplicatore-breeder e EUROFER come materiale strutturale. Tuttavia, questo progetto è in una fase pre-concettuale ed è importante analizzare con modelli numerici il comportamento del sistema dai diversi punti di vista, ad es. neutronica, termomeccanica e termoidraulica.
Considerando l'alta conducibilità elettrica del metallo liquido utilizzato come moltiplicatore-breeder, il regime di flusso nel ciclo PbLi è fortemente suscettibile al campo magnetico e questo provoca l'inizio di un flusso magneto-idrodinamico (MHD). Il campo magnetico in un reattore a fusione è composto principalmente da una componente toroidale e da una poloidale che cambiano in base alla posizione all'interno del reattore. In generale, per un fluido elettroconduttivo che scorre all'interno di un campo magnetico, la caduta di pressione è la somma della caduta di pressione idrodinamica ordinaria (OHD) (Δp_{OHD}) e della caduta di pressione magneto-idrodinamica (Δp_{MHD}). Per valori di campo magnetico elevati, è possibile considerare solo il caso MHD in cui la caduta di pressione complessiva può essere suddivisa in perdite distribuite (Δp_{2D}) e concentrate (Δp_{3D}).
Rispetto al caso OHD, le perdite di carico MHD hanno correlazioni diverse in base alla geometria del canale, all'orientamento del campo magnetico, alla variazione della sezione trasversale e alla presenza di ostacoli. Lo scopo di questo lavoro è sviluppare un modello 1-D attraverso il linguaggio Modelica per il circuito PbLi, per caratterizzare la caduta di pressione all'interno della regione del BB. In questo studio, viene considerato il design del WCLL 2018 del circuito del PbLi. In primo luogo, le correlazioni per ogni tipo di perdita di pressione vengono implementate con il linguaggio Modelica e vengono confrontate e convalidate con i risultati sperimentali disponibili. Quindi, tutti i componenti del circuito del PbLi vengono modellati secondo i diversi tipi di perdite di carico (Δp_{2D} e/o Δp_{3D}), tenendo conto delle corrispondenti geometrie, proprietà del fluido e parametri del campo magnetico. Infine, il modello è applicato sia per i circuiti OB che IB in funzionamento nominale e in due possibili transitori.

Contents

List of Tables

List of Figures

Nomenclature

Acronyms and abbrevation

BB	Breeading Blanket
BoP	Balance of Plant
BSS	Back Supporting Structure
BZ	Breeding Zone
CFD	Computational Fluid Dynamics
CP	Cooling Plates
CS	Central Solenoid
DCLL	Dual-Coolant Lithium Lead
DN	Nominal Diameter
DP	Draining Pipe
EU DEMO	European Demonstration Fusion Power Reactor
FCI	Flow Channel Inserts
FP	Feeding Pipe
FV	Finite Volumes
FW	First Wall
GETTHEM	General Tokamak Thermal-hydraulic Model
HCLL	Helium-Cooled Lithium Lead
HCPB	Helium-Cooled Pebble Bed
IB	Inboard Blanket
ITER	International Thermonuclear Experimental Reactor
LOCA	Loss Of Coolant Accident

M	Manifold
MHD	MagnetoHydroDynamics
MMS	Multi Module Segmentation
OB	Outboard Blanket
OHD	Ordinary HydroDynamics
PbLi	Lithium-Lead
PFC	Poloidal Field Coil
PHTS	Primary Heat Transfer System
SMS	Single Module Segment
TBR	Tritium Breeding Ratio
TFC	Toroidal Field Coil
VV	Vacuum Vessel
WCLL	Water-Cooled Lithium-Lead

Greek

α	Thermal diffusivity
β	Volumetric thermal expansion coefficient
λ	Thermal conductivity
μ	Dynamic viscosity
ν	Kinematic viscosity
ϕ	Toroidal (reactor and blanket) direction
ρ	Density
ρ_{el}	Electrical resistivity
σ	Electrical conductivity
σ_w	Wall electrical conductivity
θ	Poloidal (blanket) direction

Subscript

eu	Eutectic
$head$	Hydrostatic head

lit	Literature data
$obst$	Obstacles
$orif$	Channel cross section variation (orifice)
pol	Poloidal direction
rad	Radial direction
sim	Modelica simulation value
tor	Toroidal direction
ver	Vertical direction

Symbols

Δp_{2D}	2D pressure drops (distributed losses)
Δp_{3D}	3D pressure drops (concentrated losses)
$\dot{m}$	Mass flow rate
$\epsilon_{E,c}$	Coupling effect corrective coefficent (annular channel)
$\epsilon_{I,c}$	Coupling effect corrective coefficent (internal channel)
A	Area of channel/pipe cross section
a	Channel half width parallel to magnetic field
B	Magnetic field
b	Channel half width perpendicular to magnetic field
c	Wall conductance ratio
c_H	Hartmann wall conductance ratio
c_p	Specific heat
$c_{S,i}$	Side wall conductance ratio
d_{hyd}	Vertical (reactor) direction
d_i	Inner diameter
d_o	Outer diameter
f_{corr}	Corrective factor
f_{perc}	Percentage mass flow rate coefficient
g	Gravitational acceleration constant ($9.81\ m/s^2$)

h	Channel vertical heigth
Ha	Hartmann number
He	Helium particle
k_1, k_2	Flow around obstacle pipes correlation coefficients
k_p	2D pressure loss coefficient
k_{3D}	3D pressure loss coefficient
L	Channel length
L_{ch}	Characteristic length
n	Neutron
N_{pipes}	Obstacle pipes number
P	Channel perimeter
R	Radial (reactor) direction
r	Radial (blanket) direction
r_i	Inner radius
r_o	Outer radius
Re	Reynolds number
T_{PbLi}	Temperature
t_w	Wall thickness
u_0	Fluid mean velocity
Z	Vertical (reactor) direction
D	Deuterium
T	Tritium

Chapter 1

Introduction

1.1 EU DEMO Breeding Blanket

The European Demonstration Fusion Power Reactor (EU DEMO) [1] is a fusion reactor prototype under development by the EUROfusion Consortium. It is the successor of the ITER experimental reactor [2] in the European Roadmap to the realization of fusion energy [3]. Unlike the ITER project, which aims to demonstrate the possibility to obtain a plasma capable to sustain fusion nuclear reactions between deuterium and tritium (D-T) [4] for a long time (1000 s), the main purpose of the DEMO project is to demonstrate the capability to produce electrical energy through the nuclear fusion reactions. Figure 1.1 reports a scheme of a general layout of EU DEMO reactor.

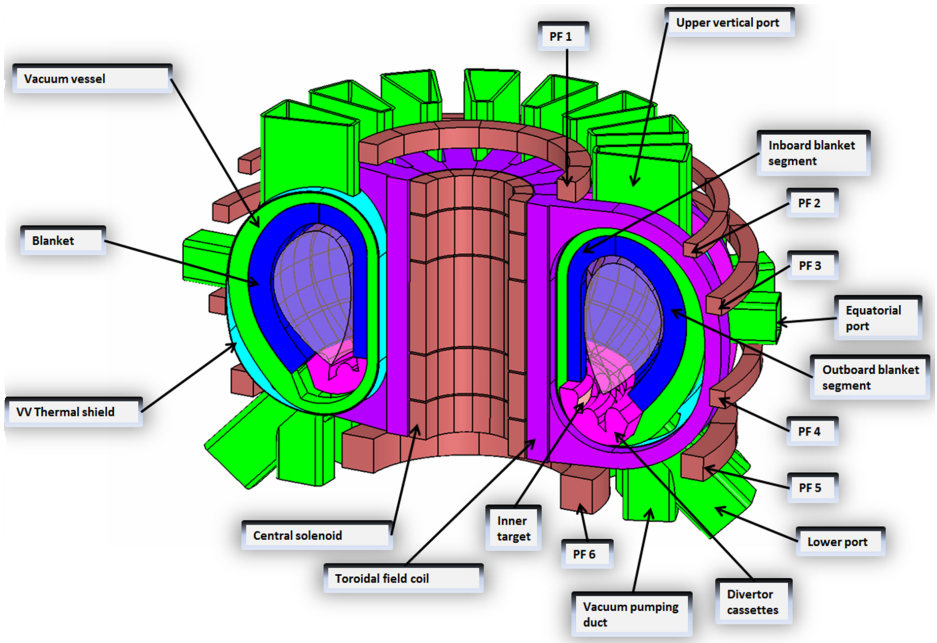

Figure 1.1: The EU DEMO tokamak general layout [5].

The thermal energy production occurs via fusion reactions between two hydrogen isotopes, deuterium (D) and tritium (T). These two isotopes are heated at a high value of temperature ($\approx$ 100 million degrees) until they ionize and become plasma. The plasma is confined trough a complex system of superconducting magnets. The products of these reactions are helium particles (He) and neutrons (n). The reaction can be expressed with the relation

$$D_1^2 + T_1^3 \rightarrow He_2^4\ (3.5\ MeV) + n^0\ (14.1\ MeV)$$

The ionized plasma is confined inside the reactor chamber through a complex system of magnetic fields. The resultant magnetic field has an helical shape that runs along the torus composed by several field components, which are generated through the superconducting magnets located in particular regions of the reactor. The toroidal field component is produced by the TFCs; the poloidal component is produced by the current circulating in the plasma which is produced by the CS; the vertical field is generated by the PFCs. The toroidal and the poloidal fields serve to give the plasma helical shape and permits the right confinement; the vertical one gives the right plasma stability. A general representation of the magnetic field components is presented in Figure 1.2. Usually, the main magnetic field component in a tokamak is the toroidal one.

The EU DEMO fusion reactor is composed by several main components:

- **Magnets**: provide the plasma confinement generating a complex system of magnetic fields. They are made by Nb_3Sn and refrigerated by liquid helium. The principal magnetic field is generated by three different systems of superconducting magnets: the central solenoid (CS), the toroidal field coils (TFC) and the poloidal field coils (PFC). The CS is placed in the centre of the reactor, the TFCs are placed around the reactor providing the main magnetic field component and the PFCs are placed outside the reactor providing the plasma stability.
- **Divertor**: removes the spent helium ashes and other impurities from the plasma. It generates an X configuration of the magnetic field (magnetic field null) that conveys the particles to the *divertor plates*.
- **Breeding Blanket (BB)**: contains a Li-rich material which is used to breed the T; it also contains the First Wall (FW), which is the first solid component facing the plasma.
- **Vacuum Vessel (VV)**: provides the ultra-high-vacuum environment for the plasma stability; it contains the BB and the divertor.
- **Cryostat**: surrounds the vacuum-vessel and superconducting magnet systems and ensures an ultra cool and vacuum environment necessary for the right operation of the reactor components.

The BB is a key part of many proposed fusion reactors. It consists of a set of modules covering the interior of the fusion reactor vessel, capable of supporting a high heat load and intense neutron flux. It serves several purposes: 1) absorbing the energy from neutrons produced in the plasma by D-T nuclear fusion reactions, acting as a power extraction system; 2) breeding further tritium fuel through the reaction of neutrons with the

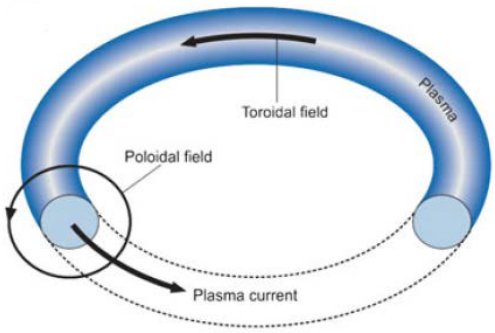

Figure 1.2: General scheme of the main magnetic field components in a tokamak [6].

lithium in the blanket, that would otherwise be difficult to obtain in sufficient quantities and ensure the necessary fuel generation for the plant self-sufficiency; 3) shielding, protecting the area outside of the the reactor and radiation-susceptible components, such as superconductive magnets, from the high-energy neutrons produced in the plasma chamber.

In the DEMO development, it has been recognized that self-sufficient fuel cycle is necessary due to the high difficulty of tritium storage and providing the self-sustainability of the reactor. The tritium production is based on fission reactions, in particular between the absorption of the neutrons, produced in the plasma, by the lithium. It is possible to exploit the reactions with the following relations:

$$n^0 + Li_3^6 \rightarrow He_2^4 + T_1^3 + 4.8\ MeV$$

$$n^0 + Li_3^7 \rightarrow He_2^4 + T_1^3 + n^0 - 2.5\ MeV$$

The candidate concepts for the EU DEMO BB under development are: Water-Cooled Lithium-Lead (WCLL) Helium-Cooled Pebble Bed (HCPB), Helium-Cooled Lithium Lead (HCLL) and Dual-Coolant Lithium Lead (DCLL) [7]. A brief review of all design is reported below.

WCLL The WCLL design is composed by two regions: the Outboard Blanket (OB) and the Inboard Blanket (IB), composed adopting the Single Module Segment (SMS) approach [8]. The current design is based on pressurized water as coolant, liquid eutectic lithium-lead (PbLi) as breeder and neutron multiplier and EUROFER 97 as structural material.

HCPB The current HCPB design is built adopting the Multi Module Segmentation (MMS) that divides the BB into seven OB and seven IB modules [9]. The modules are composed by radial-toroidal Cooling Plates (CP) in which the coolant flows and, in-between them, alternate pebble beds of Li_4SiO_4 compound and Be are used as breeder and multiplier. The EUROFER 97 is chosen as structural material and helium is used as gas coolant at 80 bar and inlet/outlet temperatures of 300/500 °C. The tritium produced by pebbled

beds is extracted by an independent low pressure gas flow. Layout and details of the HCPB design are represented is Figure 1.3.

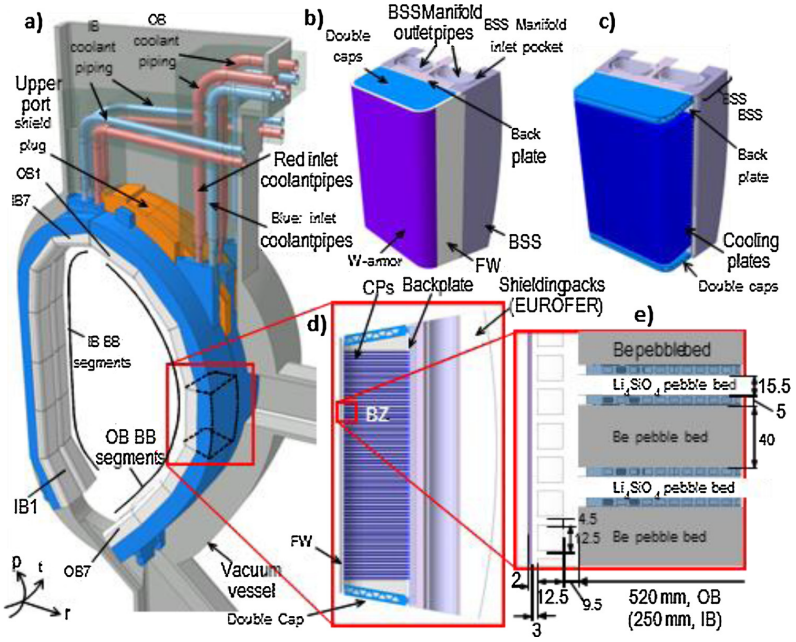

Figure 1.3: HCPB: a) HCPB DEMO sector; b), c) 3D views of a module; d) section cut of a module; e) detail of the breeder zone. Coordinate axis: p=poloidal, t=toroidal, r=radial [7].

HCLL The HCLL design adopts three alternative options: Optimized-Conservative, Advanced, and Advanced-Plus [10]. The structural material is EUROFER 97, while the helium gas is used as coolant with inlet/outlet temperature of 300/500 °C and 80 bar and the eutectic Pb–15.7Li enriched at 90% in ^{6}Li as breeder, multiplier and tritium carrier. A representation of the HCLL layout is given if Figure 1.4.

DCLL The DCLL design is composed by modules in which the breeding zone is composed by several PbLi circuits, separated by radial stiffeners, where the liquid metal flows in parallel mainly in poloidal direction [11, 12]. The DCLL is based on the use of PbLi as breeder, main coolant, neutron multiplier and tritium carrier, while helium at 80 bar is used to cool specific parts of the EUROFER structure, mainly the FW. A representation of the DCLL module is given in Figure 1.5.

The Water-Cooled Lithium-Lead (WCLL) concept has been adopted for the purpose of this work. It is one of the candidate design for the EU DEMO fusion reactor and it is in a pre-conceptual phase. The current design is based on pressurized water as coolant, liquid eutectic lithium-lead (PbLi) as breeder and neutron multiplier and EUROFER as structural material. The WCLL design is divided into two regions: the outboard blanket (OB), located on the external side of the VV, and the inboard blanket (IB), located closed

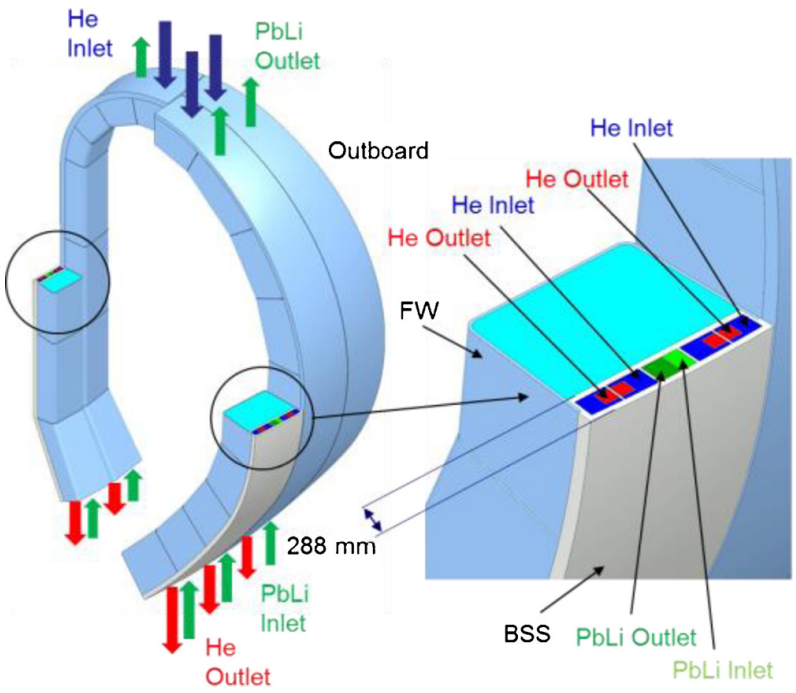

Figure 1.4: Layout of the HCLL. Left: general layout. Right: section of a module [7].

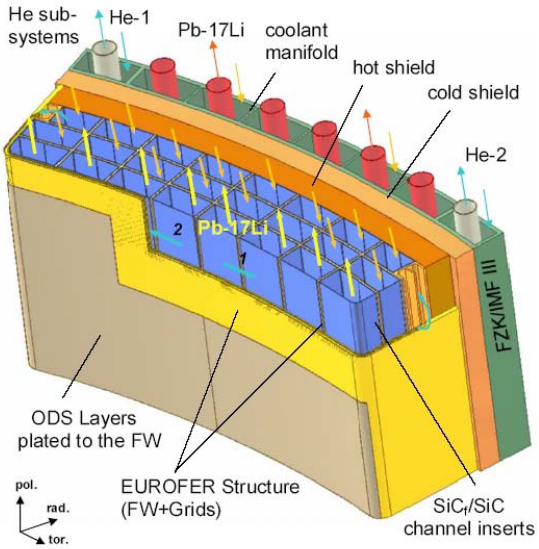

Figure 1.5: DCLL module internal structure [13].

to the CS. The general layout is presented is Figure 1.6. The WCLL BB relies on the Single Module Segment (SMS) approach, which consists on the repetition of the breeding element

along the poloidal direction constituting a large continuous segment [8]. This segment is attached with the VV through the Back Supporting Structure (BSS) and it is strengthened by a complex internal structure composed by stiffening plates. In Figure 1.7 there is a representation of these elements. The poloidal-radial stiffening plates are five vertical plates that run along the entire length of the BB segment; the toroidal-radial stiffening plates are horizontal elements repeated along the BB segment.

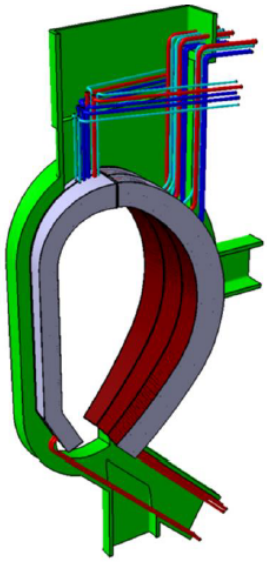

Figure 1.6: The EU DEMO WCLL general layout. Grey: manifold and breeding zone, red: first wall, green: vacuum vessel [14].

Another important component is the FW. The FW is integrated in the BB, generally covered by a thin tungsten layer; it is the surface of the blanket facing the plasma chamber [8].

As mentioned above, the WCLL BB achieves its power extraction and breeding functions trough two independent hydraulic loops of pressurized water and liquid PbLi respectively. The cooling system is employed for the refrigeration of both the first wall and the breeder, else the breeding system is employed for the tritium production. In this work the breeding system is considered, a brief description of which is reported in Section 2.1.

1.2 The GETTHEM Code

The General Tokamak Thermal-hydraulic Model (GETTHEM) is a system-level dynamic thermal-hydraulic code developed at Politecnico di Torino (NEMO group - Dipartimento Energia) for the modelling of the PHTS and Balance of Plant (BoP) of tokamak fusion reactors, in particular for the EU DEMO reactor under development by the EUROfusion

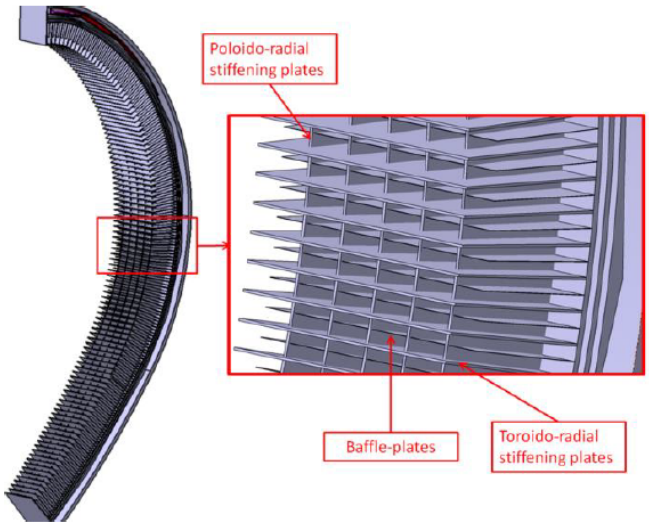

Figure 1.7: EU DEMO WCLL internal structural elements [14].

Consortium [15].

The code is developed to analyse the thermal-hydraulic transients in the entire PHTS based on the modelling of the BB cooling loops. Within the design candidates for the EU DEMO reactor, the concept designs under investigation in this code are the Helium-Cooled Pebble Bed and the WCLL. The code is based on a system-level modelling using the equation-based and object-oriented Modelica language [16, 17, 18, 19]. The Modelica language has been chosen for this code for its user-friendliness, its dynamic nature and its ease of code development through a modular structure that permits to easily update the system model as the design evolves.

The aim of this code is to have a fast and easy tool to analyse the transient behaviours of the all components relevant for the power generation of the fusion reactor and the contribution of several parameters. To answer to this aim, the different components are modelled solving the mass, momentum and energy conservation equations with a 0D approach for manifolds, pumps and valves, and 1D approach for cooling channels and pipes using the Finite Volumes (FV) method. The code can be applicable to nominal and accidental scenario using proper assumptions and simplifications. In general, the WCLL GETTHEM model is developed modelling two uncoupled models for the FW-PHTS and BZ-PHTS in which only the coolant thermal-hydraulic system is considered, i.e. the breeder is not modelled. A general scheme of the GETTHEM model is represented in Figure 1.8.

After the development, the code has been subjected to a benchmark and validation phase. For this purpose, the code has been benchmarked both in normal-operational scenario against a 3D Computational fluid dynamics (CFD) for the case of the HCPB [21] and WCLL, and in accidental scenario with the CONSEN code in the case of the HCPB [22] and experimental data from the ICE campaign. After the benchmark, the code has been

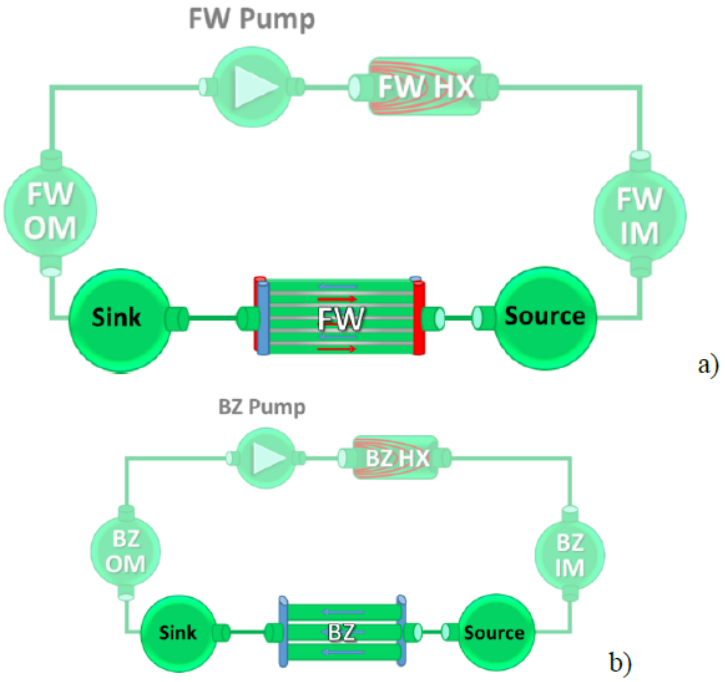

Figure 1.8: A general GETTHEM model scheme of the EU DEMO WCLL cooling system. FW PHTS (a) and BZ PHTS (b). The ex-vessel components are greyed-out. [20].

used to different EU DEMO analyses. At first, an optimization of the coolant mass flow rate distribution analysis has been done for the HCPB case [20, 23]. As further application, the code has been used also to analyse the hot-spot temperature in the EUROFER for the HCPB case, in which the EUROFER structure in some points overcomes the temperature limit (500 °C) [24], and WCLL case, in which the temperature of the EUROFER is below the threshold value [25, 26]. Moreover, the accidental scenarios, such as in-VV LOCA, for the HCPB and WCLL have been analysed [27].

1.3 Aim of the thesis

As mentioned above, the WCLL BB is in a pre-conceptual phase and it important to analyse with numerical methods the several reactor systems from different points of view. A thermal-mechanics and thermal-hydraulic analysis is necessary to understand the behaviour of the system during the normal operation and observe the dynamics of some fundamental parameters in case of accidental scenario, providing that they do not exceed the functional design limits. Another important analysis that must be done is the neutronics, to study the contribution of the neutrons absorption, the tritium breeding ratio (TBR) and the power generation inside the BB. The GETTHEM code has been developed with this purpose (see Section 1.2), in particular to analyse the thermal-hydraulic behaviour of the coolant system for the HCPB and WCLL reactor configurations. For the latter,

there is another complication due to the presence of liquid breeder inside the BB, and so a system-level modelling of the PbLi loop is needed.

In the WCLL design, an accurate estimate of the magnetohydrodynamics (MHD) pressure drop is mandatory to properly analyse the PbLi flow. For this purpose, some models have been developed to characterize the MHD losses inside the main WCLL components, in particular for the "in-magnet" sections of the PbLi loop [28, 29]. These models estimate the MHD pressure drops in four BB components (feeding pipe, manifold, breeding zone and draining pipe) singularly and independently modelled and the overall pressure drop is simply the sum of all losses, considering the four components in series. In this way, it is given a general overview of the MHD pressure drops, necessary to evaluate the pressure critical points of the WCLL design, but it is not given a complete description of the PbLi loop that takes into account all main components modelled together and the different breeding zone cells positions. A complete model for the PbLi loop allows also to characterize the breeder mass flow rate distribution for different operations and design configurations.

The aim of this work is the development of a 1D model for the PbLi loop to characterize the pressure losses inside the BB region during a normal operation of the reactor. For this purpose, the Modelica language is used. These losses, both for OB and IB case, must be lower then a threshold value corresponding to the maximum estimated value of a pump prevalence necessary to the PbLi circulation inside the BB ($\approx \quad 2MPa$). As starting point, there is a description of the WCLL configuration and the PbLi loops, with also a particular attention to the breeder fundamental properties (see Appendix A). Then, the MHD correlations for pressure drops are reported, providing a precise description of various types of pressure losses within the BB. After that, all of these kinds of losses have been implemented with the Modelica language and then validated by comparison with experimental results or literature data. Subsequently, all the main components, both for OB and IB loops, are modelled singularly and validated, keeping in mind all together the pressure losses studied before, and finally, the complete model of OB and IB loops have been implemented, at first without considering the hydrostatic head of the PbLi and then including the hydrostatic head. As final analysis, two possible transients have been studied. At the end of this work, conclusions are reported and some perspectives are indicated for further analysis that can be carried out in the future.

Chapter 2

The EU DEMO Water-Cooled Lithium-Lead Breeding Blanket

2.1 PbLi loop

The WCLL BB PbLi loop is divided into two independent branches: the OB and the IB loop. The WCLL PbLi loop system is represented in Figure 2.5. Each loop is made by four main components:

- **Feeding pipe (FP)**: The FP is a connection pipe between the PbLi ex-vessel loop and the BB, it is usually placed in the lower part of the VV. Its function is to load the liquid metal into the breeding blanket, exactly to the manifold region through a particular collector.
- **Manifold (M)**: The manifold is a long components that constitutes the major part of the blanket segment. It is composed of six rectangular parallel channels that run along the segment from the bottom to the top region of the BB (see Figure 2.1). Each channel is composed by two co-axial channels, the external one (*annular channel*) and the internal one (*internal channel*) (see Figure 2.2). Its function is to distribute and collect the PbLi inside the BB, in particular the annular channel brings the liquid metal to the breeding zone (BZ) and the internal channel receives the PbLi from the breeding zone.
- **BZ cell**: The BZ cell is an horizontal component that constitutes the bulk of the blanket. The elementary cell is composed by six rectangular parallel channels divided by poloidal-radial stiffening plates and connected in correspondence of the six manifold channels (see Figure 2.3). The entire BB is composed by a repetition of elementary cells along the segment, separated by toroidal-radial stiffening plates, and linked to the manifold. Each channel is constituted by a lower and upper radial channel separated by a baffle-plate and connected by a U bend (see Figure 2.4). The PbLi radial flow enters into the lower channel going towards the plasma chamber,

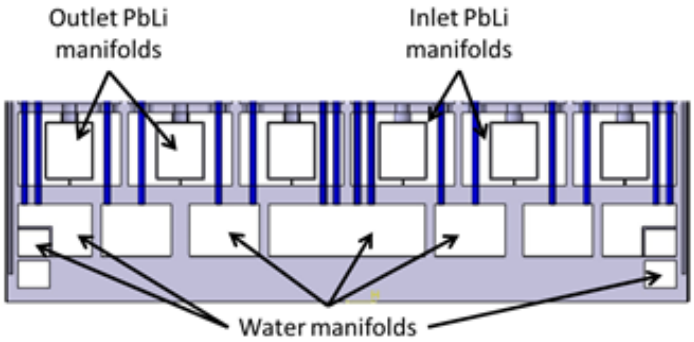

Figure 2.1: OB manifold section: toroidal-radial view [30].

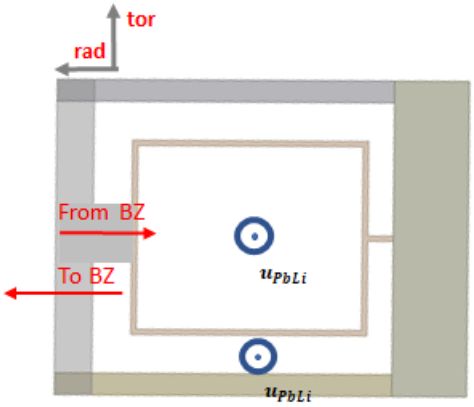

Figure 2.2: OB manifold co-axial channels: radial-toroidal view (adapted from [31]).

passes through the U turn, and goes backwards inside the upper channel exiting the BZ cell. Moreover, the liquid metal encounters the water pipes (cooling pipes) that cross the BZ cell in the perpendicular direction respect to the PbLi flow. The BZ cell is the most important region of the BB, because heat exchange occurs between the coolant (water) and breeder (PbLi) regarding the thermal power production, and neutrons-lithium reactions happen regarding the tritium production.

- **Draining pipe (DP)**: The DP is a straight connection pipe that connects the BB with the ex-vessel PbLi loop. It is usually placed in the upper region of the blanket. As the FP, the DP is connected with the manifold with a particular collector. Its function is to remove the liquid metal from the BB and bring it to the external loop.

These components are considered in this work for the system-level modelling of the PbLi loop. In the following sections, there is a more detailed description of each component regarding the OB and IB loop. For the FP and DP, the geometry dimensions are based on a conventional parameter indicated by a nominal diameter (DN). For each DN there is the corresponding inner diameter (d_i), the outer diameter (d_o) and wall thickness (t_w). Regarding the manifold and BZ, they have specific geometry dimensions for the OB and IB case. The pipe dimensions are reported in Table 2.1 [30].

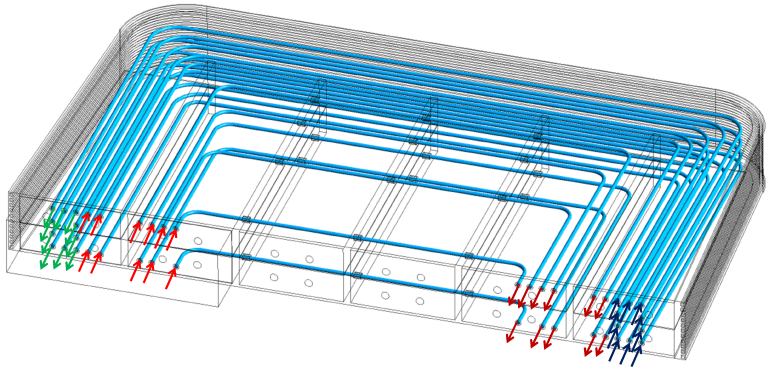

Figure 2.3: BZ elementary cell. Cooling pipes are highlighted [14].

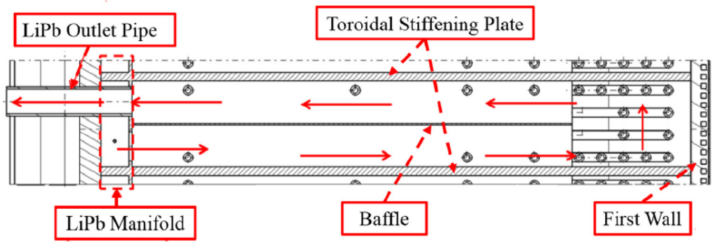

Figure 2.4: BZ channel section: radial-polidal view. The left side (LiPb Outlet Pipe and LiPb Manifold) is not considered in this work [32].

2.1.1 Outboard blanket (OB)

The OB loop is located in the outer side of the VV, in correspondence with the external curvature of the "D shape" of the VV. It is composed by the OB FP, OB manifold, OB BZ and OB DP, as shown in Figure 2.5.

OB Feeding pipe The OB FP is a straight electro-conductive pipe situated at the bottom region of the BB. Its design scheme is based on the 2018 DEMO WCLL configuration. It is routed from the PbLi loop through the VV lower port and into the blanket segment, where it feeds the manifold. The geometry parameters refers to DN200 (see Table 2.1). It is composed by three straight section, two obliques and one vertical, connected by a 100° and a 120° bend. The major part of the OB FP is located outside of the TFC, except for the last section that crosses the TFC and is linked to the OB manifold with a collector. A representation is given in the lower part in Figure 2.5.

OB manifold A representation of the OB manifold is in Figure 2.1. For the OB FP, the design scheme of the OB manifold refers to the 2018 DEMO WCLL design. Regarding the PbLi loop, the OB manifold is composed by six parallel channels that run along the BB

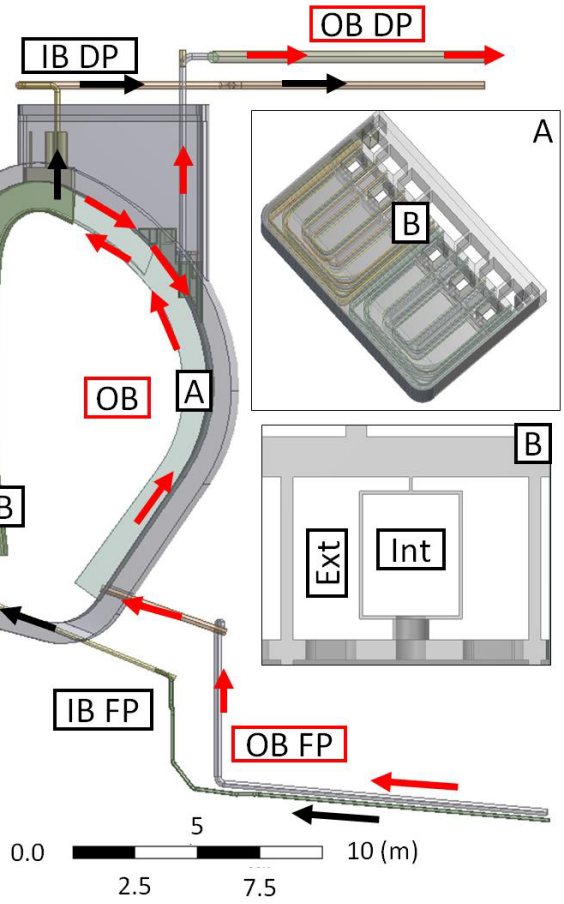

Figure 2.5: The WCLL OB/IB PbLi loop system. The OB and IB loops are highlighted by red and black arrows respectively. In the picture: detail of the OB BZ/manifold (A) and the co-axial manifold channels (B) [30].

Nominal diameter	Outer diameter	Inner diameter	Wall thickness
80	88.9	78.9	5
100	114.3	101.7	6.3
125	139.7	123.7	8
150	168.3	148.3	10
200	219.1	194.1	12.5
250	273	241	16
300	323.9	288.9	17.5
350	365	346	19

Table 2.1: FP and DP dimensions for the corresponding DN. Values expressed in mm. The DN350 case is obtained by extrapolation due to lack of data [30].

segment. Each channel is subdivided into two co-axial channels, the annular channel that distributes the liquid metal to the BZ and the internal channel that collects the PbLi from the BZ. The PbLi flow enters the BZ through a rectangular orifice and goes out from the BZ through a circular orifice. A detail of the two co-axial channels is reported in Figure 2.2. The cooling pipes cross the annular channels to bring the coolant into the water manifold, located near the PbLi manifolds. In this work the coolant manifold is not considered.

OB Breeding zone In this work, the OB BZ layout in based on the TO1.A configuration of the 2016 DEMO WCLL design. The TO1.A configuration is represented in Figure 2.3. In this configuration, the BZ in formed by an elementary cell that covers the blanket segment toroidal width and is divided into six parallel channels. The PbLi flows radially in the channels, at first going towards the FW and then going backward. It is linked with the manifold co-axial channels with a rectangular and circular orifice. In Figure 2.4, the PbLi flow is highlighted.

OB Draining Pipe The OB DP is a straight electro-conductive pipe situated in the upper region of the BB. As the OB FP, the DP is based on the 2018 DEMO WCLL configuration. It is attached to the BB at around two-third of the poloidal height through a collector that runs along the blanket segment. It is composed by a vertical and horizontal section, connected by a 90° bend, which brings the PbLi from the blanket to the ex-vessel loop crossing the VV upper port. A schematic representation is given in the upper part in Figure 2.5. The two sections have different geometry parameters: DN200 for the vertical one and DN350 for the horizontal one (see Table 2.1). As for the OB FP, the major part of the OB DP is located outside of the TFC, except for the collector and a small piece of the vertical pipe.

2.1.2 Inboard blanket (IB)

The IB loop is located in the inner part of the reactor, close the CS, and it si principally straight except for the terminal part of the segment which is bent. It is composed by IB FP, IB manifold, IB BZ and IB DP, as shown in Figure 2.5.

IB Feeding pipe The IB FP, as the OB one, is a straight electro-conductive pipe situated in the lower part of the BB. Its design scheme is based on the 2018 DEMO WCLL configuration. It enters from the VV lower port and feeds the PbLi into the IB manifold. The geometry parameter refers to DN125 (see Table 2.1). Unlike the OB FP, the IB FP has a more complex structure. It is composed at first by a horizontal section followed by two 45° bends; then, there are a vertical and a oblique section connected by a 135° bend; the latter section enters through the TFC and ends with a 45° curvature. The IB FP scheme is represented in the lower part in Figure 2.5.

IB manifold The design scheme of the IB manifold refers to the 2018 DEMO WCLL design. As the OB manifold, the IB manifold is composed by six co-axial channels, in turn subdivided in the annular channel that distributes the PbLi to the BZ and the internal channel that collects the liquid metal from the BZ. The layout of the IB manifold is

represented in Figure 2.6. The IB manifold, unlike the OB, has a shrinkage of the BSS and a smaller cross section for the water manifolds. A detailed representation of the co-axial channels is shown in Figure 2.7.

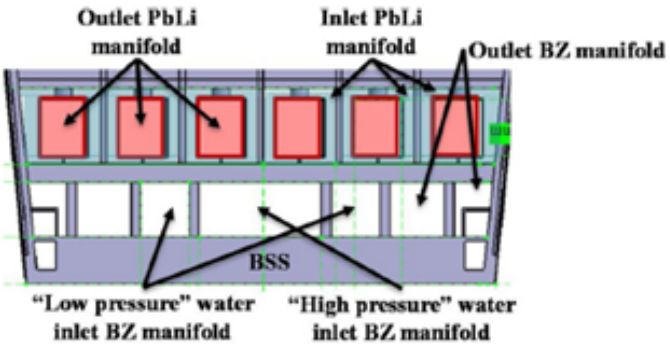

Figure 2.6: IB manifold section: toroidal-radial view [8].

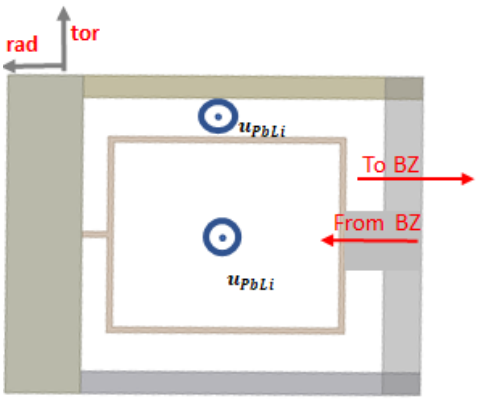

Figure 2.7: IB manifold co-axial channels: radial-toroidal view (adapted from [31]).

IB Breeding zone In general, the IB BZ has a different design respect to the OB BZ. The IB BZ should have a small shrinkage in the inlet/exit region, in correspondence of the manifold attachment. Despite this geometry difference, in this work, for simplicity and lack of information, the IB BZ has the same configuration as that of the OB BZ (TO1.A 2016 DEMO WCLL configuration).

IB Draining pipe The IB DP, as the OB case, is a straight electro-conductive pipe situated in the top region of the BB. Its layout is based on the 2018 DEMO WCLL configuration. Unlike the OB DP, the IB DP is linked directly to the upper region of the manifold and not with a long collector. It has a very simple scheme, starting with a vertical pipe (DN150) which has a small piece inside of the TFC and then a horizontal pipe (DN200), both connected by a 90° bend. For the geometry parameters see Table 2.1. A representation is shown in the upper part in Figure 2.5.

2.2 EU DEMO WCLL magnetic field profile

The plasma confinement in the EU DEMO reactor is based on a complex system of magnetic fields, generated by the CS, TFCs and PFCs. The resultant magnetic field has a helical shape that runs along the torus, composed by two main components: the toroidal magnetic field (B_{tor}) and the poloidal magnetic field (B_{pol}). There is also the vertical magnetic field (B_{ver}) that is generated by the PFCs providing the plasma stability, but in this work this component is not considered.

For this purpose, a quasi-toroidal coordinate system is used to indicate the magnetic field directions, in which the coordinates origin is placed on the plasma torus centre. The blanket coordinates scheme is presented in Figure 2.8. In this framework, we define a toroidal (ϕ), a vertical (Z) and a radial (R) direction. A second coordinate system is employed with its origin placed in the torus cross-section centre. In this new coordinates system, the toroidal direction is the same of the previous case; the radial (r) direction is now defined with the torus cross-section centre; the polidal (θ) direction that defines the position with respect to the torus horizontal plane. The difference between the R and r is that the first refers to the global reactor (torus geometry), the latter to a local region (plasma geometry).

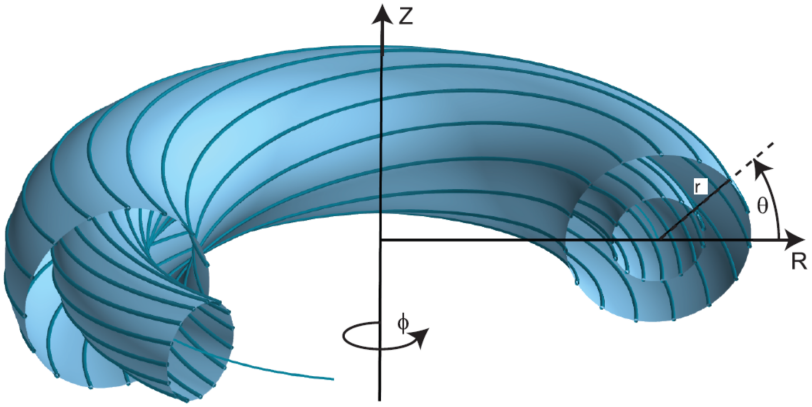

Figure 2.8: Blanket coordinate system [33].

In DEMO, the toroidal magnetic field is the highest one ($B_{tor} >> B_{pol}$) and its intensity is inversely proportional to the R-direction (B(R)). The toroidal magnetic field behaviour is described by the relation [30]:

$$B_{tor}(R) = \frac{R_0 \cdot B_0}{R} \tag{2.1}$$

where $R_0 = 8.9316$, $B_0 = 4.8935$ and R is the radial (torus) direction. This relation is only valid for the toroidal magnetic field in the region inside the TFCs, while outside it is null and the reference magnetic field is the poloidal one. For calculations, B_{tor} is used for the components that are inside the TFCs, such as the manifold and the BZ cells, while B_{pol} for the collectors, FPs and DPs. Table 2.2 collects an overview of the poloidal magnetic

field values. In general, the poloidal magnetic field decreases in the R-direction, i.e. it is higher near the TFCs while it is lower far from the TFCs.

Component	Inboard	Outboard
Feeding Pipe	0.53÷1.41	0.53÷2.96
Bottom collector	0.56	0.80
Top collector	0.41	0.42
Draining Pipe	0.29÷1.26	0.33÷0.8

Table 2.2: Poloidal magnetic field values. The values are expressed in T [30].

The region in which the toroidal magnetic field is considered is represented in Figure 2.9. The two lines represent the limiting surfaces of the blanket depending on the vertical and radial direction. In Figure 2.10, the toroidal magnetic field behaviour as a function of the R-direction is represented, according the relation 2.1, while a representation of the B_{tor} in the WCLL is represented in Figure 2.11.

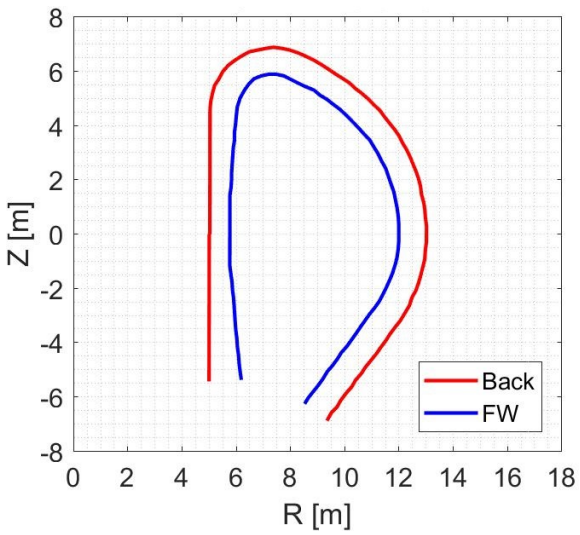

Figure 2.9: EU DEMO WCLL BB limiting surfaces (reproduced from [33]).

Instead, regarding the Z-direction dependence, the toroidal magnetic field intensity and behaviour changes for the OB and IB segment. The plot of the toroidal field on the BB surfaces is represented in Figure 2.12. Depending on the position, the magnetic field varies its intensity and behaviour in the OB and IB segment. In the OB segment, represented in Figure 2.12a, the magnetic field has a shape similar to a parabola, in which the minimum intensity is reached in the equatorial plane of the blanket ($Z = 0$), while the maximum is located in the top of the BB, in correspondence of the interface between the OB and IB segments. For the IB segment, represented in Figure 2.12b, the magnetic field has a different behaviour: it is almost constant in a large portion of the segment, in which its intensity is the highest, while it decreases in the top of the blanket, in correspondence of

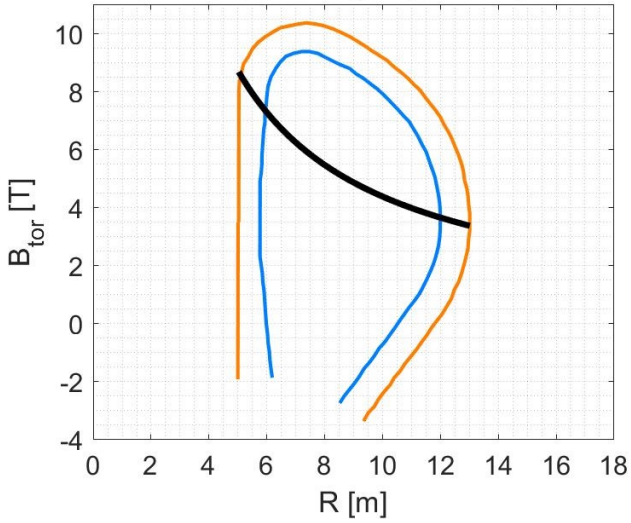

Figure 2.10: Toroidal magnetic field in function of radial direction during the magnets nominal operation. The orange and light blue line represent respectively the back of the BB and FW; the black line represents the toroidal magnetic field.

the curvature near the interface between the OB and IB segments. In general, the magnetic field intensity for the IB segment is higher then the OB case.

Regarding the poloidal magnetic field, it is commonly composed by a radial (B_r) and a vertical (B_Z) component. It is generated by the interaction of the PFCs and CS. A framework of the radial and vertical component is shown in Figure 2.13.

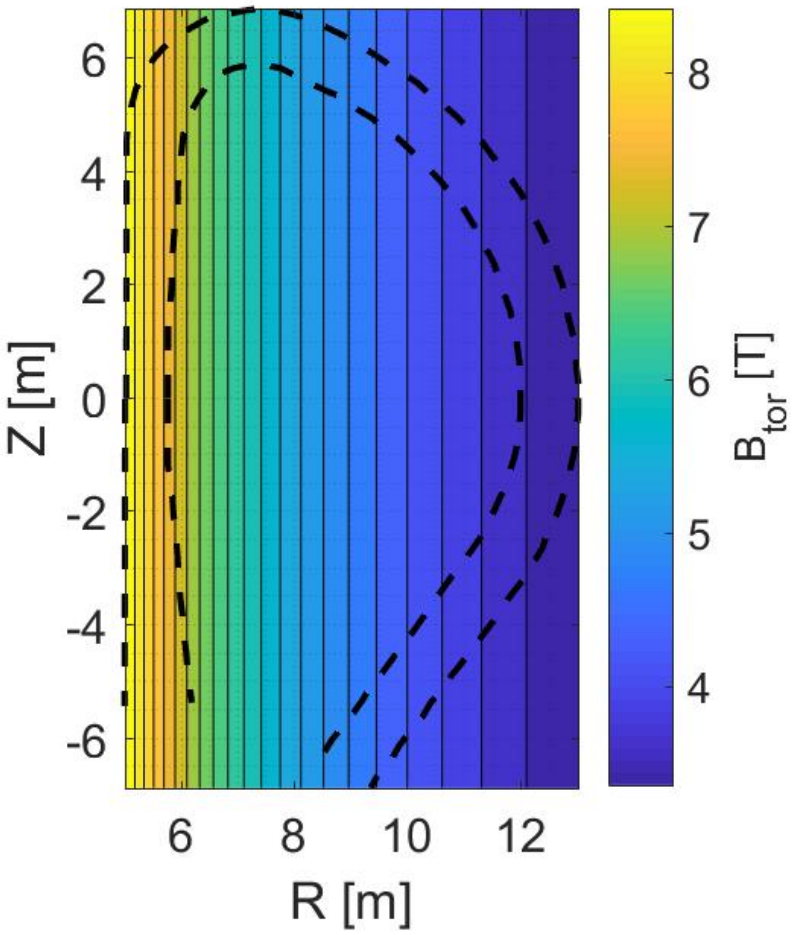

Figure 2.11: Representation of the toroidal magnetic field in the EU DEMO WCLL during the magnets nominal operation. The dashed lines represent the BB profile.

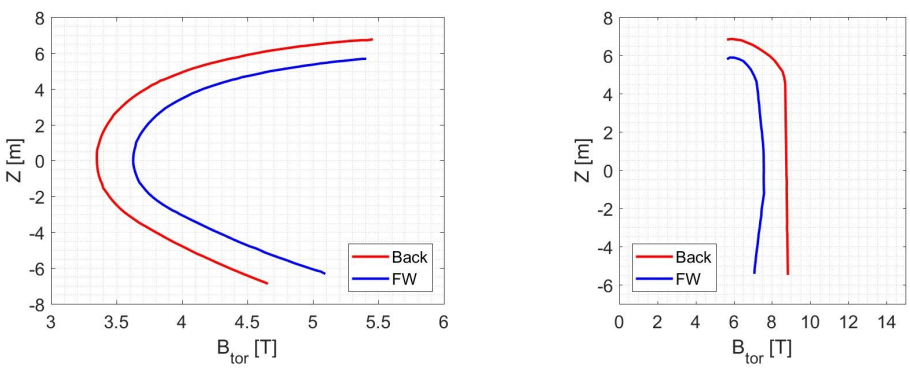

(a) OB magnetic field (b) IB magnetic field

Figure 2.12: EU DEMO WCLL toroidal magnetic field versus the vertical Z-direction during the magnets nominal operation. (a) OB segment, (b) IB segment.

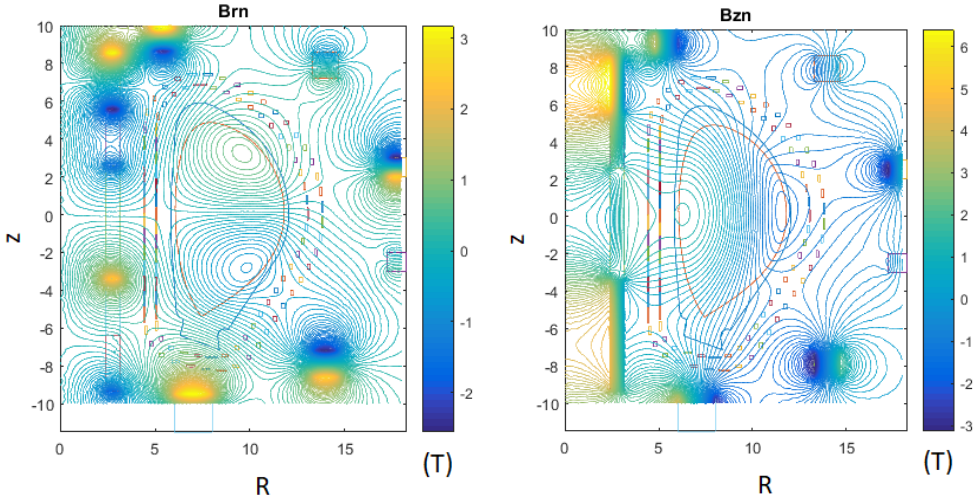

(a) Radial magnetic field component (b) Vertical magnetic field component

Figure 2.13: EU DEMO WCLL radial and vertical components of poloidal magnetic field during the magnets nominal operation. The magnetic field intensity is expressed in T [34].

Chapter 3

Fundamentals of magnetohydrodynamics pressure drop

3.1 Introduction

One of the issue that must be addressed for the WCLL design is interaction of the PbLi and the magnetic field employed for the plasma confinement. In general, the motion and the evolution of an electro-conductive fluids, such as liquid metals, molten salts and ionized gases, in presence of a magnetic field, result to be different respect to the normal fluid-dynamics behaviour. This phenomenon, called magnetohydrodynamics (MHD), modifies the features of the fluid flow in a totally different way than the normal fluid-dynamics, in this work called ordinary hydrodynamics (OHD). For this purpose, the MHD flow requires the combination of the Navier-Stokes and Maxwell equations to represent the interaction between the electro-conductive fluid and the applied magnetic field, deriving a set of physical laws. Moreover, for the aim of this work, the MHD effects determine additional pressure losses inside the hydraulic loop that are estimated with specific correlations. In this chapter, a general overview of the MHD is treated, in particular regarding the most important dimensionless numbers that characterize this phenomenon and the pressure drop correlations needed for the model implementation.

3.2 Methodology

The liquid PbLi, used as breeder-multiplier in DEMO WCLL design, has a relatively large electrical conductivity and its flow regime is strongly susceptible to magnetic field, inducing the onset of the MHD flow. The Navier-Stokes equations, that describe a linear viscous fluid, must be modified to represent the interaction with a magnetic field including the Maxwell equations. A detailed description of the methodology to derive a comprehensive and self-consistent set of physical laws for this purpose, with appropriate hypotheses and simplifications, can be found in Ref. [35], while a detailed discussion of MHD for liquid

metals can be found in Ref. [36]. In this work, just the generic and most important information is shown.

For a steady, isothermal and incompressible fluid [32], the continuity and momentum equations can be written as

$$\nabla \cdot \vec{v} = 0 \tag{3.1}$$

$$(\vec{v} \cdot \nabla)\vec{v} = -\frac{1}{\rho}\nabla p + \nu\nabla^2\vec{v} + \frac{1}{\rho}\vec{j} \times \vec{B} + \vec{S_m} \tag{3.2}$$

where $\vec{v}$ represents the fluid velocity, ρ the fluid density, p the pressure, ν the fluid kinematic viscosity, $\vec{j}$ the electric current density and $\vec{B}$ the magnetic field. The third term on the right side of Eq. 3.2 represents the Lorentz force and the fourth a momentum source, e.g. due to the buoyancy forces. The electric current density $\vec{j}$ can be obtained by the Ohm's law and the charge conservation equations

$$\vec{j} = -\nabla\phi + \vec{v} \times \vec{B} \tag{3.3}$$

$$\nabla \cdot \vec{j} = 0 \tag{3.4}$$

where ϕ is the electric potential. Combining the equations 3.3 and 3.4, the Poisson equation is found

$$\nabla^2\phi = \nabla \cdot (\vec{v} \times \vec{B}) \tag{3.5}$$

which provides the electric potential distribution and, through the Eq. 3.3, the current density one.

3.2.1 Dimensionless numbers

The MHD phenomenon can be characterized by several dimensionless numbers. The most important is the Hartmann number (Ha), that represents the ratio between the electromagnetic and viscous forces. It can be expressed with the relation

$$Ha = BL_{ch}\sqrt{\frac{\sigma}{\rho\nu}} \tag{3.6}$$

where B is the magnetic field, σ the fluid electric conductivity, ρ the fluid density, ν the fluid kinematic viscosity and L_{ch} the characteristic length, that represents the half-width of the duct in the magnetic field direction. The Hartmann number is very important because it indicates when the electromagnetic forces prevail over the viscous ones and the transition to the MHD flow regime. Another important dimensionless number, used principally for calculations, is the interaction parameter (N). It is expressed as

$$N = \frac{\sigma L_{ch} B^2}{\rho u_0} \tag{3.7}$$

where u_0 is the fluid mean velocity. Usually, it can be expressed more simply as

$$N = \frac{Ha^2}{Re} \tag{3.8}$$

i.e. the ratio between the square of the Hartmann number and the Reynolds number (Re), and in this from it can be seen as the ratio between the electromagnetic and inertial forces. Finally, another important parameter that influences the flow regime is the wall conductance ratio (c). Is is expressed as

$$c = \frac{\sigma_w t_w}{\sigma L_{ch}} \tag{3.9}$$

where σ_w is the wall electrical conductivity and t_w is the wall thickness. This parameter is the ratio between the wall and fluid electrical conductances and represents the influence of the channel wall conductivity on the flow features. Conductive walls lead to higher Lorentz forces and slower resistance of the current path compared with a channel with insulating walls.

The transition to the MHD flow regime is governed by the Hartmann number and the wall conductance ratio. Regarding the flow pattern, in the OHD regime, the hydrodynamic velocity profile has a quasi-parabolic shape, represented in Figure 3.1. When the Hartmann number has a high value ($Ha \gg 1$), the onset of the MHD flow regime appears and the velocity profile undergoes some changes. The new profile has a rearrangement on the cross-section with the appearance of a central region, called *core*, in which there is the balancing between the Lorentz force and the driving pressure gradient, and two boundary layers closed to the duct walls. The walls perpendicular to the magnetic field are called *Hartmann walls*, conversely, the walls parallel to the magnetic field are called *side walls*. Their scales are expressed with the relation $\delta_{Ha} \propto \frac{1}{Ha}$ for the Hartmann walls and $\delta_s \propto \frac{1}{\sqrt{Ha}}$ for side walls. The peculiarities of this profile are the appearance of velocity jets in the layers attached to the side walls, in which the velocity reaches the maximum value, and a valley region in the centre of the duct in which the velocity decreases and has a constant value. A representation of the MHD velocity profile is shown in Figure 3.2. In Figure 3.2a velocity profile for poorly conducting walls ($c = 0.01$) are shown. For low magnetic field, i.e low Ha, the profile has a quasi-hydrodynamic shape (red line), but increasing Ha small velocity jets appear near the side walls and the core region starts to form. For highly conducting walls ($c = 0.1$) (Figure 3.2b), the same behaviour appears but the velocity jets are promoted and the core region is most pronounced, especially for higher Ha values (red line).

3.3 Pressure drop correlations

Another key aspect that must been analysed in the MHD case is the evaluation of the pressure drop in a generic hydraulic loop. As said in Section 3.2.1, the onset of the MHD flow regime determines an adding driving pressure due to the Lorentz forces induced by the presence of the magnetic field. For this reason, an new pressure drops analysis to consider the presence of these effects and an appropriate formulation of correlations are needed.

In general, for an electrical-conductive fluid under a magnetic field, such as the PbLi for the purpose of this work, the overall pressure drop can be expressed as the sum of the OHD and MHD pressure drops [37], with the relation

$$\Delta p = \Delta p_{OHD} + \Delta p_{MHD} \tag{3.10}$$

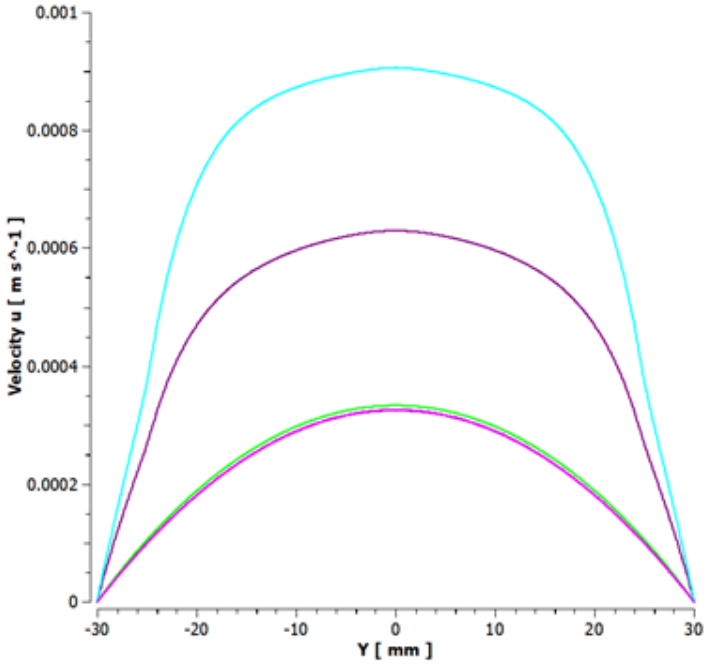

Figure 3.1: Velocity profiles for the OHD flow regime. From the innermost to the outermost (cyan): ratio between the duct length and diameter (L/d = (24; 7.2; 2.6; 1.2)) [37].

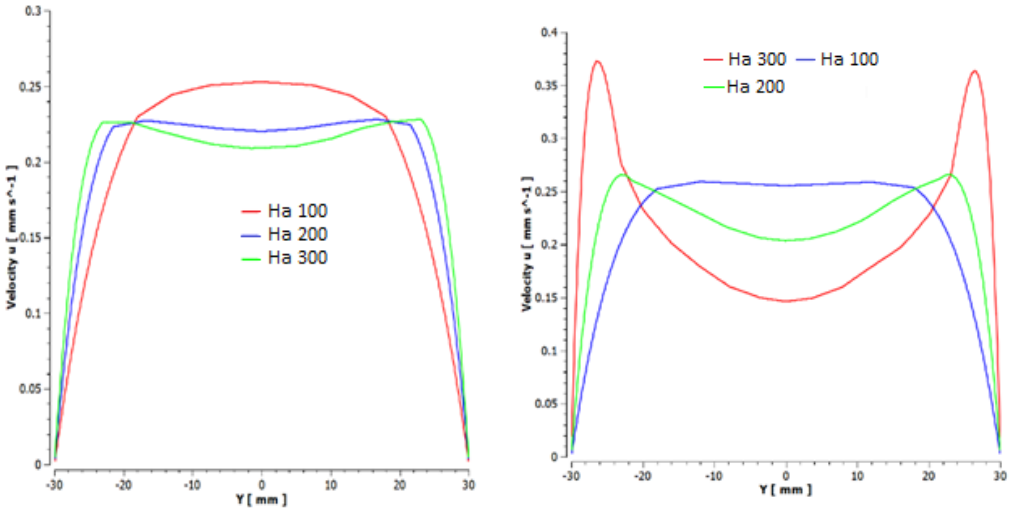

(a) (b)

Figure 3.2: Channel velocity profiles in MHD flow regime for increasing Ha: (a) velocity profiles with poorly conducting walls ($c = 0.01$), (b) velocity profiles with highly conducting walls ($c = 0.1$) [37].

But, if $Ha \gg 1$, i.e. the effects of the electro-magnetic forces prevail over the viscous ones, there is the onset of the MHD flow regime and the pressure losses are caused principally by Lorentz forces. Then, the OHD pressure drops can be neglected and the overall pressure drop is due only to the MHD losses (see Appendix B):

$$\Delta p \approx \Delta p_{MHD} \tag{3.11}$$

Then, the overall pressure drop can be split into two components:

$$\Delta p \approx \Delta p_{MHD} = \Delta p_{2D} + \Delta p_{3D} \tag{3.12}$$

The Δp_{2D} are pressure losses due to resistive Lorentz forces generated by induced currents confined in the straight channel cross-section (for this reason called 2D) and they are the analogous of the distributed hydrodynamics losses. Else, the Δp_{3D} are pressure drops due to additional Lorentz forces that are non-aligned with the stream-wise direction. In this case, a non-null velocity gradient appears along the duct axis in presence of obstacles or channel variations, and an induced electric potential difference appears driving 3D currents that will be no longer confined to the channel cross-section. Conversely, they are the analogous of the concentrated hydrodynamics losses. A representation of the induced currents for 2D and 3D losses are shown in Figure 3.3.

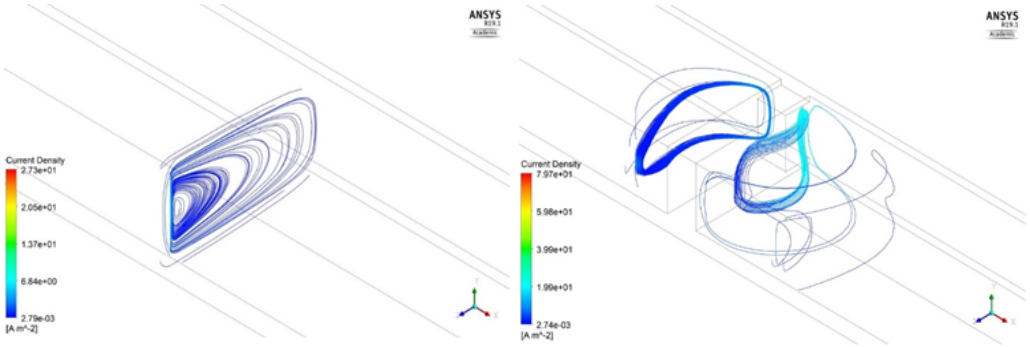

(a) (b)

Figure 3.3: Induced currents for a) 2D fully developed flow in the duct and b) 3D flow in the orifice region [37].

3.3.1 Distributed losses (2D)

In the WCLL blanket, the PbLi loop is composed principally by straight electro-conductive ducts, usually with a constant cross-section, and the distributed losses (2D pressure drops) are associated to these kind of channels. Assuming a high magnetic field intensity, uniform and uni-directional, the 2D pressure drops correlation [38] is the following

$$\Delta p_{2D} = k_p \sigma u_0 B^2 L \tag{3.13}$$

where k_p is the 2D pressure loss coefficient, σ is the PbLi electrical conductivity, u_0 is the liquid main velocity, B is the applied magnetic field perpendicular to the fluid flow and L

is the duct/pipe length. For the choice of B, it can be the toroidal or poloidal component, depending on the position in the BB. In some parts of the WCLL, especially inside the TFCs, the magnetic field is the toroidal one because the poloidal component is negligible, while outside the TFCs the toroidal component is null and the poloidal magnetic field is chosen. Regarding the 2D pressure coefficient k_p, its value is influenced by the channel geometry, cross-section and wall properties.

Rectangular channel For a straight rectangular channel with electro-conducting walls, uniform thickness and electrical conductivity (an example is shown in Figure 3.4), the 2D pressure loss coefficient can be evaluated with the following relation [39]:

$$k_p = \frac{c}{1 + c + \frac{a}{3b}} \tag{3.14}$$

where c is the wall conductance ratio, a and b are the half lengths of the channel sides, the first related to the wall parallel to the magnetic field (side wall) and the latter to the wall perpendicular to magnetic field (Hartmann wall).

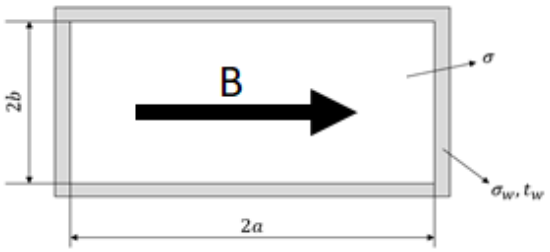

Figure 3.4: Representation of a rectangular channel with uniform thickness and electrical conductivity.

The conductance ratio in this case is calculated with Eq. 3.9 as

$$c = \frac{\sigma_w t_w}{\sigma a} \tag{3.15}$$

Else, for rectangular channels with walls of different thickness and/or electrical conductivities, the relation is the following [40]:

$$k_p = [1 + {c_H}^{-1} + \frac{a}{6b}(c_{S,1}^{-1} + c_{S,2}^{-1})]^{-1} \tag{3.16}$$

where c_H is the Hartmann wall conductance ratio, $c_{S,1}$ and $c_{S,2}$ are the side walls conductance ratios. Their values are evaluated with the Eq. 3.15 maintaining the a value fixed and changing the thickness wall value t_w according to the type of wall.

Circular pipe For a straight circular pipe, with electro-conducting walls, uniform thickness and electrical conductivity (an example is shown in Figure 3.5), the 2D pressure loss coefficient can be evaluated with the relation [41]

$$k_p = \frac{c}{1+c} \tag{3.17}$$

where c is the wall conductance ratio calculated with the relation

$$c = \frac{\sigma_w}{\sigma}\frac{r_o^2 - r_i^2}{r_o^2 + r_i^2} \tag{3.18}$$

where r_i and r_o are the inner and outer pipe radius.

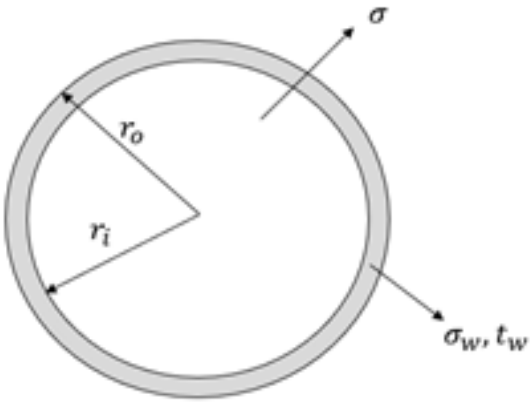

Figure 3.5: Representation of a circular pipe with uniform thickness and electrical conductivity.

Regarding the accuracy of the 2D pressure drop correlation, several authors have compared the predictions of the Eq. 3.13 with the experimentally-measured pressure drops. A representation of the deviation of the k_p coefficient is given in Figure 3.6, in which it is possible to deduce a good confidence of ±15% [28].

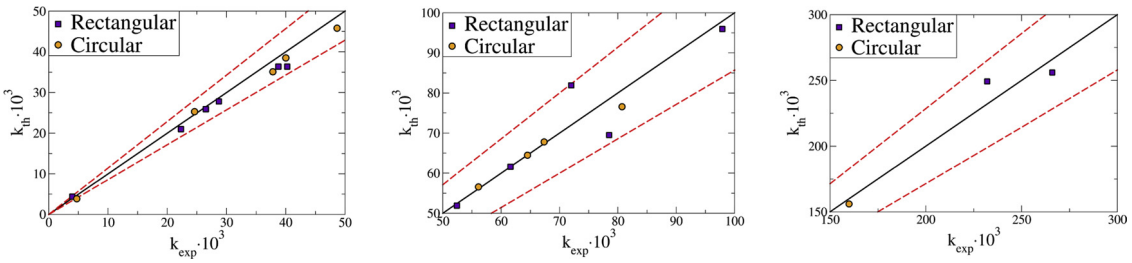

Figure 3.6: Relative error between correlation and experimental value of k_p for rectangular and circular channels. The dashed lines represent a relative error of ±15% [28].

3.3.2 Concentrated losses (3D)

The 3D MHD flows are less characterized in literature with respect to the 2D flow and moreover the pressure drops evaluation is more difficult. In general, the 3D pressure drop can be split in three terms [28]:

$$\Delta p_{3D} = \Delta p_{\infty} + \Delta p_v + \Delta p_i \tag{3.19}$$

where, on the right side of the equation, the first term called *inertia-less/inviscid*, is due mainly to the electro-magnetic forces, while the second and the third term are caused by viscous and inertial forces respectively. When $Ha \gg 1$ and $N \gg 1$, these two terms can be neglected and the 3D pressure drop can be approximated to the first term, $\Delta p_{3D} \approx \Delta p_{\infty}$ (this is usually referred to as *inertia-less approximation*). The evaluation of the 3D losses are very complicated due to its dependence on the channel geometry and the PbLi flow direction respect to the magnetic field one. The general relation for 3D pressure drop is [38]:

$$\Delta p_{3D} = k_{3D} \frac{\rho u_0^2}{2} N \tag{3.20}$$

where k_{3D} is the 3D pressure loss coefficient, ρ is the fluid density, u_0 is the main fluid velocity and N is the interaction parameter. Using the Eq. 3.8 for N, the Eq. 3.20 becomes

$$\Delta p_{3D} = k_{3D} \frac{\sigma u_0 B^2 L_{ch}}{2} \tag{3.21}$$

The local 3D pressure loss coefficient k_{3D} is strictly dependent on the channel geometry and the fluid direction with respect to the magnetic field.

In general, in the WCLL design, there are three main elements in which local 3D loss can appear. They are (see Figure 3.7):

- **Bend**: channel bend in plane parallel/perpendicular to the magnetic field direction.
- **Cross-section variation**: sudden expansion/contraction of the channel area cross-section.
- **Flow around obstacles pipes**: flow around cooling pipes which are placed perpendicularly to the fluid flow direction.

For each type of element, the estimation of k_{3D} value is calculated with an appropriate correlation, depending on the channel geometry and type (rectangular or circular) and the magnetic field direction (parallel or perpendicular).

Bend For bend losses, the 3D pressure loss coefficient is strictly dependent on magnetic field direction. There are two cases: the first is when the plane of the bend is parallel to the magnetic field ($\parallel B$) and the second when it is perpendicular ($\perp B$). The experimental relation for k_{3D}, for a 90° bend in a rectangular channel with $\parallel B$, is [42]:

$$k_{3D,\parallel} = 1.063 \frac{c}{4/3 + c} \tag{3.22}$$

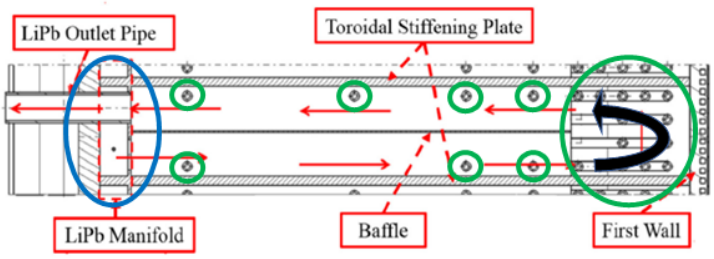

Figure 3.7: BZ channel section: radial-polidal view. Examples of 3D losses. Blue circle: cross section variations. Green circles: obstacle pipes. Black arrow: bend [32].

where c is the wall conductance ratio. While, for a circular pipe, it is possible to assume $k_{3D,\parallel} = 0.125$ [38]. For 90° bend with $\perp B$, both for rectangular and circular pipe, the $k_{3D,\perp}$ is one-third of the parallel one, i.e $k_{3D,\perp} = 0.33 k_{3D,\parallel}$.

Else, regarding other angle values, the k_{3D} estimation is proportional to the previous ones through the ratio between the effective angle (θ) and 90°. This proportionality is the same both for parallel and perpendicular magnetic field direction and both for rectangular and circular channel. In formula:

$$k_{3D,\theta,\parallel} = \frac{\theta}{\pi/2} k_{3D,\pi/2,\parallel} \tag{3.23}$$

$$k_{3D,\theta,\perp} = \frac{\theta}{\pi/2} k_{3D,\pi/2,\perp} \tag{3.24}$$

The deviation of the k_{3D} for bend losses, based on the ratio between the theoretical and experimental value, is ±20% [42].

Cross-section variation The treatment for the pressure drop due to cross-section variation is simpler. For this type of loss, the k_{3D} estimation does not depend on the magnetic field direction and the channel geometry. In this work, the 3D pressure coefficient is taken at $k_{3D} = 0.5$ both for contraction and expansion of the channel area cross-section [28]. Similarly for the bend losses, the deviation of the k_{3D} shows the same accuracy (±20%).

Flow around obstacle pipes In the WCLL design, in particular in the BZ region, there are several cooling pipes in which the pressurized water flows. These pipes are oriented with the toroidal magnetic field and the PbLi flow crosses them orthogonally. For this reason, a particular 3D pressure drop correlation has been proposed by the WCLL design team [35, 28]:

$$\Delta p_{3D} = k_1 \sigma u_0 B^{k_2} d \tag{3.25}$$

where $k_1 = 0.1931$ and $k_2 = 1.73$. The parameter d, in this correlation, is the outer diameter of the cooling pipe. This correlation is valid for one obstacle pipe that is transverse or aligned with the liquid flow direction. Regarding the correlation accuracy, it is ±11%, calculated through the Taylor approximation knowing the standard deviations of k_1 and

k_2 [35].

An overview of all 3D losses and k_{3D} estimation, is present in Table 3.1.

Loss type	Angle	B direction	Rectangular/Square	Circular
Bend	$\theta = \frac{\pi}{2}$	$\parallel B$	$1.063\frac{c}{4/3+c}$	0.125
		$\perp B$	$k_{3D,\perp} = 0.33k_{3D,\parallel}$	$k_{3D,\perp} = 0.33k_{3D,\parallel}$
	$\theta \neq \frac{\pi}{2}$	$\parallel B$	$k_{3D,\theta,\parallel} = \frac{\theta}{\pi/2}k_{3D,\pi/2,\parallel}$	
		$\perp B$	$k_{3D,\theta,\perp} = \frac{\theta}{\pi/2}k_{3D,\pi/2,\perp}$	
Cross-section variation		$\parallel B$, $\perp B$	0.5	
Obstacle pipes		$\parallel B$, $\perp B$	$\Delta p_{3D} = k_1\sigma u_0 B^{k_2} d$ $k_1 = 0.1931$, $k_2 = 1.73$	–

Table 3.1: k_{3D} estimation for different type of losses, magnetic field direction and channel geometry. For flow around obstacle pipes the pressure drop correlation is reported.

Chapter 4

GETTHEM models for magnetohydrodynamics pressure drop

4.1 Introduction

In this chapter, there is a complete review of all kind of pressure drops that occur in the WCLL BB. For the purpose of the WCLL modelling, such pressure drops must be singularly analysed and evaluated to verify the correlations validity and to have a set of models that can be used for the complete model of the BB. As starting point, all property and pressure drop correlations are implemented. Regarding the properties (see Appendix A), they are implemented in the Modelica library, else the pressure drop correlations in the GETTHEM library. Then, the distributed losses (Δp_{2D}) for rectangular and circular channels are modelled for different cases of magnetic field (or Hartmann number), velocity (or mass flowrate) and temperature. After that, the concentrated losses (Δp_{3D}) for bends, cross section variations (contraction and expansion) and flow around obstacle pipes are modelled. For all these kinds of losses, a verification of the PbLi properties implementation and a models comparison and verification with experimental/literature data are done.

4.2 2D pressure drops

In this section, the 2D pressure drops are analysed, in particular regarding the distributed losses for rectangular/square and circular channels. The models are implemented according to several experiments made by different authors and compared with the experimental results.

4.2.1 Rectangular/square channel

In this subsection, the rectangular/square channel pressure drop is modelled. For this purpose, the reference experiment is described in Ref. [43]. The geometry of the channel

is represented in Figure 4.1 and the relative geometry parameters are indicated in Table 4.1 [43].

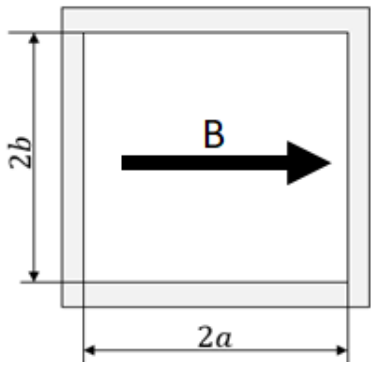

Figure 4.1: Representation of the square channel.

Parameter	Value	Units
$2a$	18	mm
$2b$	18	mm
t_w	3	mm
Channel length	1.4	mm

Table 4.1: Geometry parameters for the square channel [43].

The wall thickness, in this experiment, is considered uniform, while the wall electric conductivity is affected by the temperature. The experiments have been conducted at different PbLi temperatures (430 °C, 540 °C and 650 °C) and, neglecting the heat exchange between the liquid fluid and wall, the wall electrical conductivity has been estimated at the same PbLi temperatures according to EUROFER properties [44]. In Table 4.2 the electrical conductivities for PbLi and EUROFER are indicated.

The magnetic field value depends on the applied currents in experiment channel. The distribution along the channel length is represented in Figure 4.2, in which it is possible to see two fringing magnetic field in the inlet and the outlet of the channel, and a uniform magnetic field in the central region. In the central region, the applied magnetic field increases as the coil currents, and these values of B are used for the purpose of this experiment. The magnetic field values are 0.544 T, 1.088 T, 1.563 T, 1.88 T and 2.03. To measure the MHD pressure drop, the chosen channel length is of $L = 400\ mm$, i.e. the interval in which all the applied magnetic fields are considered uniform. Regarding the characteristic length, its value is the half-width of the channel in the magnetic field direction; referring to Figure 4.2, the characteristic length is equal to a, i.e. $L_{ch} = 0.9\ mm$.

The 2D MHD pressure drop Modelica model for rectangular channel is represented in Figure 4.3. This model is composed by three components: a mass flow rate source, one distributed pressure drop component and a pressure sink. In the first component, the input

Electrical conductivity (S/m)	430 °C	540 °C	650 °C
PbLi [52]	$8.39 \cdot 10^5$	$7.97 \cdot 10^5$	$7.53 \cdot 10^5$
EUROFER [44]	$1.01 \cdot 10^6$	$9.06 \cdot 10^5$	$8.24 \cdot 10^5$

Table 4.2: Electrical conductivities at different temperatures for the MHD experiment channel.

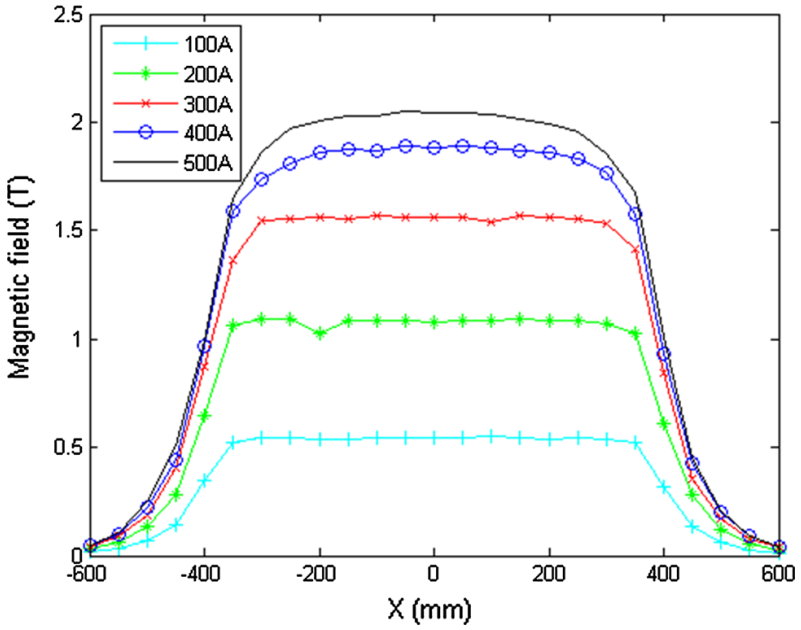

Figure 4.2: Magnetic field distribution along the channel length for different current values [43].

parameters are the mass flow rate $\dot{m}$ and the PbLi temperature T_{PbLi}. The second component is a 2D pressure drop component that evaluates the corresponding 2D pressure loss, in which the input parameters are the applied magnetic field B, the channel geometry ($2a$, $2b$, t_w), the wall electrical conductivity σ_w and the channel length L in which the magnetic field is uniform. The correlations have been implemented starting from a component in the ThermoPower library [45, 46] called "flow1DFV", used for straight channels pressure losses and heat exchange modelling. The 2D pressure drop is evaluated with Eq. 3.13, where the PbLi electrical conductivity σ is calculated knowing the fluid temperature through the relations A.7 and A.8, while the PbLi main velocity u_0 through the mass flow rate and the area of channel cross section. The k_p coefficient is evaluated through the Eq. 3.14 in which the wall conductance ratio is calculated with Eq. 3.15. Finally, the third component, is a pressure sink component.

This model has been simulated for every magnetic field and PbLi temperature value previously indicated, evaluating the 2D pressure drop in the channel for different fluid main velocities. Each pressure loss has been obtained changing $\dot{m}$ and T_{PbbLi} in the mass flow

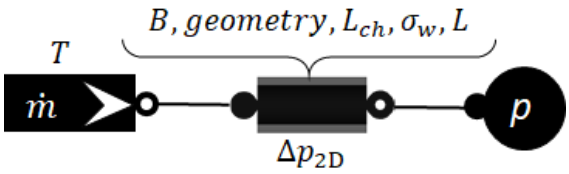

Figure 4.3: 2D pressure drop Modelica model for rectangular/square channel. Above each components input parameters are indicated.

rate source and B and σ_w in the 2D pressure drop component, while the other parameters are fixed. In Figure 4.4, the pressure drop results as a function on the PbLi main velocity are represented. In all the cases, the Modelica results agree very well with the theoretical and experimental results, with a maximum relative error of $\approx 9\%$, that is below the acceptable value of $\pm 15\%$, expressed in Subsection 3.3.1, represented by error bars in the Figure 4.4.

The pressure drop has a linear dependence with the fluid main velocity and it is strongly dependent on the applied magnetic field: these characteristics are due to the MHD effects happening inside the channel. In MHD cases, the flows are in a laminar state due to the strong MHD effect on suppression of turbulence, nevertheless the Reynolds numbers are relatively high ($Re > 8000$) . For this reason, the pressure drop behaviour, in the MHD case, is always linearly dependent on the main velocity, while, for smaller value of B (low Ha), the transition between OHD and MHD happens and the evaluation of the pressure loss depends on the flow regime (laminar or turbulent). The pressure drop is also strongly dependent on the applied magnetic field. This feature is shown by the increasing slope of the curve for higher magnetic field value. In the range of 0.544 T - 2.030 T, at smaller velocities, the pressure drop difference is more or less of one order of magnitude and tends to be larger for increasing liquid velocity, for instance, seeing the Figures 4.4a and 4.4e. Moreover, for lower magnetic field values, the difference between two curves slope is high, while increasing the applied B, it tends to be less accentuated. Another important aspect is the fluid temperature. For all the cases, a lower PbLi temperature tends to increase the pressure drop in the channel, due to the fact that fluid electrical conductivity increases while its dynamic viscosity and density decrease. In conclusion, the Modelica model agrees very well with the correlation theoretical values and experimental data and seems to represent with a good approximation the general 2D pressure drop behaviour for electro-conducting rectangular/square channel.

4.2.2 Circular pipe

In this subsection, the circular pipe pressure drop is modelled. The reference experiment for this case is described in Ref. [47]. The geometry of the channel is represented in Figure 4.5 and the relative geometry parameters are indicated in Table 4.3 [47].

The wall thickness, in this experiment, is considered uniform, while the wall electrical-conductivity is affected by the temperature. The PbLi properties (see Appendix A) are

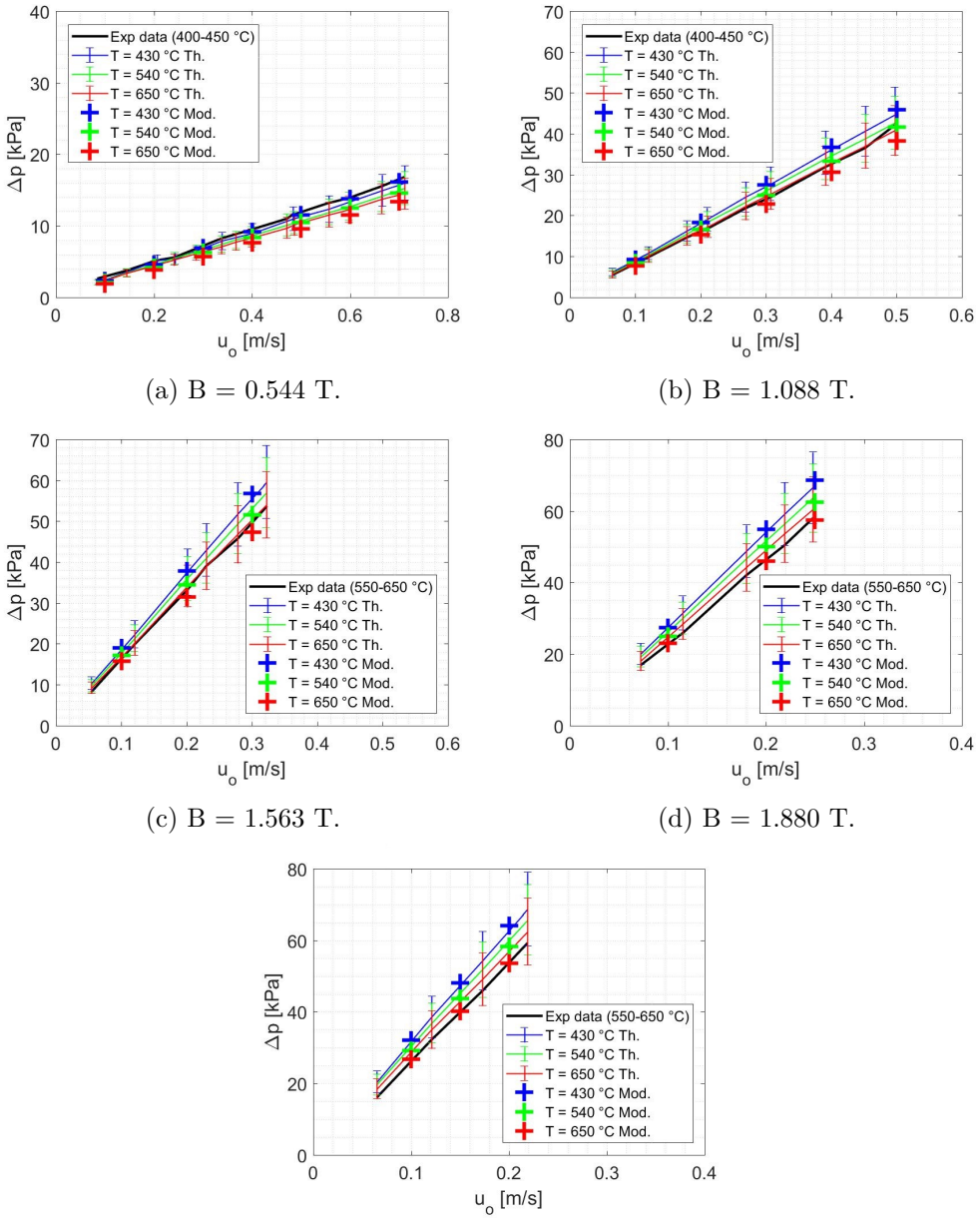

(a) B = 0.544 T.

(b) B = 1.088 T.

(c) B = 1.563 T.

(d) B = 1.880 T.

(e) B = 2.030 T.

Figure 4.4: Rectangular channel 2D pressure losses for different magnetic fields and PbLi temperatures. The continuous lines represent the correlation values, the crosses represent the Modelica simulation values and the black lines represents the experimental data from [43]. (a) B = 0.544 T, (b) B = 1.088 T, (c) B = 1.563 T, (d) B = 1.880 T and (e) B = 2.030 T.

calculated at 300 °C (573.15 K) and the EUROFER properties [44], in particular its electrical conductivity σ_w, neglecting the heat exchange between the wall and the fluid, is

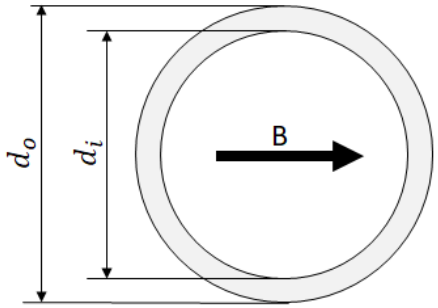

Figure 4.5: Representation of the circular pipe.

Parameter	Value	Units
d_i	22.2	mm
d_o	25.4	mm
t_w	1.6	mm

Table 4.3: Geometry parameters for the square channel [47].

calculated at the same PbLi temperature. Regarding the pressure drops evaluation, several runs have been carried out, with different fluid velocity and magnetic field values. The parameters of the different runs are collected in Table 4.4 [47]. The magnetic field, in this experiment, presents two fringing regions and a central region where it is uniform. Its distribution is represented in Figure 4.6. The region in which the applied magnetic field is uniform is considered for the Modelica simulations, i.e. $L = 0.8\ m$.

The 2D MHD pressure drop Modelica model for circular channel is represented in Figure 4.7. This model is composed, as the rectangular case, by three components: a mass flow rate source, one distributed pressure drop component and a pressure sink. In the first component, the input parameters are the mass flow rate $\dot{m}$ and the PbLi temperature T_{PbLi}. The second is a 2D pressure drop component that evaluates the corresponding 2D pressure loss, in which the input parameters are the magnetic field B, the channel geometry (d_i, d_o, t_w), the wall electrical conductivity σ_w and the channel length L. The correlations have been implemented starting from a component in the ThermoPower library ("flow1DFV"). The 2D pressure drop is evaluated with Eq. 3.13, where the PbLi electrical conductivity σ is calculated knowing the liquid temperature through the relations A.7 and A.8, while the PbLi main velocity u_0 through the mass flow rate and the area of channel cross section. The k_p coefficient is evaluated through the Eq. 3.17 in which the wall conductance ratio is calculated with the Eq. 3.18. Finally, the third component, is a pressure sink.

This model has been simulated for every magnetic field, evaluating the 2D pressure drop in the pipe for several liquid main velocities. The magnetic field and velocity values used for each simulation, are indicated in Table 4.4. Every pressure drop value has been obtained changing $\dot{m}$ in the mass flow rate source and B in the 2D component, while the other parameters are fixed. In Figure 4.8, the pressure drop results as a function on the

Run	B = 0.475 T (Ha = 108)	B = 0.946 T (Ha = 215)	B = 1.417 T (Ha = 322)
1	0.2085	0.2085	0.0502
2	0.4170	0.3128	0.1236
3	0.6236	0.4170	0.1873
4	0.8341	0.5213	0.2703
5	1.0426	0.6236	0.3533

Table 4.4: PbLi velocities in the different runs. The value are in m/s [47].

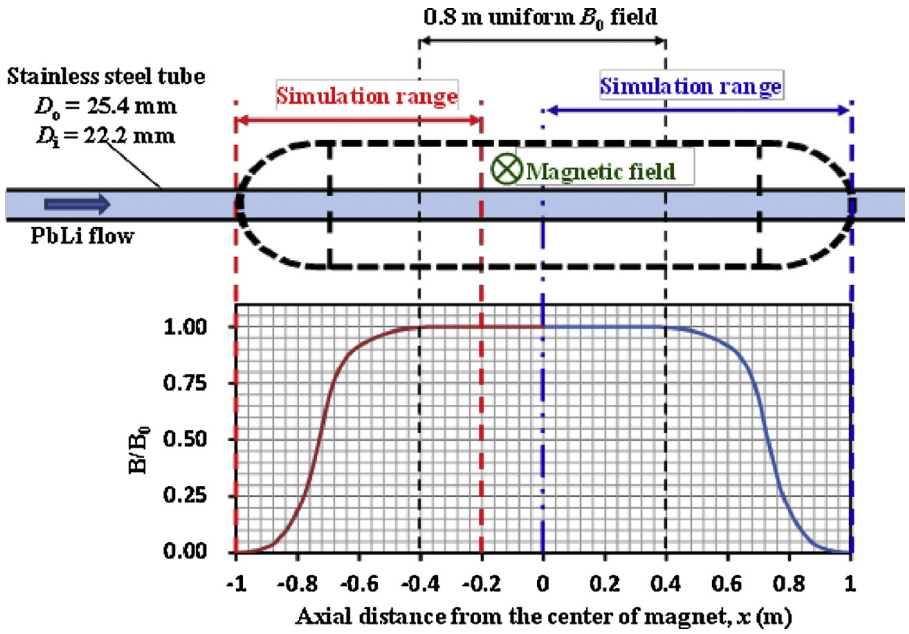

Figure 4.6: Schematic representation of the pipe geometry and magnetic field distribution along the pipe [47].

PbLi main velocity, are represented. In all cases, the Modelica results agree very well with the theoretical and measured results, with a maximum relative error of $\approx 7\%$, that is below the acceptable value of $\pm 15\%$, the same one of the rectangular channel case (see Subsection 3.3.1).

As for the rectangular/square channel, in the circular pipe case, the pressure drop has a linear dependence with the main velocity due to the MHD effects. Such effects suppress the fluid turbulent regime despite the high Reynolds numbers ($Re > 8000$), establishing a laminar state expressed by the linear behaviour of the curves. A comparison between the OHD and MHD regime with the model used in this section is described in the Appendix B. The slope of the curves increases greatly with raising the applied magnetic field, due to its strong dependence. For $\sim 1\ T$, in the range of 0.475 T - 1.417 T, for lower velocities the difference between pressure drops can be of one order of magnitude, and it can increasing more for higher velocities, as can be seen in Figures 4.8a and 4.8c. In conclusion, also for the circular pipe case, the 2D pressure drop model implemented in Modelica agrees

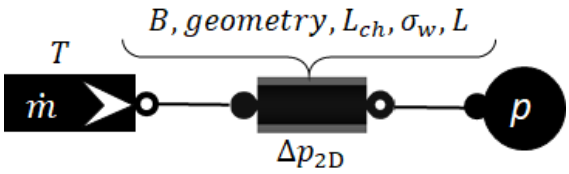

Figure 4.7: 2D pressure drop Modelica model for circular channel. Input parameters are indicated above each components.

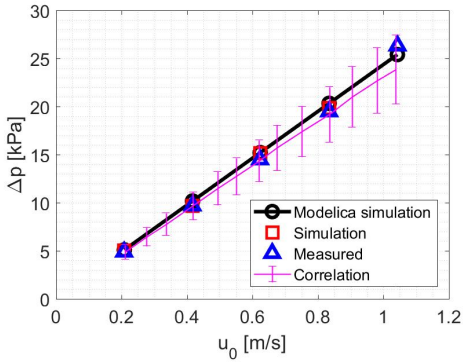

(a) B = 0.475 T (Ha = 108).

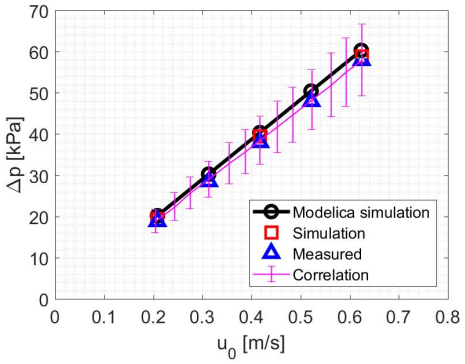

(b) B = 0.946 T (Ha = 215).

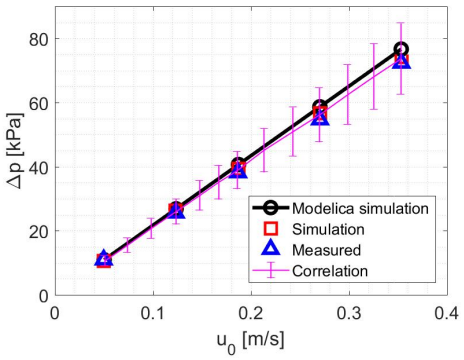

(c) B = 1.417 T (Ha = 322).

Figure 4.8: Circular channel 2D pressure losses for different magnetic fields. The black line represents the Modelica simulation, the red squares the simulation results (from [47]), the blue triangles the measured results (from [47]), and the magenta line the correlation results with the corresponding error bars. (a) B = 0.475 T (Ha = 108), (b) B = 0.946 T (Ha = 215) and (c) B = 1.417 T (Ha = 322).

very well with the experimental and theoretical results, and it can represent with a good accuracy the 2D pressure loss for an electro-conducting circular channel.

4.3 3D pressure drops

In this section, the 3D pressure drops are analysed, in particular regarding the liquid flow bends with respect to the magnetic field direction, channel cross section variations (contractions and expansions) and liquid flow through obstacle pipes placed transversely. The models are implemented according to the several examples taken in literature and compared with such data.

4.3.1 Bends

One of the most frequent 3D pressure drop inside the PbLi loop is the liquid flow bend. Such loss is strongly dependent to the curvature angle and the magnetic field direction respect to the bend plane, in particular when B is parallel or perpendicular to it, as described in the Section 3.3.2. In this subsection, these two types of losses are analysed and compared with data taken from the literature.

The Modelica model used for the simulation is represented in Figure 4.9. The first component represents a mass flow rate source where the input parameters are the liquid fluid mass flow rate and the PbLi temperature, thanks to which its properties (see Appendix A) are calculated. The second one is a 3D MHD pressure drop component (based on the "pressDrop" component in the ThermoPower libary) in which the 3D MHD correlation has been implemented according to the Eq. 3.21. The k_{3D} coefficient has been estimated with the relation corresponding to the type of the loss, i. e. the bend loss for this case (see Table 3.1). For such component, the input parameters are the applied magnetic field B and its direction, the channel geometry, the characteristic length L_{ch}, the wall electrical conductivity σ_w and the curvature angle θ. Finally, the third component is a pressure sink. In the following, flow bends parallel and perpendicular to B are analysed and the specific details are described.

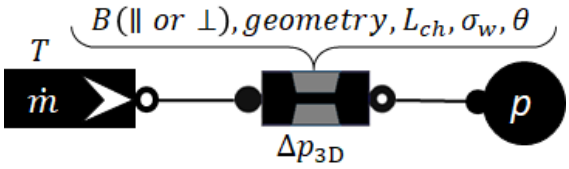

Figure 4.9: 3D pressure drop Modelica model for liquid flow bends. Input parameters are indicated above each components.

Bend parallel to B For this kind of loss, a portion of the OB draining pipe is taken, as represented in Figure 4.10. In this specific case, the curvature angle is 90° and the poloidal magnetic filed direction is parallel to the curvature plane of the PbLi flow. The input parameters, regarding the magnetic field, PbLi properties (see Appendix A) and channel geometry, are indicated in Table 4.5.

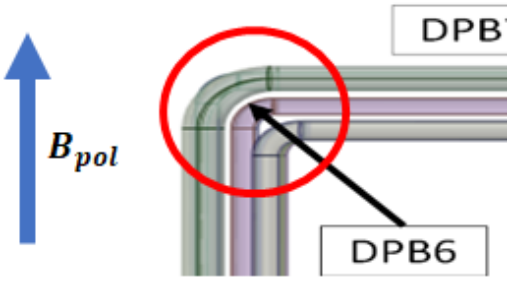

Figure 4.10: OB draining pipe portion: radial-poloidal view. The 90° bend is highlighted in the red circle and the poloidal magnetic field is indicated by a blue arrow [28].

Parameter	Value	Units
$\dot{m}$	16.38	kg/s
T	600	K
B_{pol}	0.8	T
r_i	17.3	cm
r_o	19.2	cm
t_w	1.9	cm
σ_w	$1.14 \cdot 10^6$	S/m

Table 4.5: Input parameters for the 90° bend parallel to the magnetic field [28].

For the estimation of the 3D loss, the k_{3D} coefficient is equal to $k_{3D,\parallel}$ and calculated with the Eq. 3.22. Regarding wall conductance ratio c, necessary for the evaluation of the k_{3D} coefficient, and the 3D pressure drop, the corresponding equations are 3.9 and 3.21 respectively. In this case, but in general for circular pipes, the corresponding characteristic length L_{ch} is equal to the inner radius. Then, the equations used for the calculations are:

$$\Delta p_{90^\circ} = \frac{k_{3D,\parallel}\sigma u_0 B^2 r_i}{2} \tag{4.1}$$

$$c = \frac{\sigma_w t_w}{\sigma r_i} \tag{4.2}$$

$$k_{3D_\parallel} = 1.063\frac{c}{4/3 + c} \tag{4.3}$$

The corresponding 3D pressure drop value obtained from literature [48] is

$$\Delta p_{3D,90^\circ,lit} = 0.2\ kPa \pm 20\%$$

while the Modelica simulation result carried out by the model represented in Figure 4.9, obtained with the input parameters mentioned above, is

$$\Delta p_{3D,90^\circ,sim} = 0.191\ kPa$$

where the relative error with respect to the literature result is ≈ 4.5 %, calculated with the relation: $\frac{|\Delta p_{3D,lit} - \Delta p_{3D,sim}|}{\Delta p_{3D,lit}} \cdot 100$. In conclusion, the relative error is lower then the acceptable

one (± 20 %), therefore this model can represent with a good approximation the liquid flow bend parallel to B.

Bend perpendicular to B An example of bend perpendicular to the magnetic filed is taken from the U-turn of the BZ cell, represented in Figure 4.11. In this case, the applied magnetic filed direction (toroidal component) is perpendicular to the PbLi curvature plain and the angle is 180°. In the MHD case in general, for this kind of loss, the inertial effects can be neglected and a 180° bend (U-turn) can be represented by two successive 90° bends, as mentioned also in Subsection 3.3.2. In the BZ, the U-turn presents a channel cross section variation. In this analysis, as the other ones described in the follow of this work, the lower channel area cross section has been considered for this kind of loss as conservative choice. The input parameters, regarding the magnetic field, PbLi properties (see Appendix A) and channel geometry, are indicated in Table 4.6.

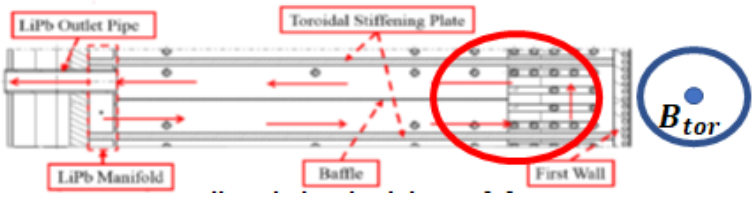

Figure 4.11: BZ cell: radial-poloidal view. The U-turn is highlighted in the red circle and the toroidal magnetic field is indicated by a blue arrow (perpendicular to the figure) [32].

Parameter	Value	Units
$\dot{m}$	0.025	kg/s
T	599	K
B_{tor}	3.49	T
$2a$ (Channel depth)	234	mm
$2b$ (Channel height)	60.5	mm
t_w (Baffle plate)	2	mm
σ_w	$1.15 \cdot 10^6$	S/m

Table 4.6: Input parameters for the 180° bend perpendicular to the magnetic field [28].

As mentioned in the Subsection 3.3.2, the k_{3D} coefficient for bend perpendicular to B is one third of $k_{3D,\parallel}$, i.e. $k_{3D,\perp} = 0.33 k_{3D,\parallel}$. Regarding the wall conductance ratio c and the 3D pressure drop, the corresponding equations are 3.9 and 3.21 respectively. In this case, but in general for rectangular bends, the corresponding characteristic length L_{ch} is equal to the half-hydraulic diameter ($d_{hyd}/2$). The equations used for the calculations are:

$$\Delta p_{90^\circ} = \frac{k_{3D,\parallel} \sigma u_0 B^2 (d_{hyd}/2)}{2} \tag{4.4}$$

$$c = \frac{\sigma_w t_w}{\sigma d_{hyd}} \tag{4.5}$$

$$k_{3D_\perp} = 0.33 k_{3D,\parallel} = 0.33 \cdot 1.063 \frac{c}{4/3 + c} \tag{4.6}$$

in which the hydraulic diameter as calculated with the following equation

$$d_{hyd} = \frac{4A}{P} \tag{4.7}$$

where A is the lower channel are cross section and P is its perimeter.

For this specific case, the 180° bend is the double of one 90° bend, i.e. $\Delta p_{180^\circ} = 2\Delta p_{90^\circ}$. The corresponding 3D pressure drop value obtained from the literature [28] is

$$\Delta p_{3D,180^\circ,lit} = 0.044\ kPa \pm 20\%$$

while the Modelica simulation result carried out by the model represented in Figure 4.9, obtained with the input parameters mentioned above, is

$$\Delta p_{3D,180^\circ,sim} = 0.0399\ kPa$$

where the relative error with respect to the literature result is ≈ 10.3 %, calculated with the relation: $\frac{|\Delta p_{3D,lit} - \Delta p_{3D,sim}|}{\Delta p_{3D,lit}} \cdot 100$. In conclusion, the relative error is lower then the acceptable one ($\pm$ 20 %), therefore this model can represent with a good approximation also the liquid flow bend perpendicular to B.

4.3.2 Channel cross section variation (contraction/expansion)

Another important and frequent 3D loss inside the PbLi loop is the channel cross section variation, i.e. contraction or expansion of the channel area. Such loss is very simple to be modelled, since it is not dependent on the magnetic field direction and its estimation method is equal for rectangular and circular channel.

The Modelica model used for the simulation is represented in Figure 4.12. This model is the same adopted for the bend loss (see Subsection 4.3.1), except for the 3D component in which the 3D MHD correlation has been implemented according the Eq. 3.21. The input parameters are the applied magnetic field B, the channel geometry, the characteristic length L_{ch} and the wall electrical conductivity σ_w..

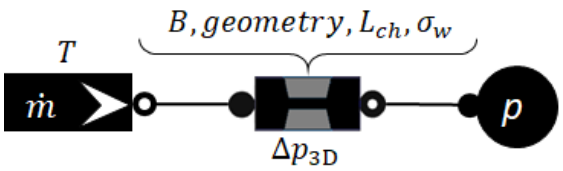

Figure 4.12: 3D pressure drop Modelica model for channel contraction or expansion. Input parameters are indicated above each components.

For this kind of loss, the channel expansion (inlet opening) and contraction (outlet pipe) of the BZ zone are considered (see Figure 4.13). In this particular example, both losses are the same due to the same channel contraction/expansion dimensions, therefore just one of them is analysed. The input parameters regarding the magnetic field, PbLi properties (see Appendix A) and channel dimensions, are indicated in Table 4.7.

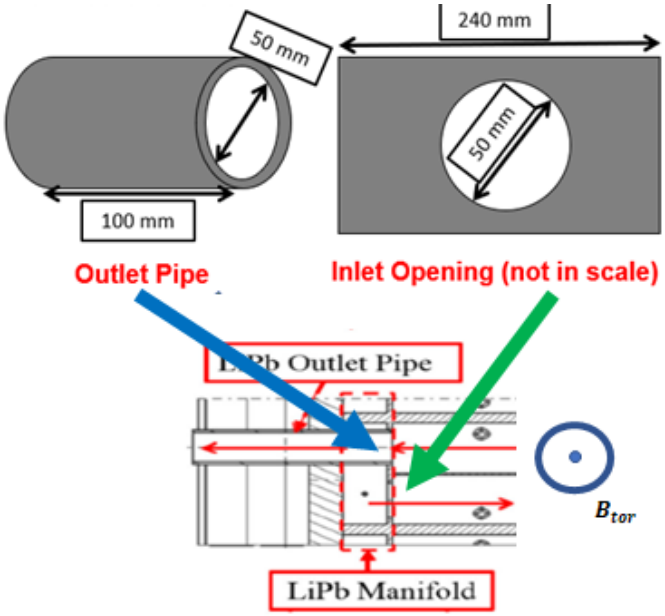

Figure 4.13: BZ cell portion: radial-poloidal view. The inlet opening (expansion) and outlet pipe (contraction) are indicated by two arrows and the toroidal magnetic field is indicated by a blue arrow (perpendicular to the figure). Above, sketches of the two orifices are represented with the corresponding geometry dimensions (adapted from [48]).

Parameter	Value	Units
$\dot{m}$	0.025	kg/s
T	599	K
B_{tor}	3.49	T
r_i	21	mm
σ_w	$1.15 \cdot 10^6$	S/m

Table 4.7: Input parameters for the channel cross section variation [48].

For channel variation cross section loss, the k_{3D} is independent on the magnetic field direction and channel geometry, in fact for such loss the wall conductance ratio c is not used. As mentioned is Subsection 3.3.2, the k_{3D} for channel contraction/expansion is equal to 0.5, while the characteristic length L_{ch} is equal to the inner radius r_i for circular channel or to the hydraulic diameter d_{hyd} for rectangular one. The equation used for the calculation in this example (circular channel) are:

$$k_{3D,orif} = 0.5 \tag{4.8}$$

$$\Delta p_{orif} = \frac{k_{3D,orif}\sigma u_0 B^2 r_i}{2} \tag{4.9}$$

The corresponding 3D pressure drop value obtained from the literature [28] is

$$\Delta p_{3D,orif,lit} = 0.091\ kPa \pm 20\%$$

while the Modelica simulation result carried out by the model represented in Figure 4.12, obtained with the input parameters mentioned above, is

$$\Delta p_{3D,orif,sim} = 0.101\ kPa$$

where the relative error respect to the literature result is $\approx$ 11 %, calculated with the relation: $\frac{|\Delta p_{3D,lit} - \Delta p_{3D,sim}|}{\Delta p_{3D,lit}} \cdot 100$. In conclusion, the relative error is lower then the acceptable one ($\pm$ 20 %), therefore this model can represent with a good approximation the channel cross section variation (contraction/expansion).

4.3.3 Flow around obstacle pipes

The third and the last 3D loss in the PbLi loop is the liquid flow around obstacle pipes. Such loss is located principally inside the BZ zone, where the PbLi flow crosses transversely the water cooling pipes. The estimation of this 3D pressure drop is very different with respect to the others, as mentioned in the Subsection 3.3.2, with an appropriate correlation [28].

The Modelica model used for the simulation is represented in Figure 4.14. This model is the same adopted for the bend (see Subsection 4.3.1) and channel cross section variation losses (see Subsection 4.3.2), except for the 3D component in which the 3D MHD corrleation has been implemented according the Eq. 3.25. The input parameters are the applied magnetic field B, the channel geometry, two constant coefficient, k_1 and k_2, needed for the 3D pressure drop estimation, the obstacle pipes outer diameter d and the number of obstacle pipes N_{pipes} that are in the PbLi hydraulic path.

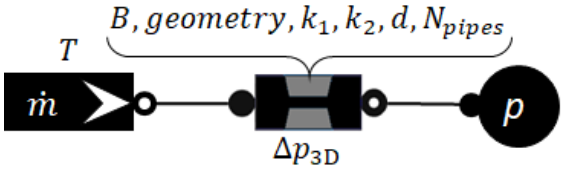

Figure 4.14: 3D pressure drop Modelica model for liquid flow around obstacle pipes. Input parameters are indicated above each components.

The example model for this kind of loss is taken from the BZ, represented in Figure 4.15. In general, in the BZ of T01.A WCLL configuration, the cooling pipes run along the

radial direction and then curve along the toroidal one. In this subsection, the case in which the cooling pipes are parallel to the magnetic field is considered, due to the fact that this is the most relevant pressure drop. The PbLi flow crosses transversely the cooling pipes and on each of them the pressure loss happens, therefore the overall pressure drop is estimated taking into account the total number of pipes. The distribution of the cooling pipes inside the BZ is different, for instance near the FW they are very close while in the sub-channel or in the upper channel they are spaced, therefore the overall 3D pressure drop is obtained taking into account the number of cooling pipes that are in the mean liquid hydraulic path. In this configuration there are 21 pipes with the same outer diameter, but for the calculation, the number of pipes N_{pipes} taken into account is 13, according to the pipe number on the hydrualic path [48]. The other input parameters are indicated in Table 4.8. The simulations have been carried out with three magnetic field values based on the BZ cell position.

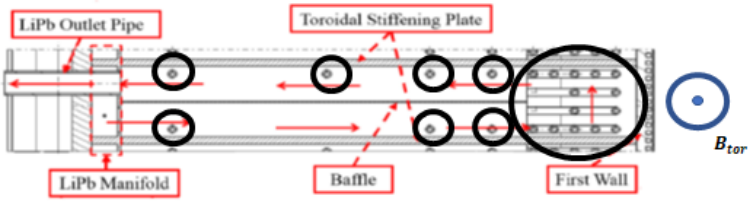

Figure 4.15: BZ cell portion: radial-poloidal view. The cooling pipes (obstacle pipes) are highlighted with black circles and the magnetic field in indicated by a blue arrow (perpendicular to the figure) (adapted from [48]).

Parameter	Value	Units
$\dot{m}$	0.025	kg/s
T	599	K
d (pipes diameter)	13.5	mm
N_{pipes} (hydraulic path)	13	-
B_{tor} (Bottom blanket BZ)	5.1	T
B_{tor} (Equatorial blanket BZ)	3.49	T
B_{tor} (Top blanket BZ)	5.46	T

Table 4.8: Input parameters for PbLi flow around obstacle pipes simulations [48].

As mentioned in the subsection 3.3.2, the obstacle pipes loss is estimated with an appropriate correlation [28]. In this case in which there are several pipes, all obstacles are concentrated in one component (always based on ThermoPower "pressDrop" model) and the overall loss is calculated with a single pressure drop multiplied times the number of pipes N_{pipes}, considering that they are in series along the hydraulic path. Then, the equation used for calculations is:

$$\Delta p_{3D,obst} = N_{pipes} k_1 \sigma u_0 B^{k_2} d \tag{4.10}$$

where $k_1 = 0.1931$ and $k_2 = 1.73$.

The results are represented in Figure 4.16. The Modelica results accomplish very well the literature values, being inside the error bars. However, to achieve this result, the 3D pressure drops of Modelica results have been corrected with a corrective factor $f_{corr} = 1.1$ to conform them with a precise accuracy respect to the literature data. The relative error results are represented in Figure 4.17. The accuracy of the Modelica results, corrected with the f_{corr} factor, is good respect to the acceptable relative error (≈ 11 %) calculated with the Taylor approximation knowing the relative standard deviations [35], as mentioned in subsection 3.3.2.

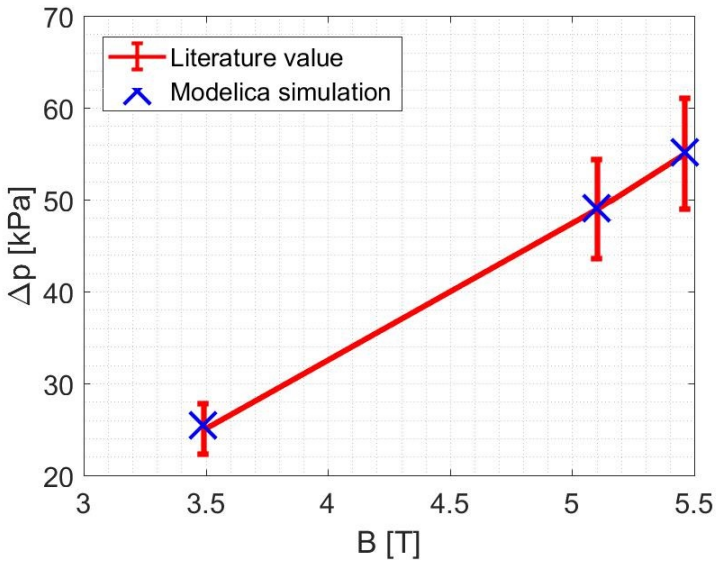

Figure 4.16: Obstacle pipes pressure drops in function of the applied magnetic field. The red line represents the literature data while the blues crosses the Modelica results. A corrective factor $f_{corr} = 1.1$ is used to Modelica results to conform to the literature values.

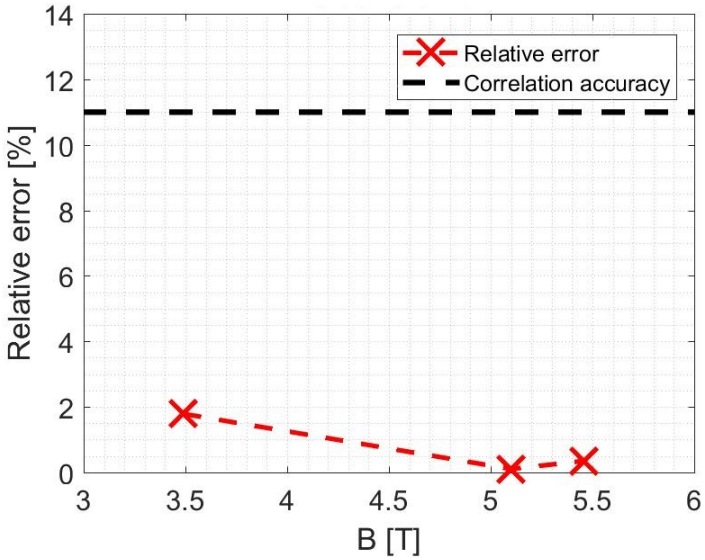

Figure 4.17: 3D obstacle pipes pressure drop relative errors respect to the applied magnetic field. The red dashed line/red crosses represents the relative errors while the black dashed line the maximum acceptable error (≈ 11 %).

Chapter 5

Application to the WCLL PbLi loop

5.1 Component-level modelling

In this section, the previous models for 2D and 3D pressure losses are applied to the WCLL PbLi loop modelling. As a first step, the principal BB components are singularly modelled to evaluate the corresponding pressure drop at each region and then they are compared and verified with literature data. The BB components that are analysed are: feeding pipe (FP), manifold, breeding zone (BZ) cell and draining pipe (DP). For each component, the OB and IB case has been considered.

5.1.1 Breeding zone

The first component that has been analysed is the BZ. For the BZ the TO1.A configuration of DEMO WCLL 2016 design has been chosen, as mentioned in section 2.1. A representation of such component is represented in Figure 5.1. The PbLi enters the BZ from the inlet opening and then runs along the radial direction in the lower channel, then crosses the U-turn near the FW and comes back radially in the upper channel, finally exiting through the outlet pipe. In this region there are several losses, both 2D and 3D, due to the channel bends and cross section variations and the presence of many obstacle. Regarding the applied magnetic field B, the toroidal component is considered, due to the fact that inside the WCLL it is predominant respect to the poloidal one. This BZ configuration is considered both for the OB and IB PbLi loop.

The reference model taken into account is described in the Ref. [28]. The equatorial BZ cell of the OB loop is considered for this analysis, in which the applied toroidal magnetic field B_{tor} is equal to 3.49 T for the entire BZ region. The PbLi mass flow rate that enters in the BZ is supposed to be equal to 0.025 kg/s, while its temperature is fixed to 599 K. Regarding the TO1.A channel geometrical parameters, they are indicated in Table 5.1. The number of cooling pipes that crosses inside the BZ is 21.

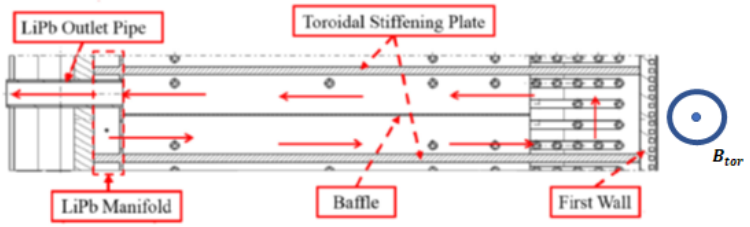

Figure 5.1: BZ channel section: radial-polidal view. The red arrows highlights the PbLi hydraulic path while the toroidal magnetic field is indicated by a blue arrow (perpendicular to the figure) (adapted from [32]).

Parameter	Symbol	Value	Units
Toroidal width	$2a$	234	mm
Poloidal width	$2b$	60.5	mm
Cell poloidal height	H	135	mm
Radial length	R_1	400	mm
Bend length	R_2	150	mm
Cooling pipes diameter	d	13.5	mm
Radial-poloidal stiffening plate	$2t_{r,p}$	19	mm
Toroidal-radial stiffening plate	$2t_{r,t}$	12	mm
Baffle plate thickness	$2t_b$	2	mm
FW thickness	$2t_{FW}$	25	mm
Orifice diameter (inlet/outlet)	d_{orif}	50	mm

Table 5.1: TO1.A channel geometrical parameters [28].

Model description

The Modelica model used to evaluated the pressure drop inside the BZ cell is represented in Figure 5.2. The model is composed by the following objects:

- **Mass flow rate source**: the first component is the mass flow rate source. The input parameters are the PbLi mass flow rate $\dot{m}_{PbLi} = 0.025\ kg/s$ and its temperature $T_{PbLi} = 599\ K$.
- **InletOpening**: this component represents the inlet opening orifice, in which the PbLi enters inside the BZ. It is a 3D loss for circular pipe cross section variation. The corresponding characteristic length L_{ch} is equal to the channel inner radius.
- **subChannel**: this component represents the lower channel of the BZ cell where the PbLi runs in the radial direction towards the FW. It is a 2D pressure drop component in which the characteristic length is equal to the half toroidal width ($L_{ch} = 2a$) and the channel length is 400 mm long.
- **ObstaclePipes**: this component represents the 3D loss due to the presence of the cooling obstacles pipes. All pipe losses have been concentrated inside this component

in which the number of obstacles on the PbLi mean hydraulic path is considered ($N_{pipes} = 13$).

- **Bend_01_90deg**: this component represents the first 90° bend of the U-turn. It is a 3D loss for rectangular channel bend perpendicular to the magnetic field ($\perp B$) and the characteristic length L_{ch} considered is equal to the half-hydraulic diameter ($d_{hyd}/2$). In this region there is also a channel cross section variation between inlet and outlet; the inlet channel area, i.e. the lower one, is considered for conservative reasons.
- **180deg_Bend**: this component represents the vertical flow inside the U-turn. It is a 2D loss in which L_{ch} is equal to the toroidal half-width $2a$, while the channel length is equal to 60.5 mm (considering the PbLi mean hydraulic path).
- **Bend_02_90deg**: this component represents the second 90° bend of the U-turn. It is the same of the component "Bend_01_90deg", in which the lower channel area is the outlet one.
- **upperChannel**: this component represents the upper channel of the BZ. It is the same of the component "subChannel", where, in this case, the PbLi flows radially from the FW toward the manifold region.
- **OutletPipe_3D**: this component represents the outlet pipe orifice, in which the PbLi exits from the BZ and goes toward the manifold region. As the inlet opening orifice, it is a 3D loss for circular pipe cross section variation and the corresponding characteristic length L_{ch} is equal to the channel inner radius.
- **OutletPipe_2D**: this component represents the PbLi flow inside the outlet pipe, that connects the BZ cell with the internal manifold channel. It simulates a 2D pressure drop inside the outlet pipe, where the characteristic length L_{ch} is equal to the inner radius, while the pipe length is equal to 100 mm.
- **Pressure sink**: the last is a pressure sink component, used to provide the loop pressure level as a boundary condition.

Results

The overall BZ pressure drop obtained with the Modelica simulation is reported in Table 5.2. The pressure loss and percentage of every component is indicated. The overall pressure drop obtained from the literature is $\Delta p_{BZ,lit} = 0.731\ kPa \pm 16\ \%$, while BZ loss estimated with the Modelica simulation is $\Delta p_{BZ,sim} = 0.622\ kPa$. The relative errors, obtained with the relation $\frac{|\Delta p_{BZ,lit} - \Delta p_{BZ,sim}|}{\Delta p_{BZ,lit}} \cdot 100$, are reported Table 5.2. Relative errors are high in components where the pressure drop is negligible, nevertheless the global relative error ($\approx 14.9\ \%$,) is inside the literature value error bar. In general, the largest contribution of BZ pressure drop is associated to the 3D losses, in particular for the inlet/outlet orifices, except for the outlet pipe 2D loss. This aspect is due to the fact that the PbLi velocity inside the BZ is very low giving a very poor distributed pressure drop inside it, while in the outlet pipe it is higher because its channel is narrower and the liquid velocity increases.

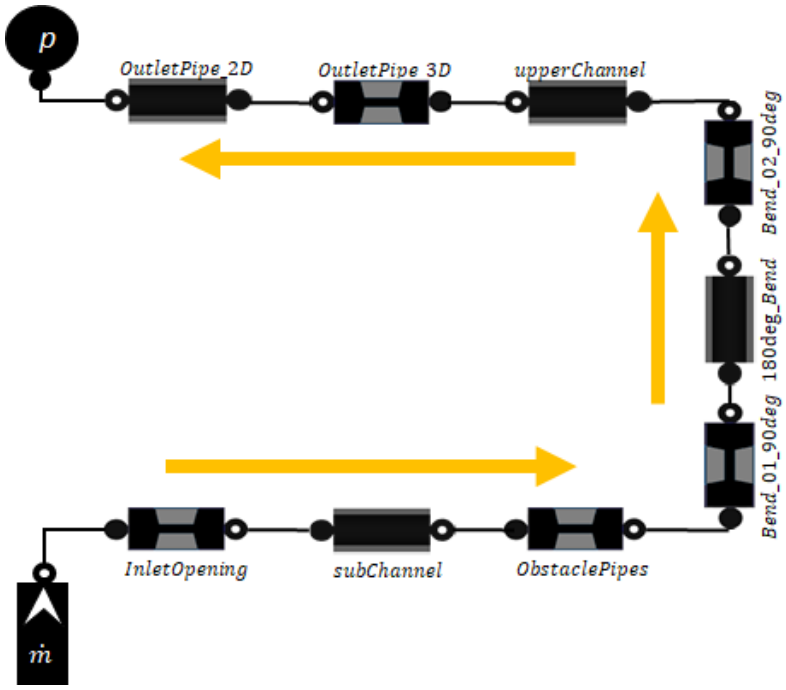

Figure 5.2: BZ Modelica model. The orange arrows indicate the PbLi flow direction.

The other 2D pressure drops are located in the lower and upper channel, where they are equal due to the same geometry, and in the vertical section of the U-turn in which there is a very small loss. Regarding the 3D losses, they occur principally in the inlet/outlet orifices, in which the losses are the same, as well as for the two 90° bends, while the smaller loss is associated to the obstacle pipes. In synthesis, the 2D overall pressure drop in the BZ is $\Delta p_{BZ,2D} = 0.350\ kPa$, while the total 3D loss is $\Delta p_{BZ,3D} = 0.272\ kPa$. In conclusion, the Modelica model can represent with a good approximation the BZ cell, nevertheless its relative error is quite large; however, this is not expected to be a strong issue as the BZ pressure drop is the smallest contributor to the overall pressure drop in the WCLL PbLi loop [29].

5.1.2 Manifold

The second component analysed in this section is the manifold region. As mentioned in section 2.1, the DEMO WCLL 2018 manifold design is chosen. This configuration presents six parallel channels that runs along the blanket segment from the bottom where PbLi enters from the FP, to the top where the liquid goes toward the DP. Each channel is subdivided into two co-axial channel, the annular channel that feeds the PbLi to the BZ and external channel that collects the liquid from the BZ (see Section 2.1 and Figures 5.3 and 5.7). In the WCLL configuration there are two independent manifolds, the OB and IB manifold, that have different dimension and design profile. In the follow, both OB and IB manifolds have been analysed.

Component	Type	Δp $[kPa]$	%	Δp_{lit} $[kPa]$	Rel. error [%]
InletOpening	3D	0.102	16.5	0.091	12.1
subChannel	2D	0.010	1.6	0.075	86.7
ObstaclePipes	3D	0.026	4.2	0.025	4
Bend_01_90deg	3D	0.020	3.2	0.022	9
180deg_Bend	2D	0.005	0.8	0.007	71.4
Bend_02_90deg	3D	0.020	3.2	0.022	9
upperChannel	2D	0.010	1.6	0.075	86.7
OutletPipe_3D	3D	0.102	16.5	0.091	12.1
OutletPipe_2D	2D	0.326	52.5	0.323	1
Total		0.622	100	0.731	

Table 5.2: Modelica simulation BZ pressure drops. Δp_{lit} $[kPa]$ values taken from Ref. [28]

OB manifold

The OB manifold layout has been described in section 2.1. A further detailed representation of the OB manifold and the co-axial channel are shown in Figure. In this region, the applied magnetic field considered for the calculation is the toroidal component that is perpendicular to the channel cross section plane, while the PbLi flows in parallel through the two channels. The geometrical parameters of the co-axial channel are reported in Table 5.3. The reference model for the MHD evaluation in the manifold region is taken from Refs. [30, 29].

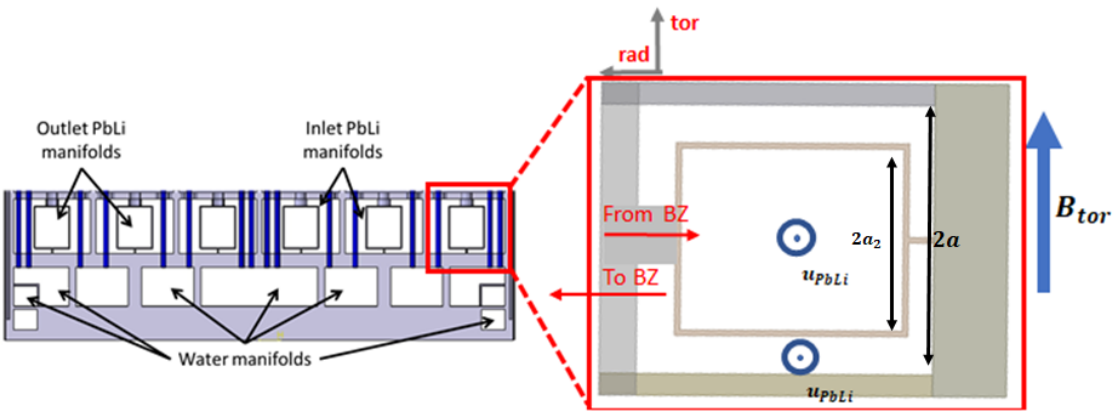

Figure 5.3: Left: OB manifold region, toroidal-radial view [30]. Right: manifold co-axial channel, radial-toroidal view [31].

One of the problem of the manifold is the presence of an unusual geometry configuration. Inside this region, the annular and external channel share an electro-conducting wall, in which currents generated in one fluid can interact with the adjacent ones and change the flow pattern. Therefore, the motion of the two adjacent electro-conducting fluids is coupled, in which they influence each other [30]. To estimate the manifold MHD loss and

Parameter	Symbol	Value	Units
Aspect ratio	$a/b = a_2/b_2$	1	
External side	2a	21.47	cm
Internal side	$2a_2$	12.60	cm
Wall thickness	t_w	0.30	cm
Annular cross section	A_{ext}	302	cm^2
Internal cross section	A_{int}	159	cm^2

Table 5.3: Geometrical parameters of OB co-axial channel

take into account this coupling effect, several correction factors are used that modified the 2D MHD pressure drop inside the channels. The 2D MHD pressure drop has been calculated at first with Eq. 3.13 and then modified with the correction factor $\epsilon_{E,c}$ for the annular channel and $\epsilon_{I,c}$ for the internal one. In the coupling scenario, in which the 2D pressure drop of both channels are modified to represent the mutual coupling effect, the corrective factor for the annular channel is $\epsilon_{E,c} = 1.59$, while for the internal channel it is $\epsilon_{I,c} = 2.41$. For a more conservative scenario, to take into account additional 3D losses due to the presence of cooling obstacle pipes and BZ outlet, the annular corrective factor is equal to the internal one ($\epsilon_{E,c} = \epsilon_{I,c} = 2.41$). These coefficient have been obtained from numerical simulations described in Refs. [49, 50].

The other critical points of this region are that the mass flow rate and the magnetic field vary along the manifold length. Regarding the first, it decreases linearly in the annular channel due to the fact that it loads the PbLi to the BZ along the blanket segment, while it increases in the internal channel for the opposite function. Else regarding the magnetic field, it varies along the manifold segment according to the WCLL field profile described in section 2.2. For this reason, a manifold discretization has been adopted for the Modelica simulation. The manifold has been divided into eight sections in which nine BZ cells equally spaced have been considered, named "OBXX", where "XX" indicates the BZ cell position (for instance "OB01" for the first BZ cell). All the cells have the same lengths and channel dimensions (annular and internal), in which the characteristic length L_{ch} corresponds to the half-width of the annular channel in the magnetic field direction, i.e. $L_{ch} = a$. For each section a different input magnetic field value is imposed, according to the position, and a flow rate corrective factor that modifies the 2D pressure drop value, to take into account the amount of the liquid flow rate that flows in that specific region. All these parameters are reported in Table 5.4, in particular the manifold spinal position (S), the section length (L), the applied magnetic field (B) and the percentage of mass flow rate in the annular and internal channel (f_{perc}). The overall blanket segment is 17 m long, in which every section has a length of 2.125 m. The magnetic field intensity is higher in the top and bottom of the BB, while it is lower in correspondence of the equatorial position. Regarding the liquid mass flow rate coefficient, it is different for annular and internal channel according to the percentage amount of flow rate that flows inside in each specific section, in particular the annular f_{perc} decreases along the spinal length to represents the reducing mass flow rate, while the internal f_{perc} increases.

Section	S [m]	L [m]	B [T]	Annular f_{perc}	Internal f_{perc}
1	0 2.125	2.125	4.92	1	0
2	2.125 4.25	2.125	4.34	0.875	0.125
3	4.25 6.375	2.125	3.91	0.750	0.250
4	6.375 8.5	2.125	3.65	0.625	0.375
5	8.5 10.625	2.125	3.73	0.500	0.500
6	10.625 12.75	2.125	4.07	0.375	0.625
7	12.75 14.875	2.125	4.72	0.250	0.750
8	14.875 17	2.125	5.10	0.125	0.875

Table 5.4: OB manifold Modelica simulation parameters.

The Modelica model used for the manifold pressure drops estimation is shown in Figure 5.4. This model is divided into two parts: the left side represents the annular channel while the right side the internal channel. Both sides are composed by eight sections modelled as a 2D pressure drop component to simulate the distributed loss along the manifold. Each section represents a portion of the annular or the internal channel with the input geometry parameters indicated in Table 5.3 and magnetic field distribution according the Table 5.4. The 2D pressure drop for every section is estimated according the Eq. 3.13 modified with the corresponding coupling coefficient ($\epsilon_{E,c}$ or $\epsilon_{I,c}$) and the percentage mass flow rate coefficient f_{perc} as discussed above. The inlet PbLi mass flow rate (2.73 kg/s) (considering one of the six parallel channel) and its temperature (600 K) are included in the flow rate source located at the starting point, while a pressure sink concludes and completes the model. The wall electrical conductivity is the same for each section ($\sigma_w = 1.15 \cdot 10^6\ S/m$).

The manifold losses have been obtained from the Modelica model simulations carried out for different BZ cell positions for one of the six parallel channels. According to the manifold discretization, there are nine BZ cells considered, where the portion of the annular and internal channel changes for each position. The calculation strategy consists considering only the corresponding annular and internal channel sections for each particular loop based on the BZ position, removing the other ones imposing $L = 0$. For example, for the OB01, the annular channel is removed and the internal channel is considered completely; for the OB02 the first section of the annular channel and the all internal channel sections, except the first, are considered, and so on. The complete strategy is reported in Table 5.5.

The MHD manifold losses are reported in Figure 5.5. The Modelica simulation results are indicated with green bars according to the BZ cell position. These results have been

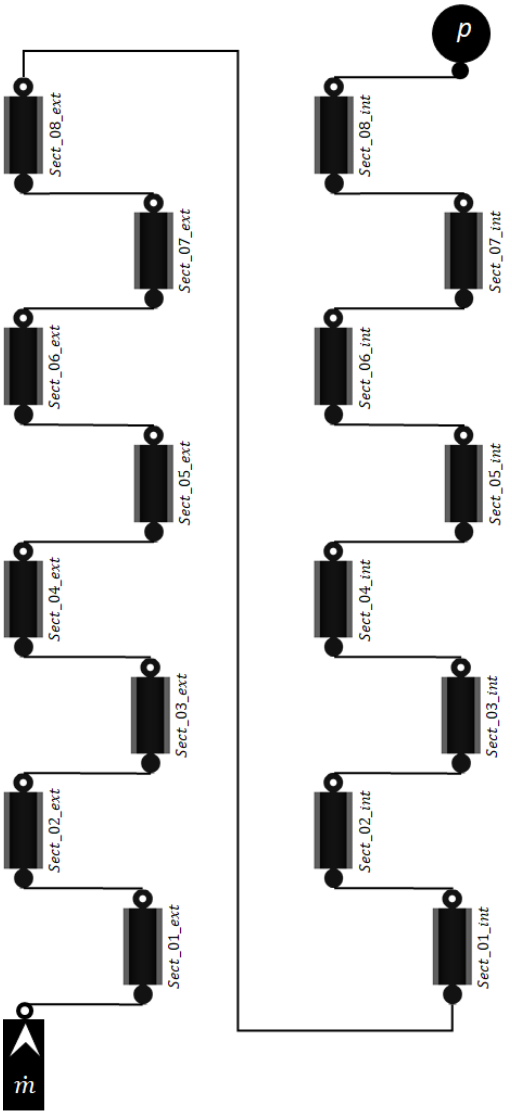

Figure 5.4: Manifold Modelica model. The left side represents the annular channel while the right side the internal one.

calculated in the conservative scenario imposing the same coupling corrective coefficient both for the annular and internal channel ($\epsilon_{E,c} = \epsilon_{I,c} = 2.41$). An additional corrective factor ($f_{corr} = 1.1$) is used for the accuracy of the simulations as explained in Subsection 4.3.3. In general, the Modelica results agree very well with the MHD manifold pressure drop taken from the literature in the conservative scenario (blue line) [29], in which the relative error (represented by the error bars) is under the acceptable one (≈ 15 %), except the last BZ cell position where it is slightly above (see Figure 5.6). In general, the pressure drop

Cell position	Annular sections	Internal sections
OB01	none	1,2,3,4,5,6,7,8
OB02	1	2,3,4,5,6,7,8
OB03	1,2	3,4,5,6,7,8
OB04	1,2,3	4,5,6,7,8
OB05	1,2,3,4	5,6,7,8
OB06	1,2,3,4,5	6,7,8
OB07	1,2,3,4,5,6	7,8
OB08	1,2,3,4,5,6,7	8
OB09	1,2,3,4,5,6,7,8	none

Table 5.5: OB manifold Modelica sections considered for each simulation based on BZ cell position

behaviour, obtained from the simulations, along the spinal manifold length is almost the same as that the conservative and simple coupling scenario (red dashed line) in which the corrective factors are $\epsilon_{E,c} = 1.59$ for the annular channel and $\epsilon_{I,c} = 2.41$ for the internal channel. The manifold losses increase from the bottom position towards the equatorial plane, where they achieve the maximum value at position OB04 ($\approx 243\ kPa$), and then they decrease towards the top of the BB where the minimum value ($\approx 100\ kPa$) is reached. This behaviour is principally ascribable to the different channel cross sections. For lower BZ positions, the major portion of the manifold is composed by the internal channel that has a smaller duct cross section ($159\ cm^2$) respect to the annular one ($302\ cm^2$), while for upper BZ positions, the manifold duct is composed principally by the annular channel. This phenomenon is then governed by other factors, such as the variable magnetic field along the BB and the decrease and increase of the PbLi mass flow rate in the annular and internal channel respectively.

IB manifold

The IB manifold layout ha been described in section 2.1. A detailed representation of the IB manifold and its co-axial channel are represented in Figure 5.7. As for the OB manifold, the applied magnetic field considered for calculations is the toroidal component that is perpendicular to the channel cross section plane, and the PbLi flows in parallel through the two channels. The geometrical dimensions of the co-axial channels are reported in Table 5.6. The reference model for the IB manifold is the same of the OB case (Refs. [30, 29]).

The IB manifold presents the same coupling effect problem of the OB manifold. For this reason, to estimated the losses in this region, the 2D MHD pressure drops are modified with the same coupling corrective coefficients adopted for the OB case both for the coupling ($\epsilon_{E,c} = 1.59$ and $\epsilon_{I,c} = 2.41$) and conservative scenario ($\epsilon_{E,c} = \epsilon_{I,c} = 2.41$). Regarding the variable magnetic field and mass flow rate inside the BB, it is adopted the same discretization of the OB manifold, in which it has been divided into eight sections and nine BZ cells equally spaced have been considered, named "IBXX" where "XX" indicates the BZ position. All the cells have the same lengths and channel dimensions (annular and internal), in which the characteristic length L_{ch} corresponds to the half-width of the

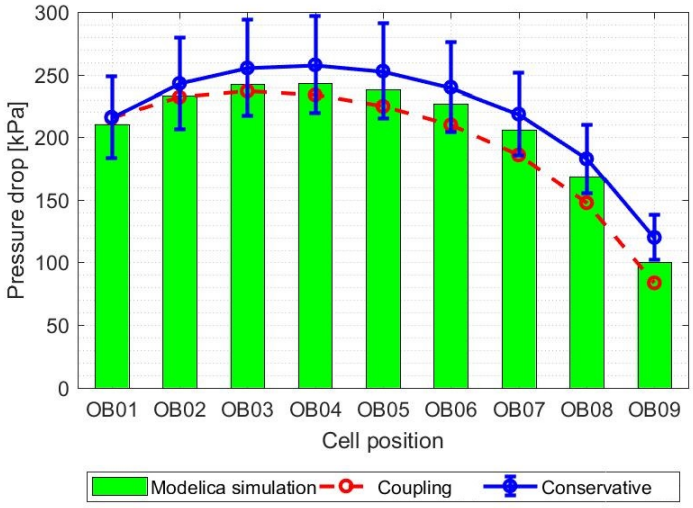

Figure 5.5: OB manifold pressure drops according to BZ cell position. The green bars represent the Modelica simulation results, the red dashed and the blue lines represents the coupling and the conservative losses respectively taken from the literature [29].

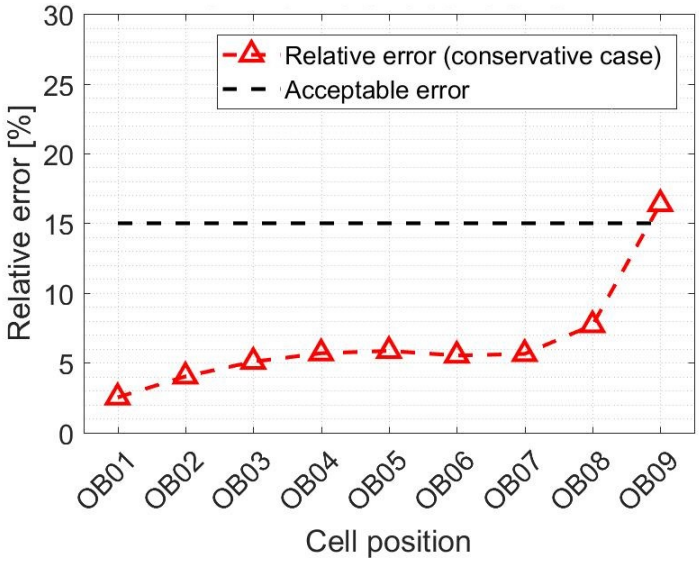

Figure 5.6: OB manifold relative error respect to the conservative scenario. The relative error is obtained with the relation: $\frac{|\Delta p_{BZ,lit} - \Delta p_{BZ,sim}|}{\Delta p_{BZ,lit}} \cdot 100$
.

annular channel in the magnetic field direction ($L_{ch} = a$). All the parameters used for each section are reported in Table 5.7. The overall IB manifold is 15.72 m long, less than the

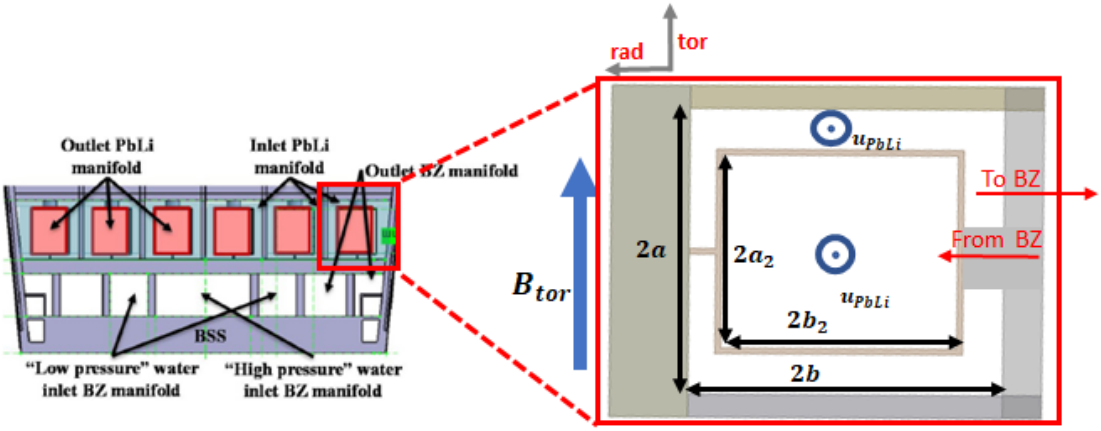

Figure 5.7: Left: IB manifold region, toroidal-radial view [8]. Right: manifold co-axial channel, radial-toroidal view [31].

Parameter	Symbol	Value	Units
Toroidal annular length	$2a$	14.8	cm
Radial annular length	$2b$	15.6	cm
Toroidal internal length	$2a_2$	10.5	cm
Radial internal length	$2b_2$	12.6	cm
Wall thickness	t_w	0.30	cm
Annular cross section	A_{ext}	104.5	cm^2
Internal cross section	A_{int}	132.3	cm^2

Table 5.6: Geometrical parameters of IB co-axial channel.

OB manifold, and each section has a length of 1.965 m. The magnetic field is the same for 2/3 of the blanket in which it reach the maximum value (8.64 T), while it decreases in the top of the BB (see 2.2). Also for the IB case, the mass flow rate percentage factor f_{perc} is used with the same purpose of the OB manifold.

The Modelica model used for the IB manifold pressure drops estimation is the same of the OB case, represented in Figure 5.4. The left and right side represents the annular and internal channel respectively, in which each section simulates the 2D pressure drop inside that specific portion of the manifold according the Eq. 3.13 modified with the coupling coefficients ($\epsilon_{E,c}$ or $\epsilon_{I,c}$) and the percentage mass flow rate factor (f_{perc}). The input geometrical and magnetic field parameters for each manifold portion are reported in Table 5.6 and 5.7, while, regarding the wall electrical conductivity, it is fixed in all manifold sections ($\sigma_w = 1.15 \cdot 10^6\ S/m$). The input PbLi mass flow rate ($0.8867 kg/s$) (considering one of the six parallel channel) and temperature (600 K) have been used in the mass flow rate source located at the starting point of the model, while a pressure sink component concludes and completes the model.

Section	S [m]	L [m]	B [T]	Annular f_{perc}	Internal f_{perc}
1	0 1.965	1.965	8.64	1	0
2	1.965 3.93	1.965	8.64	0.875	0.125
3	3.93 5.895	1.965	8.64	0.750	0.250
4	5.895 7.86	1.965	8.64	0.625	0.375
5	7.86 9.825	1.965	7.50	0.500	0.500
6	9.825 11.79	1.965	6.98	0.375	0.625
7	11.79 13.755	1.965	6.09	0.250	0.750
8	13.755 15.72	1.965	5.20	0.125	0.875

Table 5.7: IB manifold Modelica simulation parameters.

The IB manifold losses have been calculated for one of the six parallel channel with the same strategy adopted for the OB case. For each IB BZ cell position, different portions of the annular and internal channel have been considered. The complete strategy is reported in Table 5.8.

Cell position	Annular sections	Internal sections
IB01	none	1,2,3,4,5,6,7,8
IB02	1	2,3,4,5,6,7,8
IB03	1,2	3,4,5,6,7,8
IB04	1,2,3	4,5,6,7,8
IB05	1,2,3,4	5,6,7,8
IB06	1,2,3,4,5	6,7,8
IB07	1,2,3,4,5,6	7,8
IB08	1,2,3,4,5,6,7	8
IB09	1,2,3,4,5,6,7,8	none

Table 5.8: IB manifold Modelica sections considered for each simulation based on BZ cell position.

The MHD IB manifold are reported in Figure 5.8. The Modelica simulation results are indicated with green bars according to the BZ cell position. These results have been calculated in the conservative scenario imposing the same coupling corrective coefficient both for the annular and internal channel ($\epsilon_{E,c} = \epsilon_{I,c} = 2.41$). In this case, the Modelica results agrees very well with the MHD manifold pressure drop taken from the literature in the conservative scenario (blue line) [29] without any corrective factor. The accuracy

of the simulation results is evident in the fact that they are inside the conservative results error bars, further demonstrated in Figure 5.9, in which the relative error for each BZ cell position in always below the acceptable one ($\approx$ 15 %). The general behaviour of the MHD losses is inverted respect with the OB case. The MHD losses rapidly increase from the bottom BB to the equatorial plane, where they achieve the maximum value at IB05 ($\approx$ 473 kPa), and then decrease slowly towards the top BB. Unlike the OB case, in the IB manifold the largest amount of the MHD losses happens in the top part of the blanket, while they are lower in the bottom part where the minimum value ($\approx$ 245 kPa) is reached in IB01. This trend inversion is principally due to the different channel cross section, where in this case the annular one (104 cm^2) is smaller then the internal one (132.3 cm^2). Another big difference between the OB and IB case is represented by the pressure drop discrepancy, where for IB case the maximum loss is $\approx$ 473 kPa while for the IB case is $\approx$ 243 kPa, that is almost the same to the minimum for the IB manifold ($\approx$ 245 kPa). Such difference is due for two reasons: the first is the smaller cross section of the annular and internal channel in the IB manifold, as mentioned before, and the second reasons is ascribable to the higher applied magnetic field that is present in the IB blanket that contributes more to the 2D pressure drops inside this region.

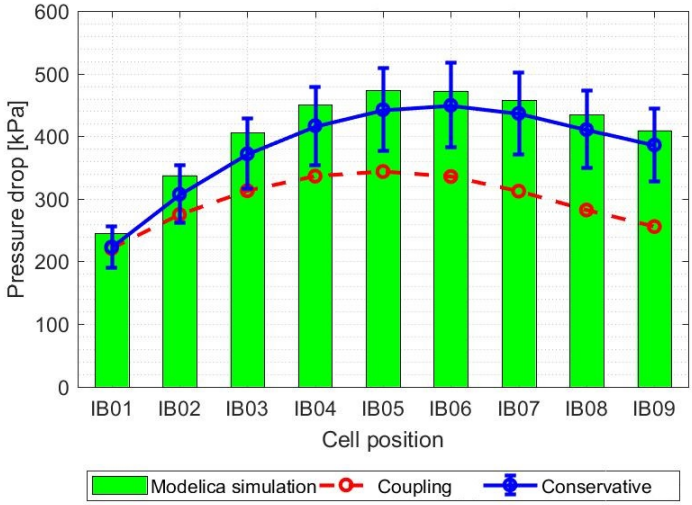

Figure 5.8: IB manifold pressure drops according to BZ cell position. The green bars represent the Modelica simulation results, the red dashed and the blue lines represents the coupling and the conservative losses respectively taken from the literature [29].

5.1.3 Feeding pipe

The third component analysed in this section is the feeding pipe. As mentioned is section 2.1, the DEMO WCLL 2018 FP design is chosen. It is an electro-conducting pipe placed in the lower part of the VV, and its function is to feed the liquid metal from the ex-vessel PbLi loop to the manifold region. In the WCLL design there are two feeding pipes, the

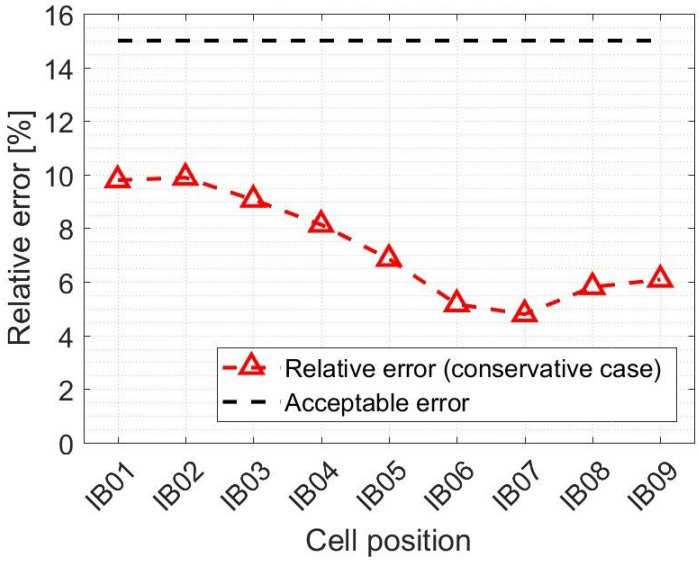

Figure 5.9: IB manifold relative error respect to the conservative scenario. The relative error is obtained with the relation: $\frac{|\Delta p_{BZ,lit} - \Delta p_{BZ,sim}|}{\Delta p_{BZ,lit}} \cdot 100$
.

OB FP and the IB FP, that have different layouts and geometrical dimensions. In the following, both OB and IB feeding pipes are analysed.

OB feeding pipe

The reference model taken into account for the OB FP is Ref. [30]. The general layout of the OB FP is shown in Figure 5.10, where the boxes report the portions of the FP implemented in the Modelica model, shown in Figure 5.11. The OB FP is an electro-conducting pipe with a nominal diameter DN200 (see Table 2.1), so the channel geometrical dimensions are reported in Table 5.9. The PbLi mass flow rate, imposed in the mass flow rate source in the Modelica model, is 16.38 kg/s, while the liquid metal temperature is 600 K. The wall electrical conductivity is fixed for all the components ($\sigma_w = 1.15 \cdot 10^6$). The Modelica model is composed by 2D and 3D pressure drop components, where the first estimate the 2D losses with the Eq. 3.13 for circular pipes and the second the 3D pressure drops with Eq. 3.21 according to the loss type as mentioned is section 3.3.2. The characteristic length L_{ch} is equal to the inner radius r_i for all the components. As usual, a pressure sink component concludes and completes the model.

The complete OB FP Modelica model is structured as follow:

- **Section 1 (FPB1)**: horizontal flow from the ex-vessel loop. 2D pressure drop component in which the applied magnetic field (poloidal) is $B_{pol} = 0.53\ T$, the channel length $L = 13\ m$.
- **Section 2 (FPB_bend1)**: 100° bend parallel to the magnetic field. 3D pressure

Parameter	Symbol	Value	Units
Inner radius	r_i	9.75	cm
Outer radius	r_o	11	cm
Wall thickness	t_w	1.25	cm
Channel cross section	A	296	cm^2

Table 5.9: OB FP geometrical parameters.

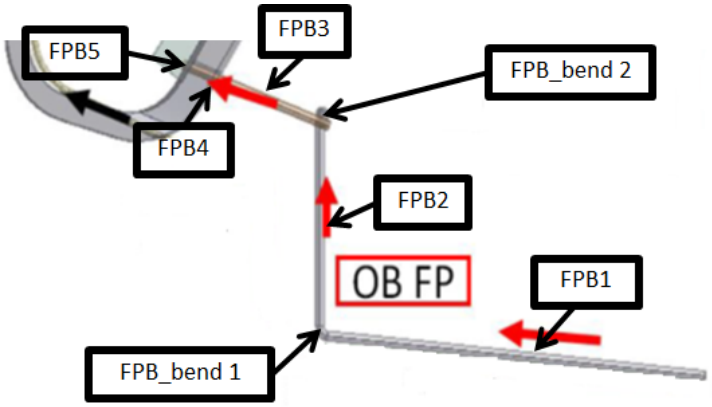

Figure 5.10: OB FP layout: radial-poloidal view. The Modelica components are indicated in boxes. The PbLi flow direction is highlighted by red arrows [30].

drop component in which the applied magnetic field (poloidal) is $B_{pol} = 1.1375\ T$.

- **Section 3 (FPB2)**: vertical flow outside TFC. 2D pressure drop component in which the applied magnetic field (poloidal) is $B_{pol} = 1.745\ T$, the channel length $L = 6\ m$.
- **Section 4 (FPB_bend2)**: 120° bend parallel to the magnetic field. 3D pressure drop component in which the applied magnetic field (poloidal) is $B_{pol} = 2.3525\ T$.
- **Section 5 (FPB3)**: flow outside TFC. 2D pressure drop component in which the applied magnetic field (poloidal) is $B_{pol} = 2.96\ T$ assumed uniform, the channel length $L = 2.5\ m$.
- **Section 6 (FPB4)**: flow through TFC. 2D pressure drop component. Magnetic field follows exponential law inside coil from zero to maximum value. For conservative reason, the maximum magnetic field value is chosen ($B_{tor} = 4.28\ T$). The channel length is $L = 1\ m$.
- **Section 7 (FPB5)**: flow inside TFC. 2D pressure drop component in which the applied magnetic field (toroidal) is $B_{tor} = 4.52\ T$, the channel length $L = 1.5\ m$.

The components FPB1, FPB_bend1, FPB2, FPB_bend2, FPB3 are outside the TFCs, while the components FPB4 and FPB5 are inside.

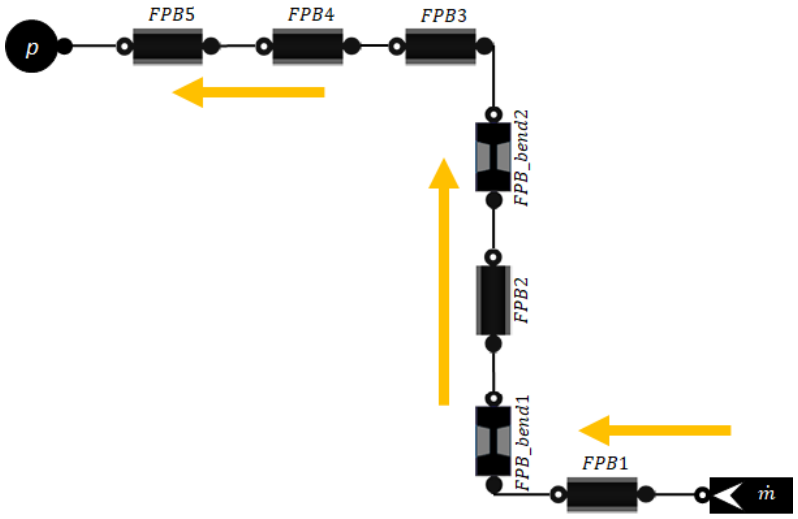

Figure 5.11: OB FP Modelica model. The orange arrows indicate the PbLi flow direction. The corresponding component are represented in Figure 5.10.

The Modelica simulation results are reported in Table 5.10. The overall OB FP pressure drop obtained in literature [29] is $\Delta p_{OB\ FP,lit} = 613\ kPa \pm 15\%$, while the total loss estimated in the simulation is $\Delta p_{OB\ FP,sim} = 617\ kPa$. The Modelica results agrees with an excellent approximation, with a relative error of $\approx 0.66\%$. In general, most losses are concentrated in the last part of the OB FP, closed the TFC where the magnetic field intensity is higher, while in the two bends the pressure drops are very low. The overall pressure drop inside the TFC is $\approx 321.1\ kPa$, while outside is $\approx 295.9\ kPa$. In conclusion, the OB FP Modelica model represents with a good approximation the OB feeding pipe.

Component	Δp [kPa]
FPB1	24.6
FPB_bend1	0.4
FPB2	122.9
FPB_bend2	2.2
FPB3	145.8
FPB4	120.2
FPB5	200.9
Total	617.0

Table 5.10: OB FP Modelica simulation pressure drops.

IB feeding pipe

The reference model taken into account for the IB FP is Ref. [30]. The general layout of the IB FP is shown in Figure 5.12, where the boxes report the portions of the FP implemented in the Modelica model, shown in Figure 5.13. The IB FP is an electro-conducting pipe with

a nominal diameter DN125 (see Table 2.1), then the channel geometrical dimensions are reported in Table 5.11.The PbLi mass flow rate, imposed in the mass flow rate source in the Modelica model, is 5.32 kg/s, while the liquid metal temperature is 600 K. The wall electrical conductivity is fixed for all the components ($\sigma_w = 1.15 \cdot 10^6$). The Modelica model is composed by 2D and 3D pressure drop components, in the same way of the OB FP. The 2D losses have been estimated with the Eq. 3.13 for circular pipes, while the 3D losses with Eq. 3.21 according to the loss type as mentioned in section 3.3.2. The characteristic length L_{ch} is always the inner radius r_i. At the end, the pressure sink component concludes the model.

Parameter	Symbol	Value	Units
Inner radius	r_i	6.19	cm
Outer radius	r_o	6.99	cm
Wall thickness	t_w	0.8	cm
Channel cross section	A	120.18	cm^2

Table 5.11: IB FP geometrical parameters.

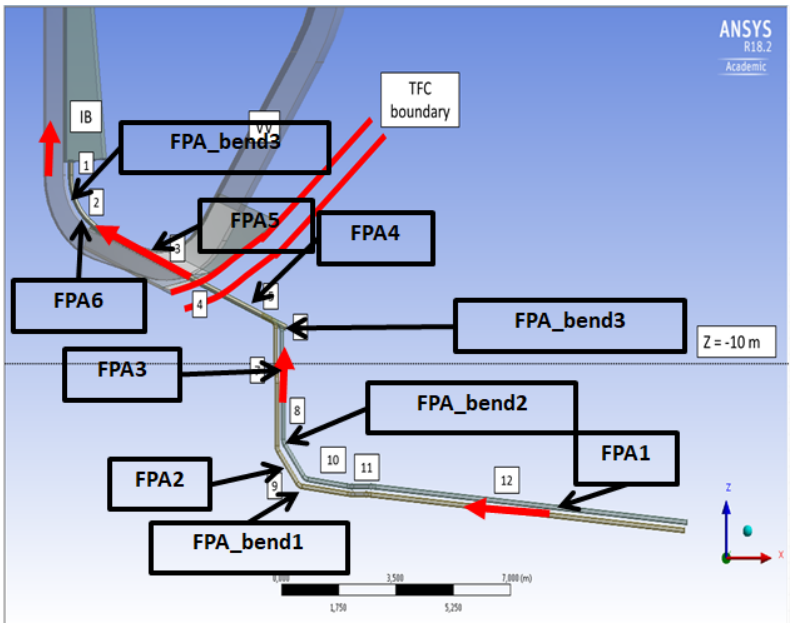

Figure 5.12: IB FP layout: radial-poloidal view. The Modelica components are indicated in boxes. The PbLi flow direction is highlighted by red arrows [31].

The complete IB FP Modelica model is structure as follow:

- **Section 1 (FPA1)**: horizontal flow from the ex-vessel loop. 2D pressure drop component in which the applied magnetic field (poloidal) is $B_{pol} = 0.53\ T$, the channel length $L = 14\ m$.
- **Section 2 (FPA_bend1)**: 45° bend parallel to the magnetic field. 3D pressure

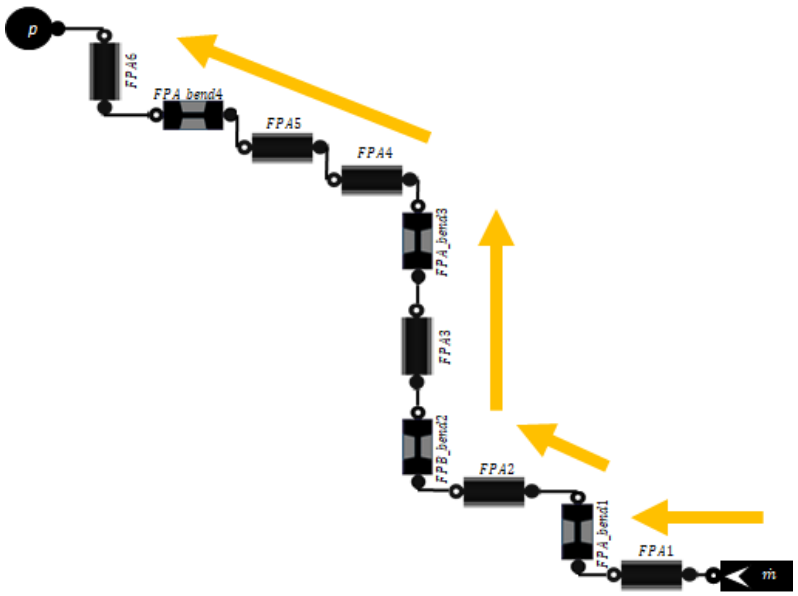

Figure 5.13: IB FP Modelica model. The orange arrows indicate the PbLi flow direction. The corresponding component are represented in Figure 5.12.

drop component in which the applied magnetic field (poloidal) is $B_{pol} = 0.53\ T$.

- **Section 3 (FPA2)**: oblique flow (45°) outside the TFC. 2D pressure drop component in which the applied magnetic field (poloidal) is $B_{pol} = 0.53\ T$, the channel length $L = 2\ m$.
- **Section 4 (FPA_bend2)**: 45° bend parallel to the magnetic field. 3D pressure drop component in which the applied magnetic field (poloidal) is $B_{pol} = 0.53\ T$.
- **Section 5 (FPA3)**: vertical flow outside the TFC. 2D pressure drop component in which the applied magnetic field (poloidal) is $B_{pol} = 0.87\ T$, the channel length $L = 5\ m$.
- **Section 6 (FPA_bend3)**: 45° bend parallel to the magnetic field. 3D pressure drop component in which the applied magnetic field (poloidal) is $B_{pol} = 0.87\ T$.
- **Section 7 (FPA4)**: oblique flow (45°) outside the TFC. 2D pressure drop component in which the applied magnetic field (poloidal) is $B_{pol} = 1.41\ T$, the channel length $L = 4\ m$.
- **Section 8 (FPA5)**: oblique flow (45°) through the TFC. 2D pressure drop component. Magnetic field follows exponential law inside coil from zero to maximum value. For conservative reason, the maximum magnetic field value is chosen ($B_{tor} = 6.08\ T$). The channel length is $L = 3\ m$.
- **Section 8 (FPA_bend4 + FPA6)**: curved flow inside the TFC. 2D component (FPA6) and 3D component (FPA_bend4) that represent the 2D flow with a 45° bend

perpendicular to the applied magnetic field (toroidal). The magnetic field value is $B_{tor} = 7.36\ T$ and the channel length is $L = 3\ m$.

The components FPA1, FPA_bend1, FPA2, FPA_bend2, FPA3, FPA_bend3 and FPA4 are outside the TFCs, while the components FPA5, FPA_bend4 and FPA6 are inside.

The Modelica simulation results are reported in Table 5.12. The overall IB FP pressure drop obtained in literature [29] is $\Delta p_{IB\ FP,lit} = 1557\ kPa \pm 15\%$, while the total loss estimated in the simulation is $\Delta p_{IB\ FP,sim} = 1567.2\ kPa$. The Modelica results agrees with an excellent approximation, with a relative error of $\approx 0.65\%$. Most losses are concentrated in the last part of the IB FP, inside the TFC where the magnetic field intensity is very high, while in the bends the pressure drops are very low. The overall pressure drop inside the TFC is $\approx 1479.4\ kPa$, while outside is $\approx 87.8\ kPa$. In general, there is a big discrepancy between the IB and OB FP, in fact the losses of the first are much higher then the latter due to the greater pipe length and the stronger magnetic field intensity in the IB segment. In conclusion, the IB FP Modelica model represents with a very good accuracy the IB feeding pipe.

Component	Δp [kPa]
FPA1	21.2
FPA_bend1	0.021
FPA2	3.03
FPA_bend2	0.021
FPA3	20.4
FPA_bend3	0.06
FPA4	42.9
FPA5	598.9
FPA_bend4	2.8
FPA6	877.7
Total	1567.2

Table 5.12: IB FP Modelica simulation pressure drops.

5.1.4 Draining pipe

The fourth and last component analysed in this section is the draining pipe. As mentioned in section 2.1, the DEMO WCLL 2018 DP design is chosen. It is an electro-conducting pipe placed in the upper part of the VV, and its function is to collect the liquid metal from the manifold and bring it up towards the ex-vessel PbLi loop. In the WCLL design there are two draining pipes, the OB DP and IB DP, that have different layouts and geometrical dimensions. In the following, both OB and IB draining pipes are analysed.

OB draining pipe

The reference model taken into account for the OB DP is Ref. [30]. The general layout of the OB DP is shown in Figure 5.14, in which the boxes report the portions of the FP implemented in the Modelica model, shown in Figure 5.15. The OB DP is an electro-conducting pipe with two sections: the first one has a nominal diameter DN200 while the second one is DN350 (see Table 2.1). This channel variation is located in correspondence of the horizontal pipe. The channel geometrical dimensions are reported in Tables 5.13 for DN200 and 5.14 for DN350. The PbLi mass flow rate, imposed in the mass flow rate source in the Modelica model, is $16.38 kg/s$ and the liquid metal temperature is 600 K. The wall electrical conductivity is fixed for all the components ($\sigma_w = 1.15 \cdot 10^6$). The Modelica model is composed by 2D and 3D pressure drop components, where the first estimate the 2D losses with the Eq. 3.13 for circular pipes and the second the 3D pressure drops with Eq. 3.21 according to the loss type as mentioned is section 3.3.2. The characteristic length L_{ch} is equal to the inner radius r_i for all the components. As usual, a pressure sink component concludes and completes the model.

Parameter	Symbol	Value	Units
Inner radius	r_i	9.75	cm
Outer radius	r_o	11	cm
Wall thickness	t_w	1.25	cm
Channel cross section	A	296	cm^2

Table 5.13: OB DP geometrical parameters for DN200.

Parameter	Symbol	Value	Units
Inner radius	r_i	17.3	cm
Outer radius	r_o	19.2	cm
Wall thickness	t_w	1.9	cm
Channel cross section	A	940	cm^2

Table 5.14: OB DP geometrical parameters for DN350.

The complete OB DP Modelica model is structure in this way:

- **Section 1 (DPB1)**: oblique flow inside the TFC. 2D pressure drop component in which the applied magnetic field (toroidal) is $B_{tor} = 3.92\ T$, the channel length $L = 0.55\ m$.
- **Section 2 (DPB2 + DPB2_bend)**: curved flow inside the TFC with a 60° bend. 2D component (DPB2) and 3D component (DPB2_bend) that represent the 2D flow with a 60° bend perpendicular to the applied magnetic field (toroidal). The magnetic field value is $B_{tor} = 3.92\ T$ and the channel length is $L = 0.52\ m$.
- **Section 3 (DPB3)**: vertical flow inside the TFC. 2D pressure drop component in which the applied magnetic field (toroidal) is $B_{tor} = 3.92\ T$, the channel length $L = 1.07\ m$.

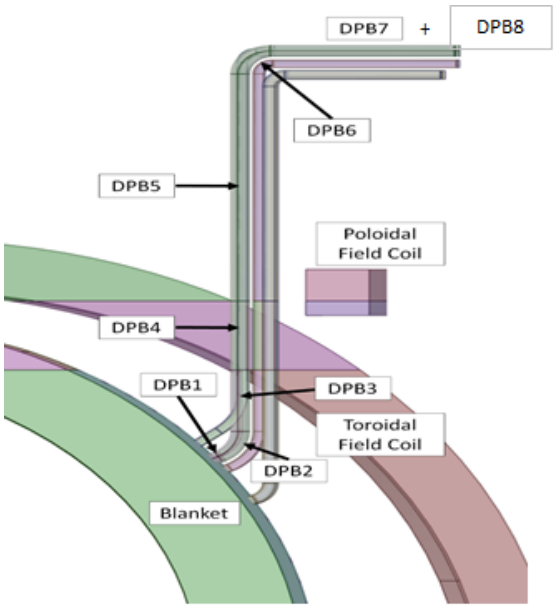

Figure 5.14: OB DP layout: radial-poloidal view. The Modelica components are indicated in boxes [28].

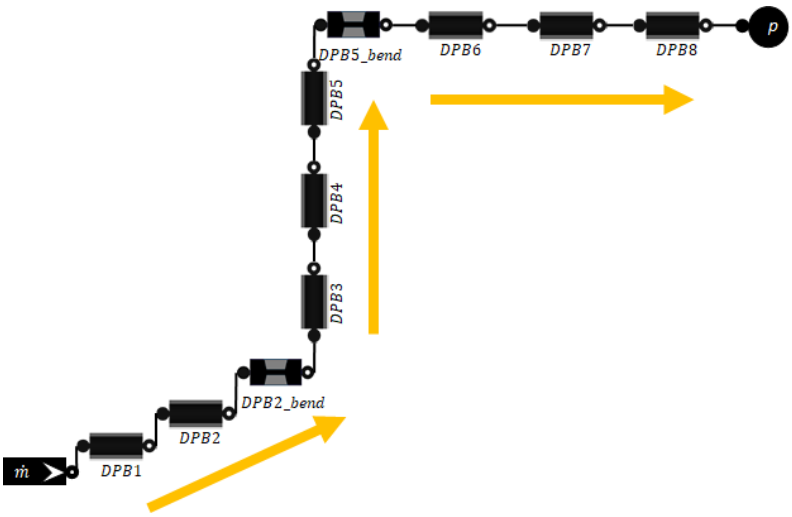

Figure 5.15: OB DP Modelica model. The orange arrows indicate the PbLi flow direction. The corresponding component are represented in Figure 5.14.

- **Section 4 (DPB4)**: vertical flow through the TFC. 2D pressure drop component. Magnetic field follows exponential law inside coil from zero to maximum value. For conservative reason, the maximum magnetic field value is chosen ($B_{tor} = 3.92\ T$). The channel length is $L = 1.20\ m$.

- **Section 5 (DPB5)**: vertical flow outside the TFC. 2D pressure drop component in which the applied magnetic field (poloidal) is $B_{pol} = 0.33\ T$, the channel length $L = 8\ m$.
- **Section 6 (DPB6 + DPB6_bend)**: curved flow outside the TFC with a 90° bend. 2D component (DPB6) and 3D component (DPB6_bend) that represent the 2D flow with a 90° bend parallel to the applied magnetic field (poloidal). The magnetic field value is $B_{pol} = 0.8\ T$ and the channel length is $L = 0.63\ m$.
- **Section 7 (DPB7 + DPB8)**: horizontal flow outside the TFC. This section is divided in two components due the channel cross section variation (here not modelled): the DPB7 is the pipe DN200 and the DPB8 is the pipe DN350. Both are 2D pressure drop components in which the applied magnetic field (poloidal) is $B_{pol} = 0.8\ T$. The DPB7 and DPB8 lengths are $L = 2.30\ m$ and $L = 11\ m$ respectively.

The components DPB1, DPB2, DPB2_bend, DPB3 and DPB4 are inside the TFCs, while the components DPB5, DPB6, DPB6_bend, DPB7 and DPB8 are outside.

The Modelica simulation results are reported in Table 5.15. The overal OB DP pressure drop taken in literature [29] is $\Delta p_{OB\ DP,lit} = 376\ kPa \pm 15\%$, while the total loss estimated in the simulation is $\Delta p_{OB\ DP,sim} = 376.54\ kPa$. The Modelica results agrees with an excellent approximation, with a relative error of $\approx 0.14\%$. Most losses are concentrated in the first part of the OB DP, in that components that are inside the TFC where the magnetic field intensity is high. The overall pressure drop inside the TFC is $\approx 345.45\ kPa$, while in the external side is $\approx 31.09\ kPa$, revealing the large discrepancy between the two regions. In conclusion, the OB DP Modelica model represents with a very good approximation the OB draining pipe.

Component	Δp [kPa]
DPB1	56.72
DPB2	53.63
DPB2_bend	1.01
DPB3	110.34
DPB4	123.75
DPB5	5.85
DPB6	2.68
DPB6_bend	0.19
DPB7	9.66
DPB8	12.71
Total	376.54

Table 5.15: OB DP Modelica simulation pressure drops.

IB draining pipe

As for the OB DP, the reference model considered for the IB DP is Ref. [30]. The general layout of the IB DP is shown in Figure 5.16, in which the boxes report the portions of

the FP implemented in the Modelica model, shown in Figure 5.17. As the OB DP, the IB DP is an electro-conductive pipe divided in two sections, the vertical one has a nominal diameter DN150 while the horizontal one has DN200 (see Table 2.1). The pipe geometrical dimensions are reported in 5.16 for DN150 and 5.17 for DN200. The PbLi mass flow rate, imposed in the mass flow rate source of the Modelica model, is $5.32 kg/s$ and the liquid metal temperature is 600 K. The wall electrical conductivity is fixed for all the components ($\sigma_w = 1.15 \cdot 10^6$). The Modelica model is composed by 2D and 3D pressure drop components, where the first estimate the 2D losses with the Eq. 3.13 for circular pipes and the second the 3D pressure drops with Eq. 3.21 according to the loss type as mentioned is section 3.3.2. The characteristic length L_{ch} is equal to the inner radius r_i for all the components. At the end, a pressure sink component concludes and completes the model.

Parameter	Symbol	Value	Units
Inner radius	r_i	7.4	cm
Outer radius	r_o	8.4	cm
Wall thickness	t_w	1.0	cm
Channel cross section	A	172.7	cm^2

Table 5.16: IB DP geometrical parameters for DN150.

Parameter	Symbol	Value	Units
Inner radius	r_i	9.75	cm
Outer radius	r_o	11	cm
Wall thickness	t_w	1.25	cm
Channel cross section	A	296	cm^2

Table 5.17: IB DP geometrical parameters for DN200.

The complete IB DP Modelica model is structure as follow:

- **Section 1 (DPA1)**: vertical flow inside the TFC. 2D pressure drop component in which the applied magnetic field (toroidal) is $B_{tor} = 5.46\ T$, the channel length $L = 1\ m$.
- **Section 2 (DPA2)**: vertical flow through the TFC. 2D pressure drop component. Magnetic field follows exponential law inside coil from zero to maximum value. For conservative reason, the maximum magnetic field value is chosen ($B_{tor} = 5.46\ T$). The channel length is $L = 1\ m$.
- **Section 3 (DPA3)**: vertical flow outside the TFC. 2D pressure drop component in which the applied magnetic field (poloidal) is $B_{pol} = 0.314\ T$, the channel length $L = 3\ m$.
- **Section 4 (DPA4_bend)**: 90° bend parallel to the magnetic field. 3D pressure drop component in which the applied magnetic field (poloidal) is $B_{pol} = 1\ T$.

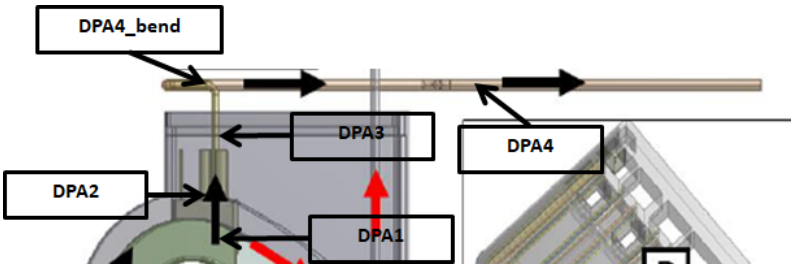

Figure 5.16: IB DP layout: radial-poloidal view. The Modelica components are indicated in boxes. The PbLi flow direction is indicated by black arrows [30].

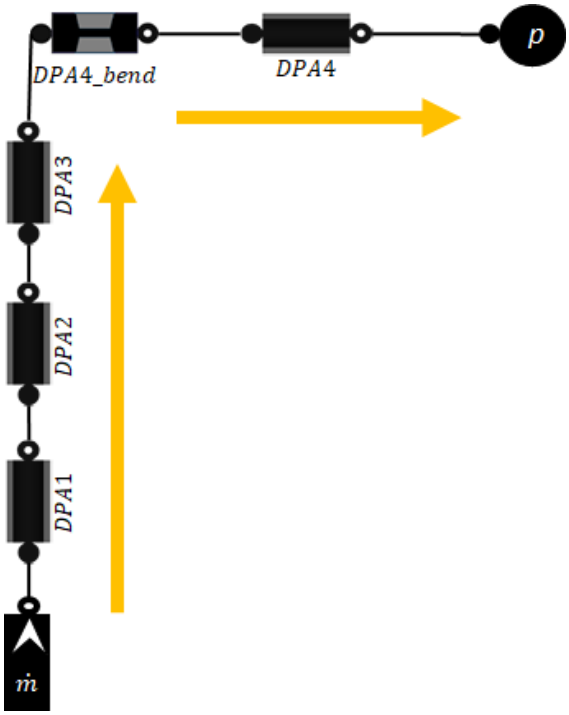

Figure 5.17: IB DP Modelica model. The orange arrows indicate the PbLi flow direction. The corresponding component are represented in Figure 5.16.

- **Section 5 (DPA4)**: horizontal flow outside the TFC. This section is modelled with DN200. 2D pressure drop component in which the applied magnetic field (poloidal) is $B_{pol} = 1\ T$, the channel length $L = 17\ m$.

The components DPA1 and DPA2 are inside the TFC, while the components DPA3, DPA4_bend and DPA4 are outside.

The Modelica simulation results are reported in Table 5.18. The overall IB DP pressure drop taken in literature [29] is $\Delta p_{IB\ DP,lit} = 260\ kPa \pm 15\%$, while the total loss estimated in the simulation is $\Delta p_{IB\ DP,sim} = 263.67\ kPa$. The Modelica results agrees with an excellent approximation, with a relative error of $\approx 1.14\%$. Most losses are concentrated in

the first part of the IB DP, in the components that are inside the TFC where the magnetic field intensity is high. The overall pressure drop inside the TFC is $\approx 231.72\ kPa$, while in the external side is $\approx 31.95\ kPa$, revealing the large discrepancy between the two regions. The IB DP has a lower pressure drop respect to the OB case, due to its smaller length despite the field intensity is higher. In conclusion, the IB DP Modelica model represents with a good approximation the IB draining pipe.

Component	Δp [kPa]
DPA1	115.86
DPA2	115.86
DPA3	1.15
DPA4_bend	0.11
DPA4	30.69
Total	263.67

Table 5.18: IB DP Modelica simulation pressure drops.

5.2 System-level modelling

In this section, the system-level modelling of the PbLi loop for the WCLL reactor design is treated. As a first step, the equatorial case has been analysed, both OB and IB case, to verify the correctness of the model with all four components implemented together and control that the Modelica simulation works completely. After that, the complete WCLL PbLi Modelica model has been developed for the OB and IB, at first considering only the MHD pressure drops inside the loop and then considering also the hydrostatic head in all the components.

5.2.1 Equatorial case model

The equatorial case model considers the PbLi loop with all four components (draining pipe, manifold, breeding zone cell and feeding pipe) implemented together, in which the BZ cell is located in the equatorial plane. For this analysis, the component models developed in the previous section, are implemented in the same system-level model, both for the OB and IB case, in which the PbLi mass flow rate and temperature are imposed. Moreover, the applied magnetic field values have been kept the same as the previous models, according to field profile in the WCLL design. At the end of this subsection, the OB and IB losses have been compared with the all four components ones summed together to control the completeness of the Modelica model, since they are placed in series.

Model description

The PbLi model is structured as follow: the first component is the feeding pipe, modelled according to the OB and IB FP: then there is the annular channel of the manifold in which the PbLi is brought from the FP to the BZ; after that there is the equatorial BZ cell (position OB05 or IB05 based on the OB and IB loop), and then the manifold internal

channel in which the PbLi goes from the BZ to the DP; at the end, the last component is the draining pipe where the PbLi is collected and goes towards the rest of the loop. In this configuration, the manifold is divided into two equals parts, in fact, because the BZ cell is located in the equatorial plane (centre of the BB), the half length of the annular and internal channels have been considered, in particular the first half for the annular duct and the second half for the internal duct. Regarding the input parameters for the channel geometries, magnetic fields and PbLi properties (see Appendix A), they have been kept the same as the previous models described in the section 5.1. In the following, both OB and IB equatorial case models are analysed.

OB Model

The WCLL PbLi loop for the OB equatorial case is represented in Figure 5.18, while the Modelica model is shown in Figure 5.19. The model is composed at first by the mass flow rate source (located in the bottom part), the OB FP, four manifold annular channel portions that represent the first half length of such duct, the equatorial BZ cell (OB05), the four manifold internal channel portions, simulating the second half length of the internal duct, the OB DP, and in the end, the pressure sink component. All components have been implemented in the same way as the previous section, maintaining the same geometry layouts, dimensions and the applied magnetic field values according to the position (toroidal or poloidal). The applied magnetic field in the BZ OB05 is 3.61 T. The PbLi temperature is fixed at 600 K and the wall electrical conductivity is equal to $1.15 \cdot 10^6$ S/m, while the PbLi mass flow rate value is 16.38 kg/s, imposed in the mass flow rate source. As mentioned in section 5.1, the manifold and the BZ cell have six parallel channels, then just one of them is considered in this simulation. Therefore, the PbLi mass flow rate is different in these components and the MHD losses have been modified taking into account the mass flow rate variation. In general, the MHD losses are linearly dependent to the liquid mass flow rate, therefore the MHD pressure drop can be modified multiplying or dividing for the portion of the mass flow rate that flows in that region. For the manifold, the liquid metal mass flow rate is one sixth of the total, so the MHD losses have been divided by six, while for the BZ pressure drop is adopted a corrective factor of 0.00153 that is the ratio between the mass flow rate in the BZ (0.025 kg/s) and the total one (16.38 kg/s). In this model, the bottom and top collectors have not been modelled, due of lack of information, concentrating to the main PbLi components.

The Modelica simulation results, expressed for each component, are reported in Table 5.19. The OB loss with the four components singularly simulated in the previous subsection is $\Delta p_{OB} = 1227.18$ kPa, obtained summing all the four pressure drops because they can be considered in series. The overall MHD pressure drop inside the OB equatorial case (OB05), obtained with this Modelica simulation, is $\Delta p_{OB,sim} = 1226.54$ kPa, that agrees very well with the loss results estimated considering the four components separately, so this model can represents with a very good accuracy the OB PbLi loop. Most of the losses appear in the OB FP (51.1 %) and in the OB DP (30.8 %) due to their greatest length and channel geometry; the rest is ascribable to the manifold region with a 18.1 %, while the BZ pressure drop can be neglected with a very low MHD loss. In these results, the collectors have not been modelled and the liquid metal hydrostatic head has not been considered.

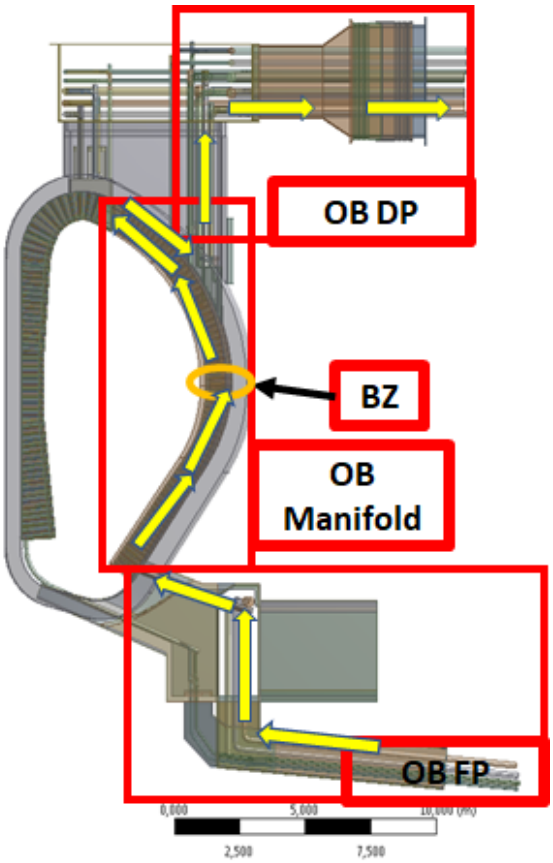

Figure 5.18: WCLL BB: radial-poloidal view. The PbLi loop is highlighted by yellow arrows. In the red boxes are indicated the several WCLL components. The equatorial BZ cell (OB05) is indicated by a orange circle (adapted from [31]).

Component	Δp [kPa]	% [-]
Feeding pipe	626.88	51.1
Manifold	221.56	18.1
Breeding zone	0.64	0.1
Draining pipe	377.46	30.8
Total	1226.54	100

Table 5.19: OB Modelica simulation pressure drops for equatorial case.

IB model

The WCLL PbLi loop for the IB equatorial case is represented in Figure 5.20, while the Modelica model is shown in Figure 5.21. This model is structurally composed as the OB case, with the mass flow rate source (located in the bottom part), the IB DP, four manifold annular channel sections, the IB BZ at the equatorial plane (IB05), four manifold internal

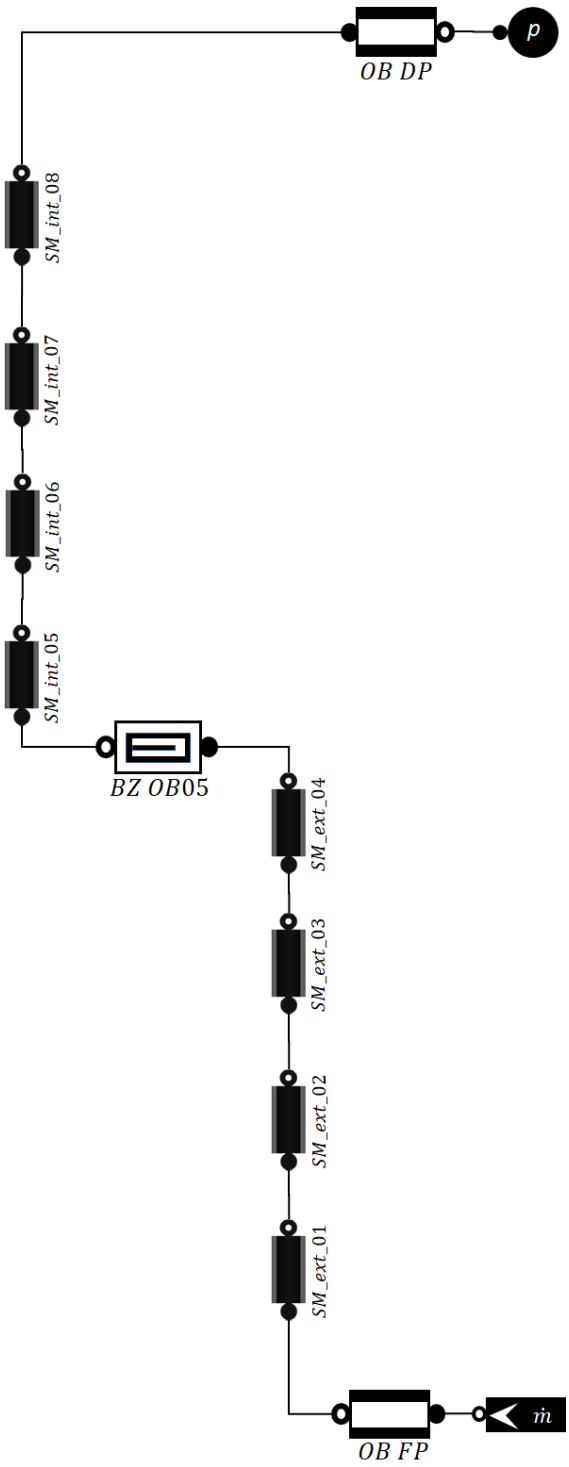

Figure 5.19: OB PbLi loop Modelica model for the equatorial case (OB05 loop).

channel sections, the IB DP and the pressure sink component. Also in this case, all components have been implemented in the same way as the previous section, maintaining the same dimension and the magnetic field intensities according to the position. The applied magnetic field in the IB05 is 8.07 T. The PbLi temperature is fixed at 600 K and the wall electrical conductivity is equal to $1.15 \cdot 10^6$ S/m, while the PbLi mass flow rate is 5.32 kg/s, imposed in the mass flow rate source. In this case, as the OB loop, the IB manifold and IB BZ cell are composed by six parallel channels. Considering one of the six channels in this simulation, the MHD pressure losses have been modified taking into account the mass flow rate portion that flow inside these components with the same strategy adopted in the OB case. For the manifold, the liquid metal mass flow rate is one sixth of the total, so the MHD losses have been divided by six, while for the BZ pressure drop is adopted a corrective factor of 0.0047 that is the ratio between the mass flow rate in the BZ (0.025 kg/s) and the total one (5.32 kg/s). In this model, the bottom and top collectors have not been modelled, due of lack of information, concentrating to the main PbLi components.

The Modelica simulation results, expressed for each component, are reported in Table 5.20. The IB loss with the four components singularly simulated in the previous subsection is $\Delta p_{IB} = 2307$ kPa, obtained summing all the four pressure drops because they can be considered in series. The overall MHD pressure drop inside the IB equatorial case (IB05), obtained with this Modelica simulation, is $\Delta p_{IB,sim} = 2321.09$ kPa, that agrees very well with the loss results estimated considering the four components separately, so this model can represents with a very good accuracy the IB PbLi loop. Most of the losses appear in the IB FP (67.5 %) principally due to its greatest length, channel dimensions and the very high magnetic field in the portion close to the TFC. In this case, the IB DP loss is lower then the OB case because of its smaller length, while the manifold pressure drop is greater due to the higher magnetic field intensity in the IB segment. The IB BZ pressure drop, as the OB one, is negligible though in this case is higher. In general, the overall IB MHD pressure drop is higher then the OB one by $\approx 1MPa$, due principally to its nearness to the CS where the applied magnetic field is stronger, therefore increasing the MHD affects and pressure drops. As the OB model, in these results the collectors pressure drops have not been modelled and the liquid metal hydrostatic head has not been considered.

Component	Δp [kPa]	% [-]
Feeding pipe	1567.17	67.5
Manifold	487.06	21.0
Breeding zone	3.19	0.1
Draining pipe	263.67	11.4
Total	2321.09	100

Table 5.20: IB Modelica simulation pressure drops for equatorial case.

5.2.2 Complete model

The complete model considers the complete PbLi loop with all fours components (draining pipe, manifold, breeding zone and feeding pipe) implemented together, simulating at the

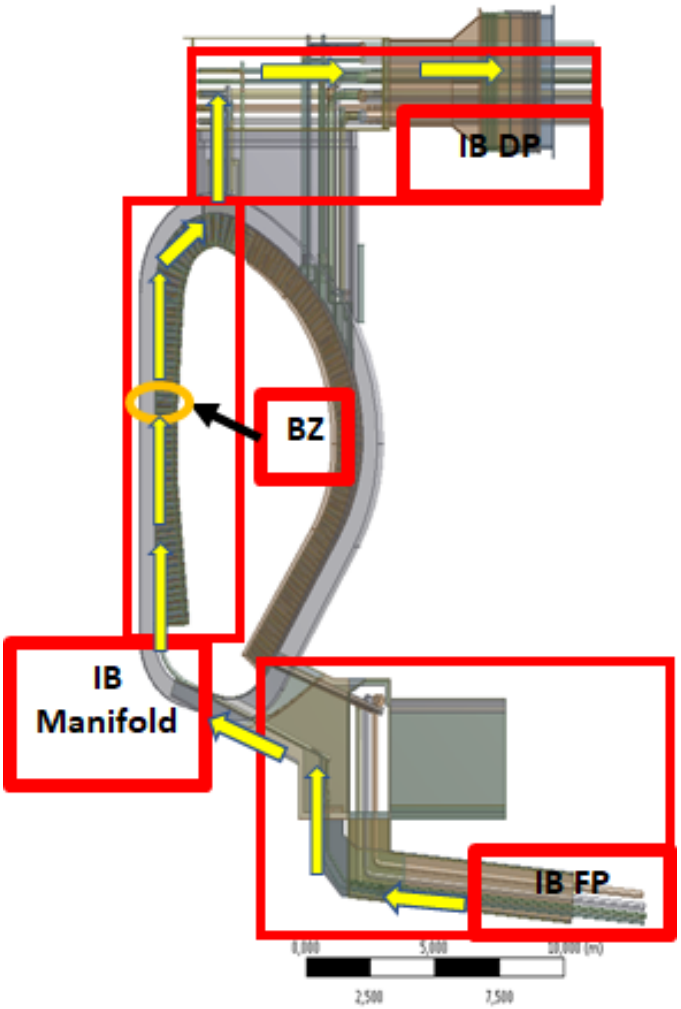

Figure 5.20: WCLL BB: radial-poloidal view. The PbLi loop is highlighted by yellow arrows. In the red boxes are indicated the several WCLL components. The equatorial BZ cell (IB05) is indicated by a orange circle (adapted from [31]).

same time all the BZ cells. For this purpose, it adopted the same strategy for the manifold pressure drops estimation, described in subsection 5.1.2, considering nine different BZ cell positions. For this analysis, the component models developed in the Section 5.1 have been implemented in the same system-level model, both for the OB and IB case, in which the PbLi mass flow rate and temperature are imposed. Regarding the applied magnetic field valued, they have been kept the same as the models described in the Section 5.1 and according to the field profile in the WCLL mentioned in section 2.2.

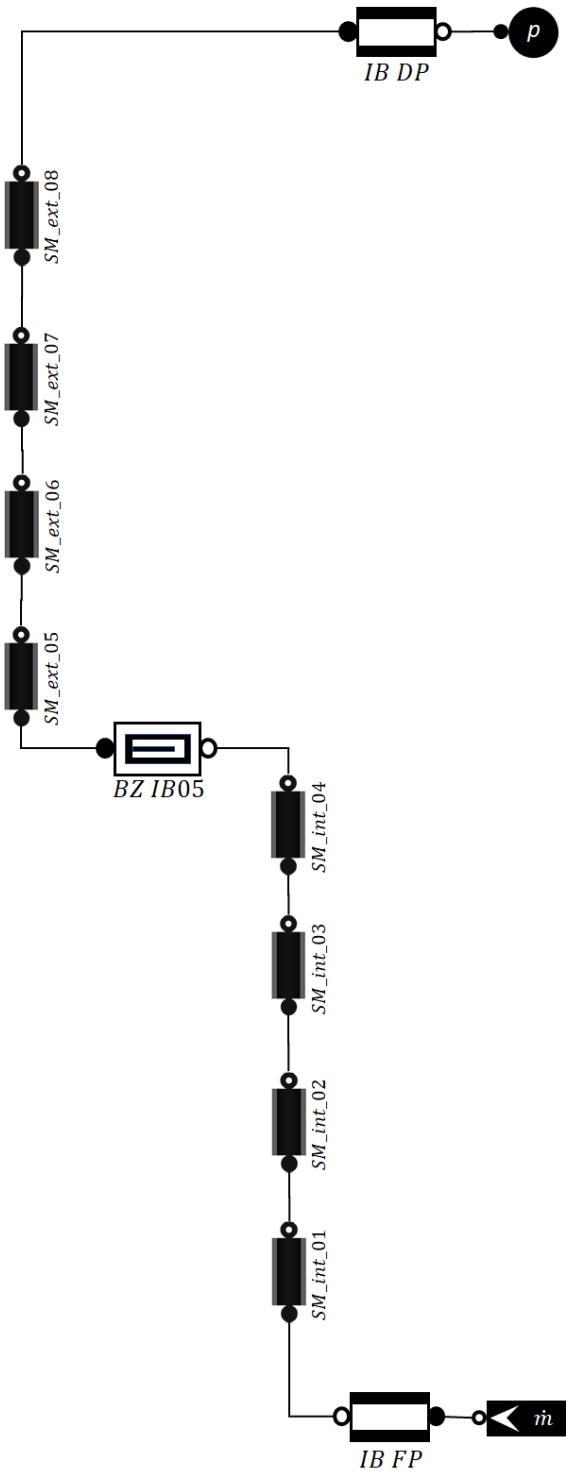

Figure 5.21: IB PbLi loop Modelica model for the equatorial case (IB05 loop).

Model description

The complete PbLi model is structured in a different way with respect to the equatorial case. The first component is the mass flow rate source in which is imposed the the liquid mass flow rate and its temperature. After that there is the feeding pipe, modelled according to the OB and IB FP, that brings the PbLi to the manifold. Then there is the manifold and BZ cells region. This region is composed by two branches that represent the annular and the internal manifold channels, connected to the different BZ cells. In this simulation, nine BZ cell positions have been considered, therefore the two manifold channels have been divided into eight sections in the same way described in the Subsection 5.1.2. This region, at the top, is linked to the draining pipe that collects all the PbLi, and in the end, a pressure sink component completes the model. Regarding the input parameters for FP, manifold sections and FP, such as the channel geometries, magnetic fields and PbLi properties (see Appendix A), they have been kept the same as the models described in the Section 5.1, while for the BZ cell, the applied magnetic field value has been modified according to its position in the BB. In the following, both OB and IB complete models are analysed.

OB Model

The WCLL PbLi loop of the OB is represented in Figure 5.22, where the magnetic field values adopted for each BZ cell position are reported in the table (right side of the figure), while the Modelica model is shown in Figure 5.23. The model is composed at first by a mass flow rate source (located in the bottom-right side) in which the liquid metal mass flow rate and temperature are imposed, and then by the OB FP that brings the PbLi towards the manifold region. The OB manifold region is divide by two sides, each of them composed by eight sections, where the right one represents the annular channel and the left one that represents the internal channel. In the centre there are nine OB BZ cells located in nine different positions along the OB segment, that have the same geometrical dimensions but different magnetic field values. For each OB BZ cell, the portion of the annular and internal OB manifold channel is different, varying according to the BZ position. After this region, there is the OB DP that collects all the PbLi from the manifold and the model concludes with a pressure sink component (located in the top-right side). The applied magnetic fields in the OB BZ cells are reported in the table in Figure 5.22. The PbLi temperature is fixed to 600 K and its inlet mass flow rate is 16.38 kg/s (both imposed in the mass flow rate source), while the wall electrical conductivity is $\sigma_w = 1.15 \cdot 10^6\ S/m$. Also for the complete model, the OB manifold and all OB BZ cells are constituted by six parallel channels, therefore the Modelica simulation is obtained simulating one of them dividing the MHD pressure drop by six, while for the OB FP and OB DP, being a single channel, the MHD losses have not been changed. For this simulation, the bottom and top collectors have not been modelled and the hydrostatic loss have not been considered.

The Modelica simulation results, expressed for each OB loop and for each component, are shown in Figure 5.24 and reported in Table 5.21. The overall MHD pressure drop for all poloidal locations is $\Delta p_{OB} = 1160.3\ kPa$, being in parallel, but its distribution among the components is different. This MHD pressure drop agrees perfectly with threshold value expressed in the section 1.3, corresponding to the maximum estimated value of a pump

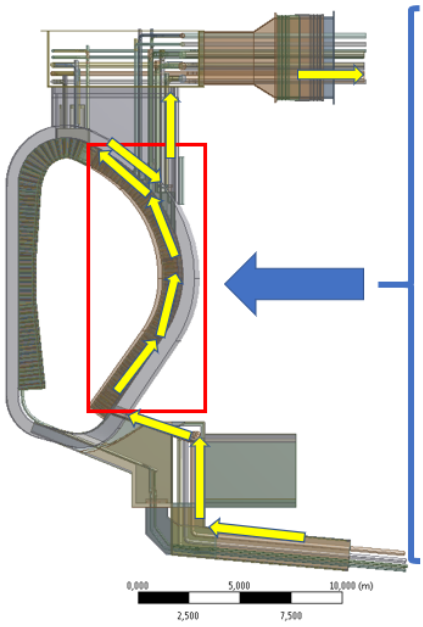

Cell position	B [T]
OB_01	4.93
OB_02	4.36
OB_03	3.92
OB_04	3.66
OB_05	3.61
OB_06	3.75
OB_07	4.08
OB_08	4.74
OB_09	5.10

Figure 5.22: WCLL BB: radial-poloidal view. Left: The PbLi loop is highlighted by yellow arrows. Right: magnetic field values for each BZ cell in the BB segment (highlighted by a red rectangular) (adapted from [31]).

prevalence necessary to the PbLi circulation inside the BB ($\approx$ 2 MPa). Most of losses are concentrated in the OB FP and OB DP, due principally to their length and channel dimensions, and moreover their MHD pressure drops are the same (626.9 kPa for OB FP and 378.1 kPa for the OB DP) because of these components are shared with all the OB poloidal locations. Regarding the OB manifold and OB BZ, their MHD pressure drops are lower and change according the BZ cell position. The OB manifold MHD losses increase towards the equatorial plane, reaching the maximum value in the OB05 poloidal location, and decrease rapidly to the top blanket, with the same trend described in subsection 5.1.2. Conversely, the OB BZ losses are higher in the bottom and top blanket and minimal in the equatorial plane, with a inverse behaviour respect to the OB manifold. This particular trend is due principally to balance and compensate the OB manifold losses to reach the overall MHD pressure drop in the OB, and an other important factor is due to the magnetic field intensity that is higher in the bottom and top part of the blanket segment. Comparing the Modelica results with literature data ($\Delta p_{OB,lit}$ = 1609 kPa) [29], the MHD pressure drops accuracy is good, although the literature data has been estimated considering each OB poloidal location singularly and not simulated in a complete model. In conclusion, the complete model for the OB can represent with a good approximation the general MHD pressure drops behaviour inside the OB, in particular the overall loss estimation for the PbLi loop and the MHD pressure drop trends of each main component.

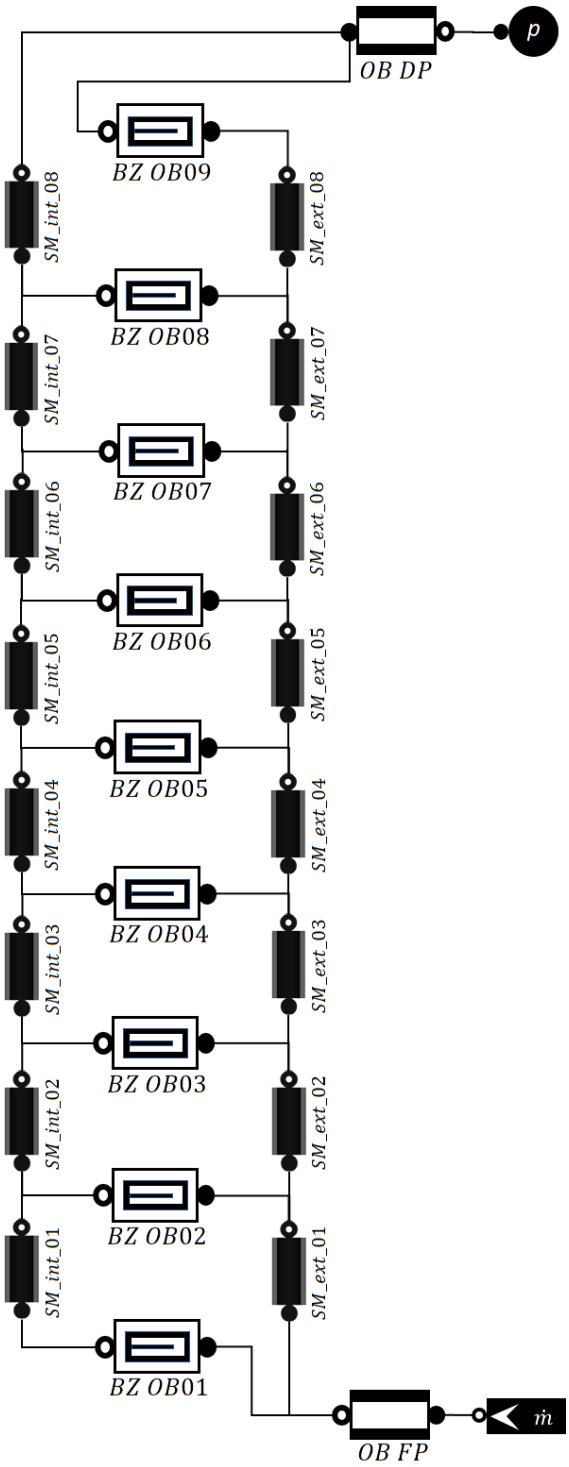

Figure 5.23: OB PbLi loop Modelica complete model.

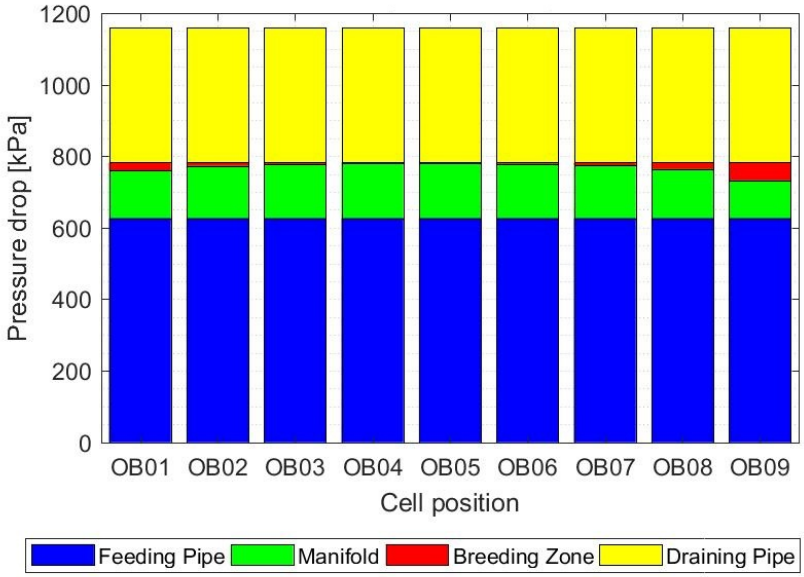

Figure 5.24: OB PbLi polidal locations Modelica complete model results.

Cell position	FP [kPa]	Manifold [kPa]	BZ [kPa]	DP [kPa]	Total [kPa]
OB01		132.6	22.8		
OB02		146.4	9.0		
OB03		151.4	4.0		
OB04		153.1	2.3		
OB05	626.9	153.3	2.1	378.1	1160.3
OB06		152.0	3.4		
OB07		148.2	7.2		
OB08		137.2	18.2		
OB09		105.6	49.8		

Table 5.21: OB PbLi poloidal locations Modelica complete model pressure drops, expressed for each component and BZ positions.

OB model with hydrostatic head

In this subsection, the contribution of the hydrostatic head in the WCLL OB PbLi poloidal locations is analysed. In general, for a closed hydraulic loop, the contribution of the hydrostatic head pressure is not an issue from the pump point ov view, but it is interesting to evaluate the additional contribution of the PbLi hydrostatic head, to be able to evaluate the breeder distribution among the different BZ cells. The PbLi density is ten times greater then the water one, then an higher contribution of its hydrostatic pressure, due to its big weight, to the overall loss is predictable. For this purpose, the same Modelica model of the previous subsection, represented in Figure 5.23, is adopted for this analysis, with the

same input parameters. In this simulation, the overall pressure drops for OB and each component, have been evaluated considering the MHD loss adding the contribution of the PbLi hydrostatic head, expressed with the relation:

$$\Delta p_{head} = \rho g h \tag{5.1}$$

where ρ is the liquid metal density, g is the gravitational acceleration constant (9.81 m/s^2) and h is the channel vertical height. This relation is implemented in the Modelica model to evaluate the contribution of the hydrostatic head loss for all vertical sections of each WCLL component. Therefore, the overall pressure drop is calculated as the sum of the MHD and hydrostatic head losses with the relation:

$$\Delta p_{tot} = \Delta p_{MHD} + \Delta p_{head} \tag{5.2}$$

The Modelica simulation results considering the PbLi hydrostatic head, expressed for each OB poloidal location and for each component, are shown in Figure 5.25 and reported in Table 5.22. The overall pressure drop for all poloidal locations is $\Delta p_{OB} = 4097.5\ kPa$ and, compared with the case without the hydrostatic head (1160.3 kPa), this value is about four times higher, demonstrating the big effect of the PbLi weight and the contribution of the hydrostatic head to the pressure drop. In the figure, the portions of the hydrostatic head loss are represented with lighter colours, and it is possible to see that the bigger contribution of the hydrostatic head is located in correspondence of the manifold region, due principally to the high vertical length of this segment. Regarding the OB FP and OB DP, the hydrostatic head contribution is lower, though it is slightly greater in the DP that presents more vertical sections in its layout. At the end, the contribution of the hydrostatic head in the BZ is very small and can be neglected. The Modelica model for the OB PbLi loop considering the liquid metal hydrostatic head, presents very high pressure drop values in the overall WCLL and in its components, as they were expected, demonstrating the importance to analyse these aspects.

Cell position	FP [kPa]	Manifold [kPa]	BZ [kPa]	DP [kPa]	Total [kPa]
OB01		1433.4	43.1		
OB02		1447.1	29.4		
OB03		1452.2	24.4		
OB04		1453.8	22.7		
OB05	1203.9	1453.9	22.6	1417.1	4097.5
OB06		1452.6	24.0		
OB07		1448.5	28.1		
OB08		1436.7	39.8		
OB09		1409.7	66.9		

Table 5.22: OB PbLi poloidal locations Modelica complete model pressure drops considering the contribution of the liquid hydrostatic head, expressed for each component and BZ positions.

Another important aspect is to analyse the mass flow rate distribution in all BZ cells in both situations. The percentage mass flow rate for each BZ cell position is represented

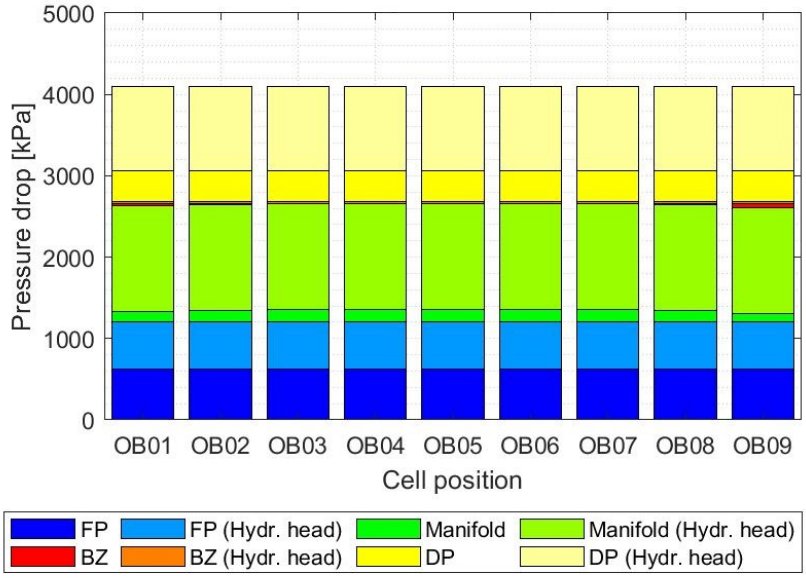

Figure 5.25: OB PbLi poloidal locations Modelica complete model results considering the contribution of the liquid hydrostatic head.

in Figure 5.26. It is possible to notice that the presence of the hydrostatic head does not affect significantly the liquid mass flow rate and the breeder distribution remains almost the same in each BZ cells. The breeder mass flow rate values for all BZ cells are reported in Table 5.23. From these results it is also possible to notice that the higher values of breeder mass flow rates are in the top and the bottom of the BB, giving an important contribution to the BZ cells losses located in these positions.

Cell position	Mass flow rate w/o hydr. head [kg/s]	Mass flow rate w/ hydr. head [kg/s]
OB01	0.477	0.479
OB02	0.242	0.242
OB03	0.132	0.132
OB04	0.086	0.088
OB05	0.083	0.087
OB06	0.122	0.129
OB07	0.220	0.235
OB08	0.412	0.442
OB09	0.956	0.898

Table 5.23: OB breeder mass flow rate in each BZ cells in the case without hydrostatic head and with hydrostatic head.

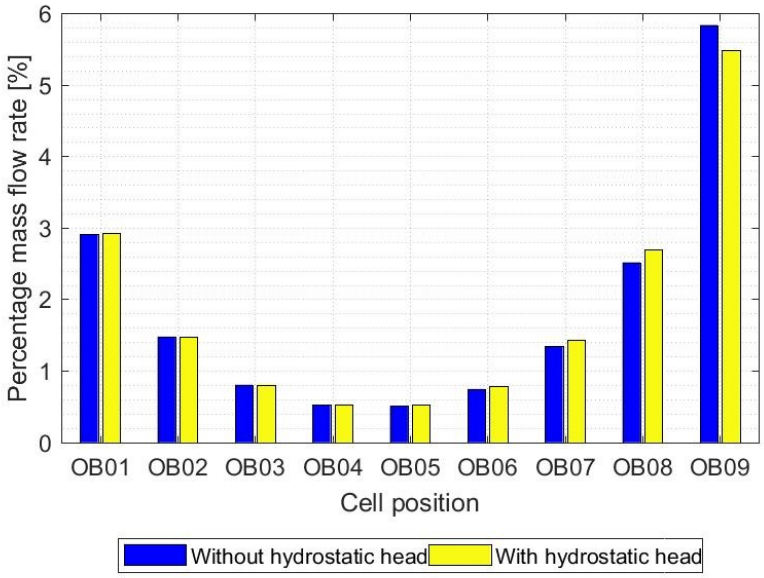

Figure 5.26: OB percentage mass flow rate for each BZ cell. Blue bars: without hydrostatic head. Yellow bars: with hydrostatic head.

IB Model

The WCLL PbLi loop for the IB is represented in Figure 5.27, where the magnetic field values adopted for each BZ cell position are reported in the table (right side of the figure), while the Modelica model is shown in Figure 5.28. The IB complete model is structured as the OB one. The PbLi temperature is fixed to 600 K and its inlet mass flow rate is 5.32 kg/s (both imposed in the mass flow rate source), while the wall electrical conductivity is $\sigma_w = 1.15 \cdot 10^6$ S/m. Also in this case, the Modelica simulation is obtained simulating one of the six parallel channel in the IB manifold and BZ cells, therefore their MHD losses have been divided by six, while for the IB FP and IB DP the MHD pressure drops have not been changed. For this simulation, the bottom and top collectors have not been modelled and the liquid hydrostatic head loss have not been considered.

The Modelica simulation results, expressed for each cell and for each component, are shown in Figure 5.29 and reported in Table 5.24. The overall MHD pressure drop for all poloidal locations is $\Delta p_{IB} = 2156.5$ kPa, being in parallel, but its distribution among the components is different. The MHD loss inside the IB, compared with the OB one, is higher by about 1 MPa, due principally to the higher magnetic field intensities in this region and smaller channel geometries. The value actually overcomes, albeit slightly, the threshold value expressed in the section 1.3, corresponding to the maximum estimated value of a pump prevalence necessary to the PbLi circulation inside the BB ($\approx$ 2 MPa). Most of the losses are concentrated in the IB FP, due principally to its length and high magnetic field intensity in correspondence of the bottom side of the BB. The IB FP and IB DP

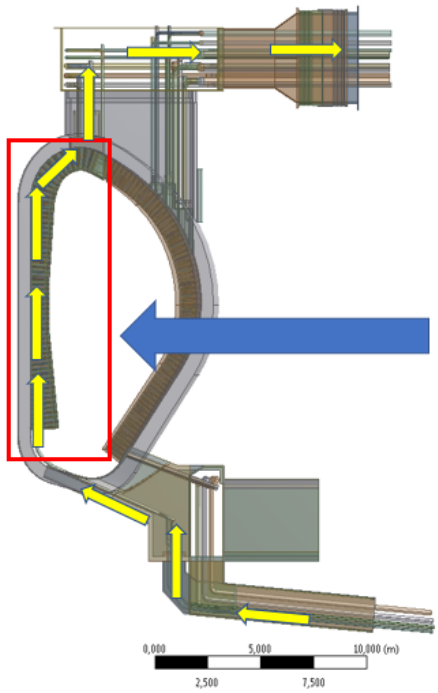

Cell position	B [T]
IB_01	8.64
IB_02	8.64
IB_03	8.64
IB_04	8.64
IB_05	8.64
IB_06	7.50
IB_07	6.98
IB_08	6.09
IB_09	5.20

Figure 5.27: WCLL BB: radial-poloidal view. Left: The PbLi loop is highlighted by yellow arrows. Right: magnetic field values for each BZ cell in the BB segment (highlighted by a red rectangular) (adapted from [31]).

losses are of course equal for all IB cases because there is a single FP and a single DP, while the IB manifold and BZ cells pressure drops change according to BZ the position. The IB manifold MHD losses increase rapidly towards the equatorial plane, reaching the maximum value in the IB05 poloidal location, and decrease to the top blanket, with the same behaviour described in subsection 5.1.2. The IB BZ cell MHD losses have a inverse trend, in which they are higher in the bottom and top side of the BB and they are lower in the equatorial zone. This particular trend is similar to the OB case, where the IB BZ losses try to balance and compensate the IB manifold pressure drops to reach the overall MHD loss inside the BB. Moreover, the maximum IB BZ MHD pressure drop happens in the lower BZ cell (IB01) where there is the highest magnetic field intensity (8.64 T), though, in general, all BZ losses are very low respect to the overall pressure drop. Comparing the Modelica results with literature data ($\Delta p_{IB,lit} = 2435\ kPa$) [29], the MHD pressure drop accuracy is good, although the literature data has been estimated considering each IB poloidal location singularly and not simulated in a complete model. In conclusion, the complete model for the IB can represent with a good approximation the general MHD pressure drops behaviour inside the IB, in particular the overall loss estimation for the PbLi loop and the MHD pressure drop trends of each main component.

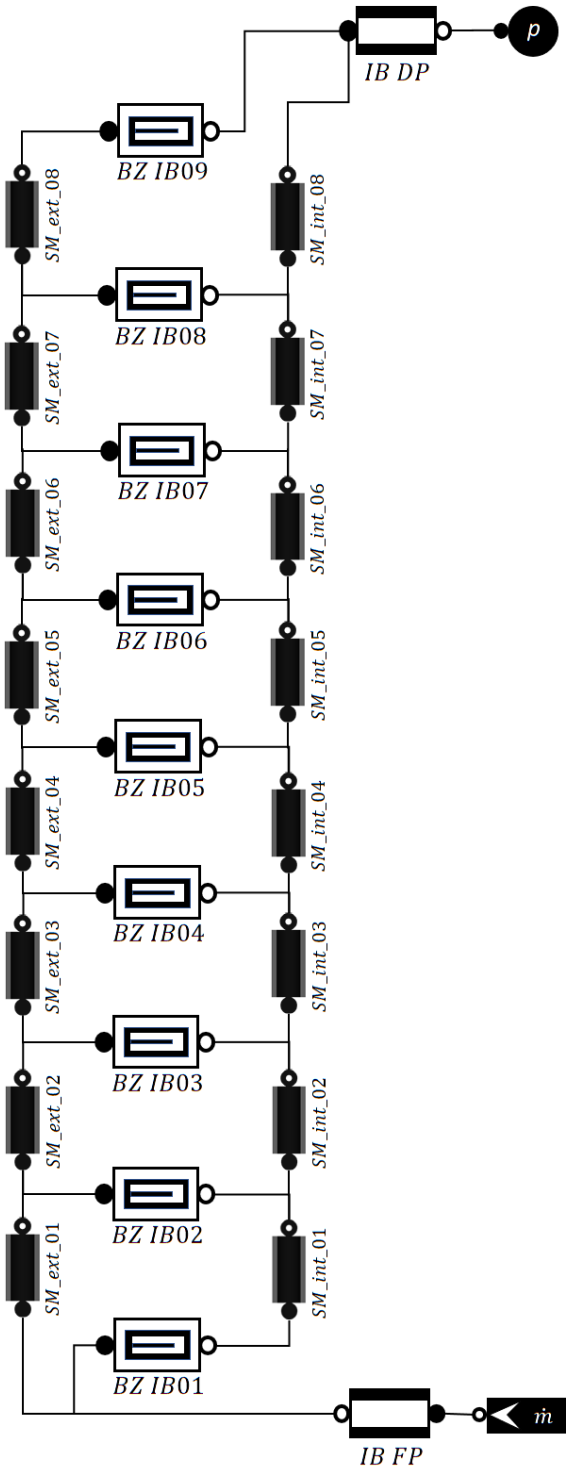

Figure 5.28: IB PbLi poloidal locations Modelica complete model.

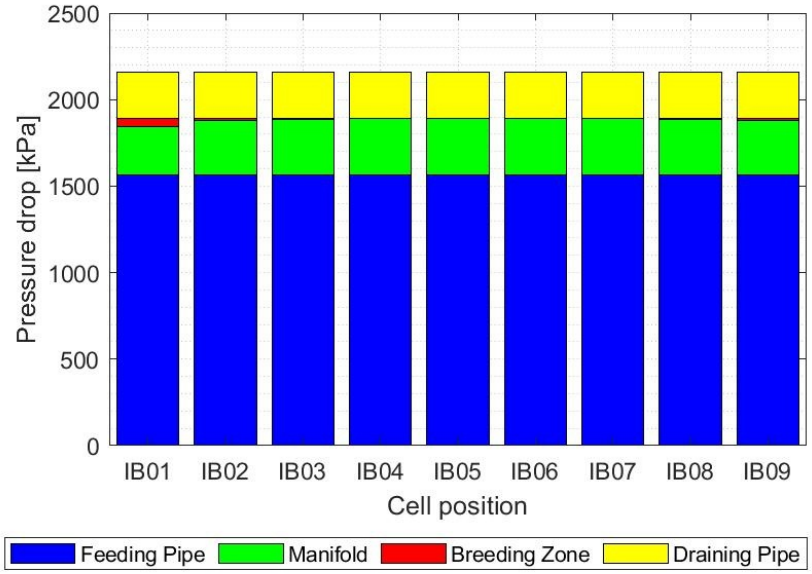

Figure 5.29: IB PbLi poloidal locations Modelica complete model results.

Cell position	FP [kPa]	Manifold [kPa]	BZ [kPa]	DP [kPa]	Total [kPa]
IB01		276.9	48.8		
IB02		310.1	15.6		
IB03		320.7	5.0		
IB04		324.0	1.7		
IB05	1567.2	324.9	0.8	263.7	2156.5
IB06		324.7	1.0		
IB07		323.4	2.3		
IB08		319.7	6.0		
IB09		310.8	14.9		

Table 5.24: IB PbLi poloidal locations Modelica complete model pressure drops, expressed for each component and BZ positions.

IB model with hydrostatic head

In this subsection, as for the OB, the contribution of the hydrostatic head in the WCLL IB PbLi poloidal locations is analysed. The same Modelica model, represented in Figure 5.28 of the previous subsection is adopted, with the same input parameters. In this simulation, the overall pressure drop for the IB and each component has been evaluated as the sum of the MHD and hydrostatic head losses with the relation 5.2, in which the latter are estimated with the relation 5.1. Both relation have been implemented in the Modelica model.

The Modelica simulation results considering the PbLi hydrostatic head, expressed for

each IB cell position and for each component, are shown in Figure 5.30 and reported in Table 5.25. The overall pressure drop for all poloidal locations is $\Delta p_{IB} = 5239.3\ kPa$ and, compared with the case without the hydrostatic head (2156.5 kPa), this value is almost three times higher, demonstrating the big effect of the PbLi weight and the contribution of the hydrostatic head pressure drop. In the figure, the portions of the of the hydrostatic head loss are represented with lighter colours, and it is possible to see that the bigger contribution of the hydrostatic head is located in correspondence of the manifold region, due principally to the high vertical length of this segment. Regarding the IB FP and IB DP, the hydrostatic head contribution is high in the FP that that presents more vertical sections in its layout, while in the DP is low. At the end, the contribution of the hydrostatic head in the BZ is very small and can be neglected. The Modelica model for the IB PbLi poloidal locations considering the liquid metal hydrostatic head, presents very high pressure drop values in the overall WCLL and in its components, as they were expected, but with a minor increase respect to the OB poloidal locations.

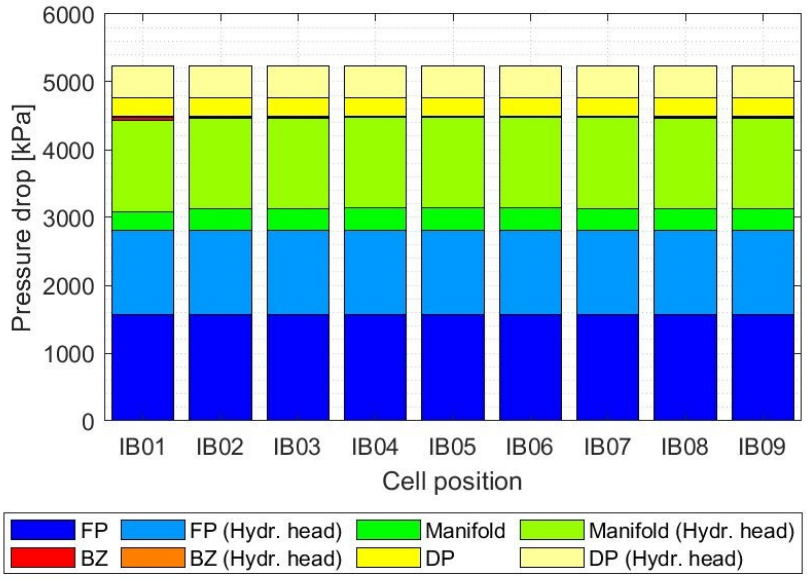

Figure 5.30: IB PbLi poloidal locations Modelica complete model results considering the contribution of the liquid hydrostatic head.

Also in the IB case, it is important to analyse the mass flow rate distribution in all BZ cells in both situations. The percentage mass flow rate for each BZ cell position is represented in Figure 5.31. Also in this case, the presence of the hydrostatic head does not affect significantly the liquid mass flow rate and the breeder distribution remains almost the same in each BZ cells. The breeder mass flow rate values for all BZ cells are reported in Table 5.26. As the OB case, in the IB the higher values of breeder mass flow rates are in the top and the bottom of the BB, giving an important contribution to the BZ cells losses located in these positions.

Cell position	FP [kPa]	Manifold [kPa]	BZ [kPa]	DP [kPa]	Total [kPa]
IB01		1613.3	69.0		
IB02		1646.4	35.9		
IB03		1656.9	25.4		
IB04		1660.1	22.1		
IB05	2812.6	1661.0	21.2	744.5	5239.3
IB06		1660.8	21.4		
IB07		1659.5	22.7		
IB08		1655.9	26.3		
IB09		1647.0	35.2		

Table 5.25: IB PbLi poloidal locations Modelica complete model pressure drops considering the contribution of the liquid hydrostatic head, expressed for each component and BZ positions.

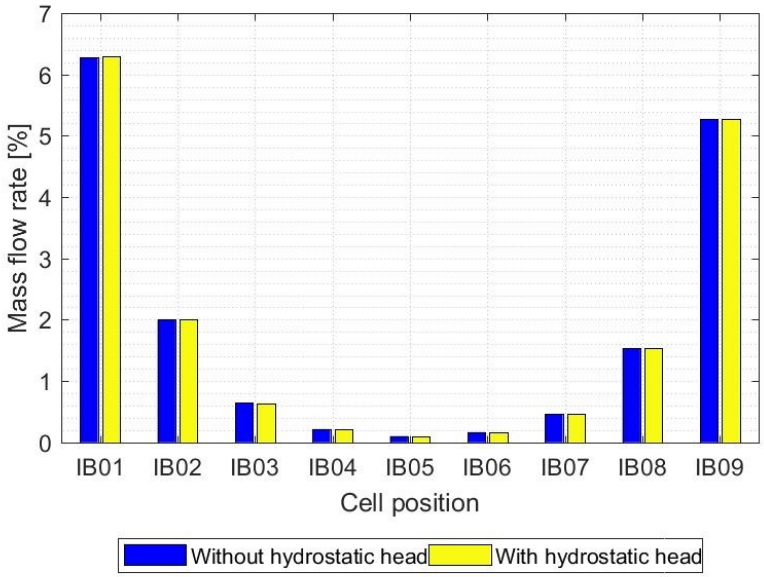

Figure 5.31: IB percentage mass flow rate for each BZ cell. Blue bars: without hydrostatic head. Yellow bars: with hydrostatic head.

5.2.3 Transient analysis

In this subsection two different transients have been analysed with the aim to verify the WCLL PbLi model simulation ability over the tokamak nominal operations. The two analyses regard the pressure drop variations inside the WCLL in the case of a possible plasma discharge and a startup of all superconducting magnets.

In the following analyses, the evaluation of the pressure drop in each PbLi poloidal

Cell position	Mass flow rate w/o hydr. head [kg/s]	Mass flow rate w/ hydr. head [kg/s]
IB01	0.334	0.335
IB02	0.107	0.106
IB03	0.034	0.034
IB04	0.011	0.011
IB05	0.005	0.005
IB06	0.009	0.009
IB07	0.024	0.024
IB08	0.082	0.082
IB09	0.280	0.281

Table 5.26: IB breeder mass flow rate in each BZ cells in the case without hydrostatic head and with hydrostatic head.

locations component takes into account the OHD and MHD flow regime modelled together. Regarding the MHD loss, they have been calculated according the correlation described in the Chapter 3, while for the OHD the adopted formula is the following [51]:

$$\Delta p_{OHD} = f_{OHD} \frac{L}{D_{hydr}} \rho \frac{u^2}{2} \tag{5.3}$$

where f_{OHD} is the OHD loss coefficient calculated with Colebrook's correlation [51], L is the channel length, D_{hydr} is the hydraulic diameter, ρ is the fluid density and u the fluid velocity. Finally the pressure drop on each component has been calculated as the sum of the OHD and MHD losses:

$$\Delta p = \Delta p_{OHD} + \Delta p_{MHD} \tag{5.4}$$

The two situations have been analysed both for OB and IB cases adopting the same poloidal locations geometries, layouts and models described in the subsections 5.2.2 and 5.2.2.

Plasma discharge

The first transient analysed in this work regards the evaluation of the pressure drop variations inside the WCLL PbLi loop during a possible plasma discharge in the reactor. For this analysis, it has been considered a plasma discharge lasting 2.5 hours (9000 s), with 30 minutes of dwell time (no plasma), during which the CS and PFCs are turned off, while they work at nominal operation for the remaining two hours; the TFCs remain operational for the whole period. During this , the toroidal field component B_{tor} remain active while the poloidal field component B_{pol}, generated by the CS and the PFCs, is null for the firsts 30 minutes and then reach the nominal value.

The pressure drop variation during this transient has been evaluated adopting the same Modelica models represented in Figure 5.23 for the OB case and Figure 5.28 for the IB case where at each component has been connected an input source for taking into account the magnetic field variation. For the components that are inside the TFCs (BZ, manifold

and parts of FP and DP), in which the toroidal component is considered, the magnetic field remains constant, while for the remaining components (that are outside the TFCs) a step variation of the poloidal field component, from zero to the nominal value, has been assumed. As a side remark, for this analysis, correlations developed for stationary problems under transient conditions were used, therefore the validity should be verified. In the following the OB and IB transient results are reported.

The overall pressure drop variations during the transient, both for OB and IB case, are reported in Figure 5.32. The loss results for each BZ position are reported in Figure 5.33 for the OB case and in Figure 5.34 for IB case. The overall pressure drops for all poloidal locations during the startup of the PFCs and CS are lower with respect to the nominal condition. In the OB case the loss passes from 824.2 kPa to 1160.3 kPa, while in the IB case from 2036.6 kPa to 2156.5 kPa. These variations are due principally to the FP and DP losses reduction that have a portion outside the TFCs in which the poloidal magnetic field is zero and there is only a OHD liquid flow regime. The highest contribution of the pressure drop variation between them is ascribable to the FP because it has the bigger portion outside the TFCs respect to the DP one. Conversely, in the components that are inside the TFCs (BZ and manifold), the toroidal magnetic field and the MHD flow regime is still present during the overall transient, then the pressure drop before and after the plasma discharge remains almost the same. In the IB case the overall pressure drop variation is lower then the OB case because in this configuration the discrepancy between the poloidal and toroidal magnetic field is very high and this has a small effect to the pressure drop variation during the plasma discharge. In general, the overall pressure drop variation is not excessively high because the poloidal magnetic field has a smaller contribution respect to the toroidal one in terms of intensity and distribution in the PbLi poloidal locations. The loss results for each WCLL component in the configuration of $B_{pol} = 0$ are reported in Table 5.27 for the OB case and in Table 5.28 for the IB case.

Cell position	FP [kPa]	Manifold [kPa]	BZ [kPa]	DP [kPa]	Total [kPa]
OB01		125.8	22.7		
OB02		139.5	9.0		
OB03		144.5	4.0		
OB04		146.2	2.3		
OB05	329.4	146.3	2.2	346.3	824.2
OB06		144.9	3.5		
OB07		140.8	7.7		
OB08		129.1	19.4		
OB09		102.0	46.5		

Table 5.27: OB PbLi poloidal locations Modelica pressure drops in the case of $B_{pol} = 0$ (regarding the results represented in Figure 5.33a), expressed for each component and BZ position.

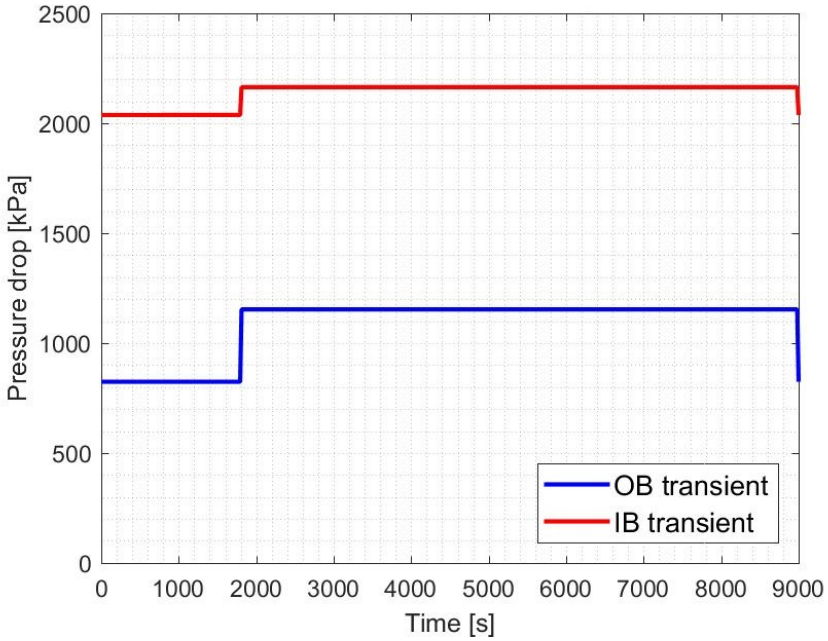

Figure 5.32: WCLL overall pressure drop behaviour during the plasma discharge with an interval time of 2.5 hours (9000 s).

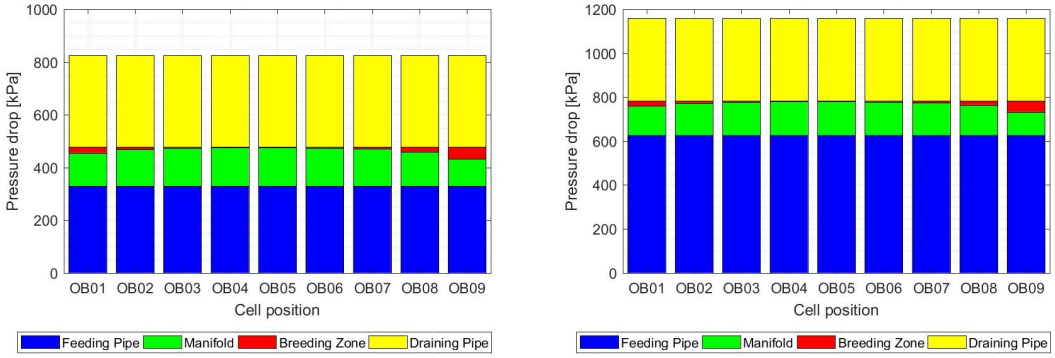

(a) $B_{pol} = 0$ (30 minutes) (b) Nominal operation (2 hours).

Figure 5.33: OB components losses during the plasma discharge. Left: PFCs and CS turned off (30 minutes) and $B_{pol} = 0$. Right: nominal operation (2 hours) with nominal values of B_{pol} and B_{tor}.

Superconducting magnets startup

The second transient analysed in this work regards the evaluation of the pressure drop inside the WCLL PbLi loop in the situation of a startup of all superconducting magnets. For this analysis, it has been considered a transient time of 30 minutes (1800 s) subdivided

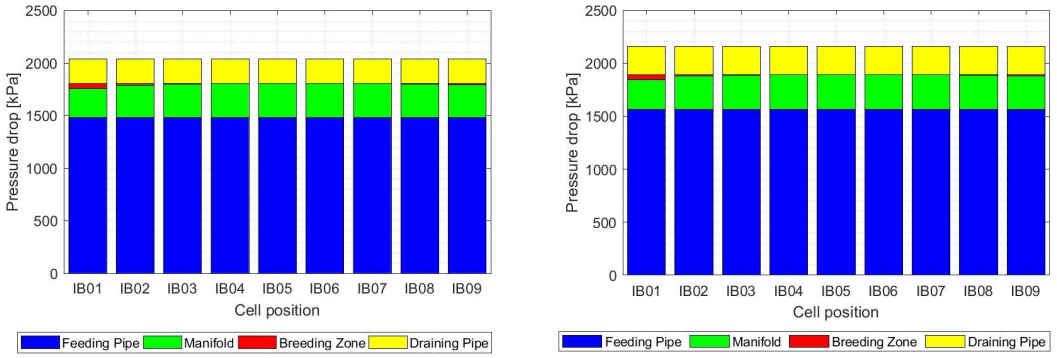

(a) $B_{pol} = 0$ (30 minutes) (b) Nominal operation (2 hours).

Figure 5.34: IB components losses during the plasma discharge. Left: PFCs and CS turned off (30 minutes) and $B_{pol} = 0$. Right: nominal operation (2 hours) with nominal values of B_{pol} and B_{tor}.

Cell position	FP [kPa]	Manifold [kPa]	BZ [kPa]	DP [kPa]	Total [kPa]
IB01		276.9	48.5		
IB02		310.1	15.4		
IB03		320.6	4.9		
IB04		323.8	1.6		
IB05	1479.4	324.7	0.8	231.7	2036.6
IB06		324.5	0.9		
IB07		323.2	2.3		
IB08		319.6	5.9		
IB09		310.7	14.8		

Table 5.28: IB PbLi poloidal locations Modelica pressure drops in the case of $B_{pol} = 0$ (regarding the results represented in Figure 5.34a), expressed for each component and BZ position.

in three phases: in the first phase (5 minutes) all superconducting magnets are turned off and all the magnetic fields (toroidal and poloidal) are equal to zero; in the second phase (20 minutes) the magnets are turned on gradually and a rump variation of the toridal and magnetic fields has been adopted; in the third phase (5 minutes) the magnets remains active and the reactor works at the nominal operation. The aim of this analysis is to verify the discrepancy between the OHD and MHD flow regime, for example in a possible startup of the superconducting magnets for a reactor maintenance.

The pressure drop variation during this transient has been evaluated adopting the same Modelica models represented in Figure 5.23 for the OB case and Figure 5.28 for the IB case where at each component has been connected an input source for taking into account

the magnetic field variation. In all components (inside and outside the TFCs) the magnetic field (toroidal or poloidal) value is set to zero for 5 minutes and then it goes to the nominal value adopting a rump curve. As the plasma discharge analysis, also in this case the correlations developed for stationary problem under transient condition were used. In the follow the OB and IB transient results are reported.

The overall pressure drop variations during the transient, both for OB and IB case, are reported in Figure 5.35. The loss results for each BZ position are reported in Figure 5.36 for the OB case and in Figure 5.37 for IB case. The overall pressure drops for all poloidal locations when the superconducting magnets are turned off are lower with respect to the nominal condition. In the OB case the loss passes from 0.079 kPa to 1160.3 kPa, while in the IB case from 0.057 kPa to 2156.5 kPa. As expected, the difference between these two phases is very high, marking also the big discrepancy between the MHD and OHD flow regime. In the first phase, the PbLi losses have been calculated according only the OHD regime, while in the second and third phases the pressure drop is composed as the sum of the OHD and MHD effects, highlighting as the OHD regime can be simply neglected when MHD effects occur. Focusing in the first phase with $B = 0$, it possible to notice that the bigger loss contribution is ascribable to the FP and DP. In the second phase, initially the pressure drop slowly raises, while, approaching the nominal phase, the increase is marked due to a stronger presence of the MHD effects. In conclusion, the overall IB loss when $B = 0$ is smaller then the OB one because of the lower liquid mass flow rate that flows inside the IB, and moreover, the bigger loss contribution is ascribable to the FP and DP, while the BZ and manifold pressure drops are negligible. The loss results for each WCLL components in the configuration of $B = 0$ are reported in Table 5.29 for the OB case and in Table 5.30 for the IB case.

Cell position	FP [kPa]	Manifold [kPa]	BZ [kPa]	DP [kPa]	Total [kPa]
OB01		$5.99 \cdot 10^{-4}$	$4.51 \cdot 10^{-5}$		
OB02		$6.36 \cdot 10^{-4}$	$8.16 \cdot 10^{-6}$		
OB03		$6.43 \cdot 10^{-4}$	$8.54 \cdot 10^{-7}$		
OB04		$6.44 \cdot 10^{-4}$	$9.99 \cdot 10^{-8}$		
OB05		$6.44 \cdot 10^{-4}$	$1.08 \cdot 10^{-7}$	0.025	0.079
OB06		$6.43 \cdot 10^{-4}$	$9.43 \cdot 10^{-7}$		
OB07		$6.35 \cdot 10^{-4}$	$9.19 \cdot 10^{-6}$		
OB08		$5.89 \cdot 10^{-4}$	$5.53 \cdot 10^{-5}$		
OB09		$4.14 \cdot 10^{-4}$	$2.30 \cdot 10^{-4}$		

Table 5.29: OB PbLi poloidal locations Modelica pressure drops in the case of $B = 0$ (regarding the results represented in Figure 5.36a), expressed for each component and BZ position.

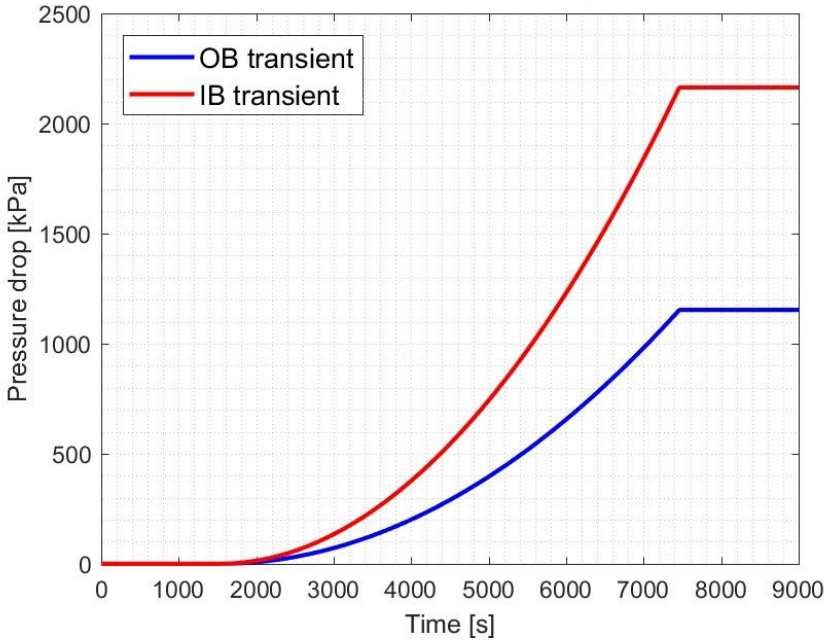

Figure 5.35: WCLL overall pressure drop behaviour during the superconducting magnets startup with an interval time of 30 minutes (1800 s).

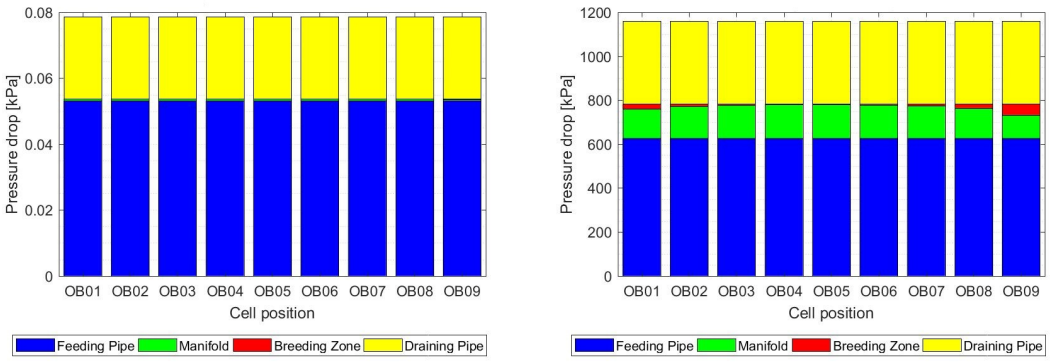

(a) $B = 0$ (5 minutes)

(b) Nominal operation (5 minutes).

Figure 5.36: OB components losses during the superconducting magnets startup. Left: all superconducting magnets turned off (5 minutes) and $B = 0$. Right: nominal operation (5 minutes) with nominal values of B_{pol} and B_{tor}.

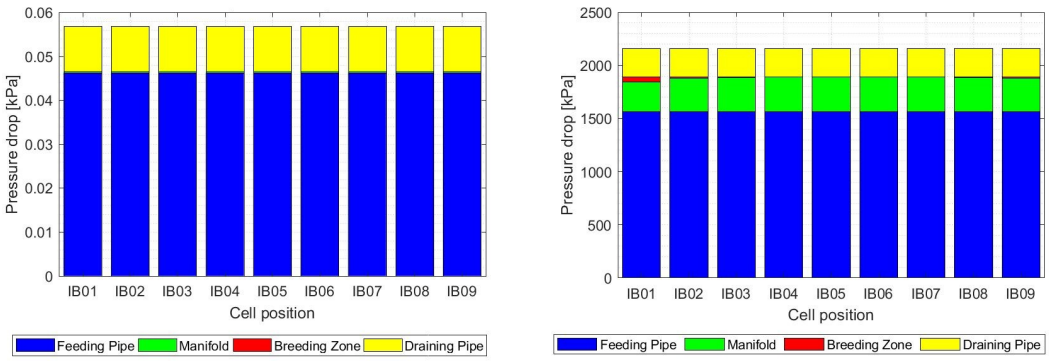

(a) $B = 0$ (5 minutes)

(b) Nominal operation (5 minutes).

Figure 5.37: IB components losses during the superconducting magnets startup. Left: all superconducting magnets turned off (5 minutes) and $B = 0$. Right: nominal operation (5 minutes) with nominal values of B_{pol} and B_{tor}.

Cell position	FP [kPa]	Manifold [kPa]	BZ [kPa]	DP [kPa]	Total [kPa]
IB01		$3.02 \cdot 10^{-4}$	$3.14 \cdot 10^{-5}$		
IB02		$3.31 \cdot 10^{-4}$	$2.59 \cdot 10^{-6}$		
IB03		$3.33 \cdot 10^{-4}$	$1.81 \cdot 10^{-7}$		
IB04		$3.33 \cdot 10^{-4}$	$1.26 \cdot 10^{-8}$		
IB05	0.046	$3.33 \cdot 10^{-4}$	$1.42 \cdot 10^{-9}$	0.0102	0.057
IB06		$3.33 \cdot 10^{-4}$	$7.99 \cdot 10^{-9}$		
IB07		$3.33 \cdot 10^{-4}$	$1.14 \cdot 10^{-7}$		
IB08		$3.32 \cdot 10^{-4}$	$1.64 \cdot 10^{-6}$		
IB09		$3.12 \cdot 10^{-4}$	$2.16 \cdot 10^{-5}$		

Table 5.30: IB PbLi poloidal locations Modelica pressure drops in the case of $B = 0$ (regarding the results represented in Figure 5.37a), expressed for each component and BZ position.

Chapter 6

Conclusions and perspectives

The development of a system-level hydraulic model for the PbLi loop of the DEMO WCLL reactor has been presented in this work. It is an implementation of the breeder hydraulic loop in the GETTHEM code, with the aim to develop a complete code integrating together the coolant and the breeder system-level modeling. The Modelica language has been used for this model.

The model focuses on the modelling of the WCLL BB, composed by two independent loops, the OB and IB, each of them divided in four main components: BZ, manifold, FP and DP. The aim of this model is to characterize the pressure drop losses inside the BB region for an electro-conductive fluid flow in presence of a strong magnetic field (MHD effects). In the Chapter 2 a complete description of the WCLL BB layout has been reported, together with the PbLi properties and the different magnetic field profile inside the reactor.

The MHD effects determine a particular flow regime for electro-conductive liquids in presence of magnetic fields, characterizing new pressure drop behaviours inside the loop. In Chapter 3, the most important dimensionless numbers have been mentioned, in particular the Hartmann number determines the onset of the MHD effects. In general, the overall pressure drop is the sum of the OHD and MHD losses, but, for high magnetic field values ($Ha \gg 1$), it is possible consider only MHD case. Then, all MHD the pressure drop correlations have been described, both for 2D and 3D losses, analysing all the possible geometries inside the WCLL BB.

In the Chapter 4, all the MHD pressure drop correlations have been reported, and their implementation in the code has been verified. Regarding the 2D pressure drops, a modeling of the distributed losses for rectangular ducts and circular pipes has been done. In both cases, the MHD pressure drops have been analysed for different magnetic filed values and increasing the fluid velocity. As result, is is possible to notice as the pressure drop is particularly affected by the magnetic field intensity and has a linear dependence with the fluid mean velocity. These results are excellent for both rectangular and circular channel. For the 3D losses, a modelling for the different types of losses inside the BB: bends, cross section variation and presence of obstacles. In all the cases, both 2D and 3D losses, the results have been validated and compared with experimental/literature results with a good

approximation.

In the Chapter 5, the models of all the BB components and of the entire WCLL loop have been described. In the first part each BB component for the OB and IB loop has been singularly modelled according to the conceptual layout, implementing together the 2D and 3D pressure drops. For each of the loop components, the pressure drops obtained from the Modelica model have been compared with the literature results. After that, all the four components have been used in the same model. For this purpose, the equatorial BZ position case has been considered, both for OB and IB. Finally, the complete model of the PbLi poloidal locations for the OB and IB case has been implemented. In this model all the four components have been simulated together, considering nine BZ cells in parallel inside the BB. The overall pressure drop is 1.16 MPa and 2.16 MPa for the OB and IB case respectively. Analysing each component losses, the biggest contribution of the overall pressure drop is ascribable to the FP and DP and their losses are the same for each poloidal locations. Regarding the manifold and BZ losses, they change according to the BZ cell position, in particular they are maximum for the manifold and minimum for the BZ in the equatorial plane. Moreover, the BZ losses are very small with respect to the overall pressure drop and therefore can be neglected. Then, the same models have been simulated considering also the contribution of the hydrostatic head. The overall pressure drop is 4.10 MPa and 5.24 MPa for the OB and IB case respectively. Also in this case the bigger contribution of the overall pressure drop is ascribable to the FP and DP and the manifold and BZ losses have the same behaviour of the previous case. In general, the PbLi hydrostatic head has a very high contribution in the entire BB poloidal locations, therefore it is an important aspect to take into account for the future works and design phases. Moreover, the breeder mass flow rate distribution for both situations has been observed, highlighting that the hydrostatic head does not affect significantly to the mass flow rate in each BZ cells. As final step, a transient analysis has been done. Two transients have been analysed: a possible plasma discharge and a startup of all superconducting magnets. In the first transient, only the CS and the PFCs are turned off and the poloidal magnetic field component is null. In this situation, a plasma discharge of 2.5 hours (with 30 minutes of dwell time) has been supposed. In the second transient, all the superconducting magnets are turned off and all the magnetic field components (poloidal and toroidal) are null. The conclusion of these two analyses is that the Modelica model is able to simulate and describe a possible breeder transient.

In perspective, two possible further improvements are foreseen. The first is to implement in the code a thermal-fluid-dynamic model, in order to study also the PbLi dynamics in terms of temperature and the heat transfer to the water coolant. With this aspect, it is possible to analyse in a general view the complete dynamics of the WCLL BB, both for the cooling and the breeding system. The second improvement could be to implement a neutronic analysis in the model. This model would allow performing TBR calculations. Moreover, the neutron absorption determine the power generation inside the BZ, which could then be computed directly inside the model, building a self-consistent tool.

Appendix A

PbLi properties

The eutectic lithium-lead ($PbLi_{eu}$) alloy is one the best candidates for tritium production and neutron multiplier for several DEMO BB concepts. The reasons that led to choose this alloy derives from the main properties of the two materials. The lithium acts as tritium breeder thanks to nuclear fission reactions with fusion neutrons, in particular the Li_3^6 has a very high cross section especially in low-energy region, and the Li_3^7 works with high energy neutrons and produces an additional n that is available for another fission reaction. Moreover, the lithium is present in great quantities in nature with an easy procurement but it can have strong reactions with water and air. The lead acts as neutron multiplier increasing the lithium fission reactions and providing an higher tritium production. This characteristic is given due to its very high cross section in high-energy region. It has further several advantages such as its high availability, low cost and the capability to be used as coolant, but also some disadvantages such as its weight, high corrosion, low melting point (≈ 235 °C) and moderate reactivity with water.

For the WCLL concept, the lithium-lead alloy is in liquid phase, in which the eutectic title of Pb in the alloy is the 15.72 at.% Li [52]. The PbLi phase diagram is represented in Figure A.1. The reasons that have led the scientific community to use an alloy near the eutectic point, derive to find a compromise between an acceptable TBR and a low lithium activity, having also the lowest melting points, an advantage for both start-up and operation.

In literature, there are several correlations for the PbLi properties. The correlations that are chosen to estimate each property, are chosen based on the reliability of the available data and the number of authors agreeing on similar values [52]. Below, are indicated the chosen correlation for each PbLi property. Each property is estimated as a function of the temperature.

Density For the PbLi density (ρ) the following correlation is chosen [53]:

$$\rho\ [kg/m^3] = 10520.35 - 1.19051 \cdot T[K] \tag{A.1}$$

Specific heat The PbLi specific heat (c_p) is expressed as following [54, 55]:

$$c_p\ [J/(g \cdot K)] = 0.195 - 9.116 \cdot 10^{-6} \cdot T[K] \tag{A.2}$$

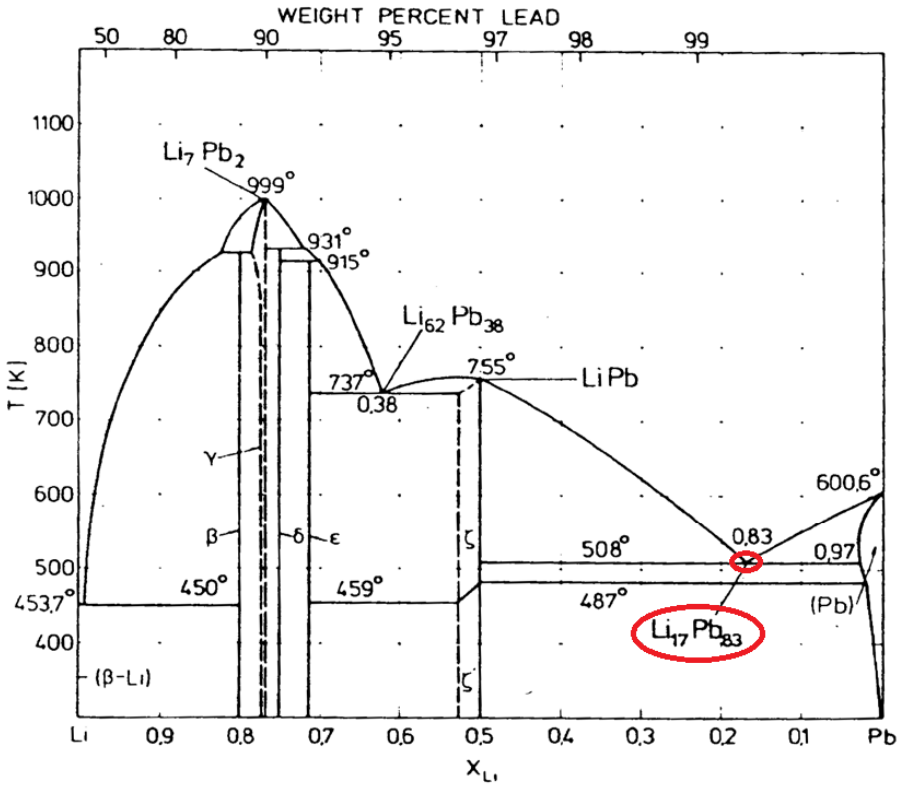

Figure A.1: PbLi phase diagram. The $PbLi_{eu}$ point is highlighted in red [13].

Thermal diffusivity The PbLi thermal diffusivity (α) is expressed with the following correlation [56]:

$$\alpha\ [cm^2/s] = 3.46 \cdot 10^{-4} \cdot T[K] - 1.05 \cdot 10^{-1} \tag{A.3}$$

Thermal conductivity For PbLi thermal conductivity (λ) the following correlation is chosen [57]:

$$\lambda\ [W/(cm \cdot K)] = 0.1451 + 1.9631 \cdot 10^{-4} \cdot T[^oC] \tag{A.4}$$

Dynamic and kinematic viscosity The PbLi dynamic viscosity (μ) is estimated with the following correlation [57]:

$$\mu\ [Pa \cdot s] = 0.0061091 - 2.2574 \cdot 10^{-5} \cdot T[^oC] + 3.766 \cdot 10^{-8} \cdot (T[^oC])^2 - 2.2887 \cdot 10^{-11} \cdot (T[^oC])^3 \tag{A.5}$$

The PbLi kinematic viscosity (ν) can be expressed with the following relation

$$\nu\ [m^2/s] = \frac{\mu}{\rho} \tag{A.6}$$

i.e. as the ratio between dynamic viscosity and density.

Electrical resistivity and conductivity The PbLi electrical resistivity (ρ_{el}) can be expressed with the relation [58]:

$$\rho_{el}\ [\Omega \cdot m] = 103.33 \cdot 10^{-8} - 6.750 \cdot 10^{-11} \cdot T[K] + 4.180 \cdot 10^{-13} \cdot (T[K])^2 \tag{A.7}$$

Else, the electrical conductivity (σ) with the relation:

$$\sigma\ [S/m] = \frac{1}{\rho_{el}} \tag{A.8}$$

i.e. as the reciprocal of the electrical resistivity.

Appendix B

OHD and MHD comparison

One of the essential aspects that must be analysed is the comparison between the OHD and MHD fluid regimes. As mentioned in the the Section 3.3, when the Hartmann number is very high ($Ha \gg 1$), the effects of the electro-magnetic forces prevail the viscous ones and the pressure losses are caused principally by Lorentz forces. For this reason, the OHD pressure drops can be neglected and the overall pressure drop is due only for the MHD losses.

In this appendix verification of this property is performed, adopting the simple model of a circular pipe already described and used in the Section 4.2.2. The Modelica model used is the same, in which in this case the pressure drop in the 2D component is evaluated as the sum of the MHD and OHD losses. The 2D MHD pressure drop is calculated with the MHD correlation for circular pipes (see Section 3.3.1), while the OHD with the Equation 5.3 [51]. The overall pressure drop in the 2D component is then evaluated as the sum of the OHD and MHD losses with the Equation 3.10.

The results of this analysis are reported in Figure B.1. These results have been calculated imposing the same geometrical parameters and fluid properties adopted in the Section 4.2.2, and the different pressure drop characteristic curves have been obtained decreasing the magnetic field values from 0.475 T to 0 T. In the same way, with fixed geometry and fluid properties (see Appendix A), the Hartmann number is proportional to the magnetic field and decreasing from 108 to 0. The first important aspect is that for decreasing magnetic fields, the pressure drop characteristic curves lower and the discrepancy between high and small Hartamann numbers is big, in some cases about of one order of magnitude. Therefore, when the $Ha >> 1$ the OHD losses can be neglected and the overall pressure drop can be approximates to the only MHD losses. The second important aspect is the curve behaviour for increasing fluid velocity. For low Ha and in turbulent regime, the OHD effect has a big contribution and the pressure drop curve has a parabolic shape (yellow curve), but for increasing Ha, the MHD effect becomes predominant and the curve assumes a linear shape (red curve). This behaviour can be seen in Figure B.1a and the parabolic shape in the Figure B.1b. Therefore, despite the fluid regime is turbulent (high Re), when the Ha becomes bigger, there is the onset of the MHD effects that inhibits the turbulent regime becoming laminar, highlighted by the linear shape of the pressure drop

characteristic curve.

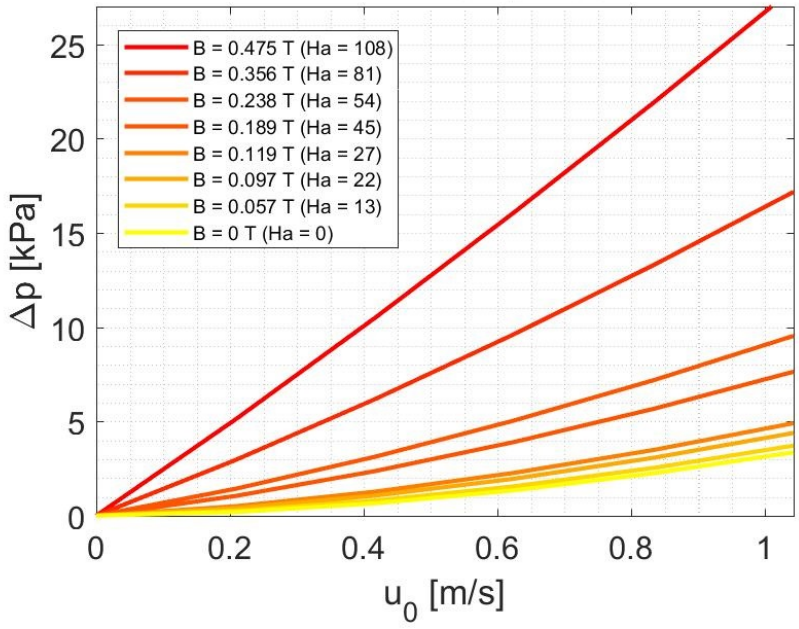

(a) OHD and MHD pressure drop comparison for different magnetic field values.

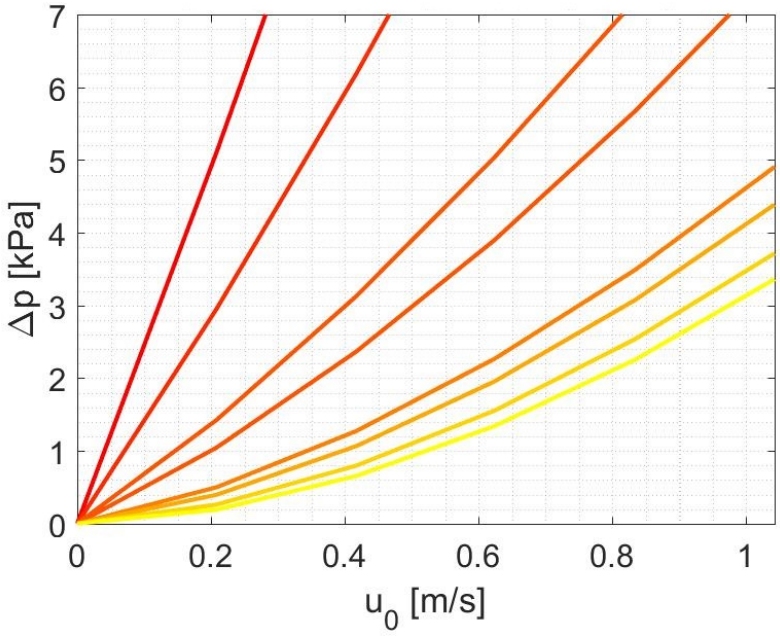

(b) OHD and MHD pressure drop comparison for different magnetic field values (zoom).

Figure B.1: OHD and MHD pressure drop comparison for different magnetic field values. Down: zoom of the top figure.

References

[1] EUROfusion Consortium, “European Consortium for the Development of Fusion Energy,” [Online]. Available: https://www.euro-fusion.org/.

[2] ITER, "International Thermonuclear Experimental Reactor" [Online]. Available: https://www.iter.org/

[3] F. Romanelli, P. Barabaschi, D. Borba, G. Federici, L. Horton, R. Neu, D. Stork and H. Zohm, “Fusion Electricity – A roadmap to the realisation of fusion energy,” European Fusion Development Agreement (EFDA), 2012, ISBN 978-3-00-040720-8T. [Online]. Available: https://www.euro-fusion.org/wpcms/wp-content/uploads/2013/01/JG12.356-web.pdf.

[4] K. Miyamoto, Plasma physics and controlled nuclear fusion, vol. 38. Springer Science and Business Media, 2006.

[5] C. Bachmann, T. Franke, F. Maviglia, M. Siccinio, S. Ciattaglia, C. Gliss, C. Vorpahl, T. Härtl, G. Keech, F. Cismondi, and G. Federici, EFDA_D_2KVWQZ, DEMO Plant Description Document, v1.4. Eurofusion, 2018. Available online for EUROfusion members at https://idm.eurofusion.org/?uid=2KVWQZ.

[6] R.G. Sharma, Superconducting magnets in fusion applications, Springer 2015.

[7] Cismondi, F., et al. "Progress in EU Breeding Blanket design and integration." Fusion Engineering and Design 136 (2018): 782-792.

[8] Del Nevo, A., et al. "Recent progress in developing a feasible and integrated conceptual design of the WCLL BB in EUROfusion project." Fusion Engineering and Design 146 (2019): 1805-1809.

[9] Hernández, Francisco A., et al. "Overview of the HCPB research activities in EUROfusion." IEEE Transactions on Plasma Science 46.6 (2018): 2247-2261.

[10] J. Aubert, et al., Status of the EU DEMO HCLL Breeding Blanket Design Development, This Conference (2018).

[11] D. Rapisarda, et al., Conceptual design of the EU-DEMO dual coolant lithium lead equatorial module, IEEE Trans. Plasma Sci. 44–49 (2016) 1603–1612.

[12] D. Rapisarda, et al., Status of the engineering activities carried out on the European DCLL, Fusion Eng. Des. 124 (2017) 876–881, http://dx.doi.org/10.1016/j.fusengdes.2017.02.022.

[13] L. V. Boccaccini, Blanket Technology for the Fusion Reactor, presentation edited by R. Zanino, 2017.

[14] A. Tassone, A. Del Nevo, P. Arena, G. Bongiovì, G. Caruso, P. A. di Maio, G. di Gironimo, M. Eboli, N. Forgione, R. Forte, et al., “Recent progress in the WCLL breeding blanket design for the DEMO fusion reactor,” IEEE Transactions on Plasma

Science, vol. 46, no. 5, pp. 1446–1457, 2018.

[15] Froio, Antonio. Multi-scale thermal-hydraulic modelling for the Primary Heat Transfer System of a tokamak. Diss. PhD Thesis, 2018.[Online]. Available: http://hdl.handle.net/11583/2704378, 2018.

[16] Modelica Association, "Modelica and the Modelica Association," 2017. [Online]. Available: https://www.modelica.org/. [Accessed 12 December 2017].

[17] Modelica Association, "Modelica® - A Unified Object-Oriented Language for Systems Modeling - Language Specification Version 3.4," 10 April 2017. [Online]. Available: https://www.modelica.org/documents/ModelicaSpec34.pdf . [Accessed 12 December 2017].

[18] P. Fritzson, Principles of object-oriented modeling and simulation with Modelica 2.2, Wiley, 2003.

[19] S. Mattsson, H. Elmqvist and M. Otter, "Physical systems modeling with Modelica," Control Engineering Practice, vol. 6, pp. 501-510, 1998.

[20] Froio, A., et al. "Dynamic thermal-hydraulic modelling of the EU DEMO HCPB breeding blanket cooling loops." Progress in Nuclear Energy 93 (2016): 116-132.

[21] A. Bertinetti, et al. "Hydraulic modeling of a segment of the EU DEMO HCPB breeding blanket back supporting structure." Fusion Engineering and Design 136 (2018): 1186-1190.

[22] A. Froio, et al. "Benchmark of the GETTHEM Vacuum Vessel Pressure Suppression System (VVPSS) model for a helium-cooled EU DEMO blanket." Proc. ESREL. 2017.

[23] A. Froio, A. Bertinetti, B.-E. Ghidersa, F. A. Hernández, L. Savoldi and R. Zanino (2019) Analysis of the Flow Distribution in the Back Supporting Structure Manifolds of the HCPB Breeding Blanket for the EU DEMO Fusion Reactor, Fusion Science and Technology, 75:5, 365-371, DOI: 10.1080/15361055.2019.1600348

[24] A. Froio, F. Cismondi, L. Savoldi and R. Zanino, "Thermal-Hydraulic Analysis of the EU DEMO Helium-Cooled Pebble Bed Breeding Blanket Using the GETTHEM Code," in IEEE Transactions on Plasma Science, vol. 46, no. 5, pp. 1436-1445, May 2018, doi: 10.1109/TPS.2018.2791678.

[25] A. Froio, et al. "Dynamic thermal-hydraulic modelling of the EU DEMO WCLL breeding blanket cooling loops." Fusion Engineering and Design 124 (2017): 887-891.

[26] A. Froio, et al. "Parametric thermal-hydraulic analysis of the EU DEMO Water-Cooled Lithium-Lead First Wall using the GETTHEM code." Fusion Engineering and Design 137 (2018): 257-267.

[27] A. Froio, et al. "Modelling an in-vessel loss of coolant accident in the EU DEMO WCLL breeding blanket with the GETTHEM code." Fusion Engineering and Design 136 (2018): 1226-1230.

[28] A. Tassone, G. Caruso, A. Del Nevo, Influence of PbLi hydraulic path and integration layout on MHD pressure losses, Fusion Engineering and Design 155, (2020) 111517.

[29] A. Tassone, et al. "MHD pressure drop estimate for the WCLL in-magnet PbLi loop." Fusion Engineering and Design 160 (2020): 111830.

[30] Arena, P.; Burlon, R.; Caruso, G.; Catanzaro, I.; Di Gironimo, G.; Di Maio, P. A.; Di Piazza, I.; Eboli, M.; Edemetti, F.; Forgione, N.; Forte, R.; Froio, A.; Giannetti, F.; Giardina, M.; Imbriani, V.; Martelli, E.; Moro, F.; Mozzillo, R.; Noce, S.; Savoldi, L.; Siriano, S.; Tassone, A.; Tomarchio, E.; Villari, R.; Del Nevo, A. WCLL BB design and

Integration studies 2019 activities. EUROfusion internal report EFDA_D_2P5NE5, 2020.

[31] A. Tassone, S. Siriano, G. Caruso, MHD loss estimate for IB PbLi loop, presented at WCLL Design Review Meeting 2019.

[32] A. Tassone, G. Caruso, A. Del Nevo, and I. Di Piazza, "CFD simulation of the magnetohydrodynamic flow inside the WCLL breeding blanket module," Fusion Engineering and Design, vol. 124, pp. 705–709, 2017.

[33] C. Bachmann and J. Anthony, EFDA D 2M8H88, Plant Definition Document. Eurofusion, 2018.

[34] R. Wenninger et al., EFDA D 2MUW9R, DEMO1 Reference Design - 2017 April ("EU DEMO1 2017") - SOF and EOF equilibria - v1.0. Eurofusion, 2018. Available online for EUROfusion members at https://idm.eurofusion.org/?uid=2MUW9R.

[35] A. Tassone, Study on Liquid Metal Magnetohydrodynamic Flows and Numerical Application to a Water-Cooled Blanket for Fusion Reactors, PhD Thesis, Sapienza University of Rome, 2019 March Available from: https://iris.uniroma1.it/retrieve/handle/11573/1243658/1054590/Tesi_dottorato_Tassone.pdf .

[36] U. Müller and L. Bühler, Magnetofluiddynamics in channels and containers. Springer Science & Business Media, 2013.

[37] A. Del Nevo, E. Martelli, P. Arena, A. Bertinetti, G. Bongiovì, G. Caruso, I. Catanzaro, L. Chiasso, G. Di Gironimo, P. A. Di Maio, M. Eboli, F. Edemetti, N. Forgione, R. Forte, A. Froio, F. Giannetti, M. Giardina, D. Giulietti, K. Jiang, S. Liu, L. Melchiorri, F. Moro, R. Mozzillo, S. Noce, S. Paci, L. Savoldi, A. Tassone, E. Tomarchio, R. Villari, R. Zanino WCLL Design Report 2018. EUROfusion internal report EFDA_D_2NUPDT, 2018.

[38] I.R. Kirillov, C.B. Reed, L. Barleon, K. Miyazaki, Present understanding of MHD and heat transfer phenomena for liquid metal blankets, Fusion Eng. Des. 27 (1995) 553–569.

[39] K. Miyazaki, S. Inoue and N. Yamaoak, Magneto-hydro-dynamic pressure drop of lithium flow in rectangular ducts, Fusion Technology 10 (1986) 830-836.

[40] T.Q. Hua, J.S. Walker, B.F. Picologlou and C.B. Reed, Three-dimensional magnetohydrodynamic flows in rectangular ducts of liquid-metal-cooled blankets, Fusion Technology 14 (1988) 1389-1398.

[41] K. Miyazaki, K. S Kotake, N. Yamaoka, S. Inoue and Y. Fujii-e, MHD pressure drop of NaK flow in stainless steel pipe, Nuclear Technology/Fusion 4 (1983) 447-452.

[42] J. Reimann, S. Molokov, I. Platnieks, E. Platacis, MHD-flow in multichannel Ubends: screening experiments and theoretical analysis, Fusion Technology 1992, Elsevier, 1993, pp. 1454–1458, https://doi.org/10.1016/B978-0-444-89995-8. 50285-X.

[43] Zi Meng et al., «Experimental studies of MHD pressure drop of PbLi flow in rectangular pipes under uniform magnetic field», J Fusion Energy, Vol. 34, pp. 759-764, 2015.

[44] Mergia, K., and N. Boukos. "Structural, thermal, electrical and magnetic properties of Eurofer 97 steel." Journal of Nuclear Materials 373.1-3 (2008): 1-8.

[45] F. Casella and A. Leva, "Modelica open library for power plant simulation: design and experimental validation," Proceedings of 3rd International Modelica Conference, pp. 41-50, Linköping, Sweden, 3-4 November 2003.

[46] F. Casella and A. Leva, “Modelling of thermo-hydraulic power generation processes using Modelica,” Mathematical and Computer Modelling of Dynamical Systems, vol. 12, no. 1, pp. 19-33, 2006.
[47] F.-C. Li et al., «Experimental and numerical studies of pressure drop in PbLi flows in a circular duct under non-uniform transverse magnetic field», Fusion Engineering and Design, vol. 88, pp. 3060-3071, 2013.
[48] A. Tassone, F. Giannetti, G. Caruso, Qualitative assessment of relevant MHD phenomena for the WCLL design, presented at WCLL Design Team Meeting, ENEA St. Teresa, La Spezia, Italy.
[49] S. Siriano, et al. "MHD forced convection flow in dielectric and electro-conductive rectangular annuli." Fusion Engineering and Design 159 (2020): 111773.
[50] S. Siriano, et al. "Electromagnetic coupling phenomena in co-axial rectangular channels." Fusion Engineering and Design 160 (2020): 111854.
[51] B. R. Munson, et al., Fluid Mechanics, 7th edition, SI version (Wiley, 2013).
[52] D. Martelli, A. Venturini and M. Utili. "Literature review of lead-lithium thermophysical properties." Fusion Engineering and Design 138 (2019): 183-195.
[53] S.V. Stankus, R.A. Khairulin, A.G. Mozgovoi, An experimental investigation of the density and thermal expansion of advanced materials and heat–transfer agents of liquid–metal systems of fusion reactor: lead–lithium eutectic, High Temp. 44 (6) (2006) 829–837.
[54] B. Schulz, Thermophysical properties of the Li(17) Pb(83) alloy, Fusion Eng. Des. 14 (1991) 199–205.
[55] U. Jauch, V. Karcher, B. Schulz, G. Haase, Thermophysical properties in the system Li-Pb, KfK Report 4144 (1986).
[56] M. Kondo, Y. Nakajima, M. Tsuji, T. Nozawa, Evaluation of thermal conductivity for liquid lead lithium alloys at various Li concentrations based on measurement and evaluation ofdensity, thermal diffusivity and specific heat of alloys, Fusion Eng. Des. 109 (111) (2016) 1345–1350.
[57] E.A. Mogahed, G.L. Kulcinski, Bibliography of a Promising Tritium Breeding Material – Pb83Li17, Fusion Technology Institute, University of Wisconsin, 1995 UWFDM-994.
[58] P. Hubberstey, M.G. Barker, T. Sample, An electrical resistivity monitor for detection of composition changes in Pb-17Li, Fusion Eng. Des. 14 (1991) 227–233.